Geological Quarterly, 2025, 69, 25
DOI: https://doi.org/10.7306/gq.1798

Laser ablation ICP-MS study of trace elements in scheelite in different types of mineralization from the Bohemian Massif

Jan PAŠAVA[1, *], Petr BOHDÁLEK[1], Jan MALEC[1], František VESELOVSKÝ[1], Ana Carolina R. MIRANDA[2], Georges BEAUDOIN[2] and Bertrand ROTTIER[2]

[1] Czech Geological Survey, Geologická 6, 15200 Praha 5, Czech Republic; ORCID: 0000-0002-1457-0165 [J.P.]

[2] Université Laval, Département de Géologie et Génie Géologique, Centre de recherche sur la géologie et l'ingénierie minérale, Québec (QC), Canada; ORCID: 0000-0002-0223-202X [A.C.M.], 0000-0002-4029-2648 [G.B.], 0000-0002-5386-0472 [B.R.]

Pašava, J., Bohdálek, P., Malec, J., Veselovský, F., Miranda, A.C.R., Beaudoin, G., Rottier, B., 2025. Laser ablation ICP-MS study of trace elements in scheelite in different types of mineralization from the Bohemian Massif. Geological Quarterly, 69, 22; https://doi.org/10.7306/gq.1798

Associate Editor: Stanisław Mikulski

We describe scheelite in five types of mineral deposit from the Bohemian Massif (greisen, orogenic Au, reduced intrusion-related gold systems (RIRGS), oxidized and reduced skarn) via cathodoluminescence (CL) imaging and laser ablation inductively coupled plasma mass spectrometry (LA-ICP-MS) analyses. We document variability in the scheelite composition within single grains and/or deposit types that reflects the nature and evolution of the ore-forming fluids. We provide scheelite typical trace element characteristics and chondrite-normalized REE patterns for different deposit types, confirming that scheelite can be used as an indicator mineral for their exploration. For example, scheelite from greisen-related deposits is usually rich in Sn, Sr, Y and HREE with various ranges of median values in individual deposits (0.05–8.0 ppm, 232.4–567.1 ppm, 0.06–465.0 ppm and 0.06–632.5 ppm, respectively) and with typical chondrite-normalized REE patterns showing Eu negative or positive anomaly. Under UV light scheelite from Sn-W deposits displays variable colours from whitish via yellowish to bluish. In contrast to greisen-related deposits, scheelite from Au-orogenic association is usually relative rich in Pb (median range in individual deposits: 6.1–11.2 ppm), and relatively poor in Mg, Mo and Nb. Flat and bell-type chondrite-normalized REE patterns show a pronounced Eu positive anomaly. Under UV light it is predominantly homogenous and bluish. Scheelite from oxidized skarn is enriched in Mo, Nb and LREE (median range in individual deposits: 311.4–7214.1 ppm, 1.3–214.9 ppm, and 1.1–1375.8 ppm, respectively), and scheelite from reduced skarns is characterized by the lowest median ranges of Nb (1.7–107.8 ppm), Y (0.69–41.1 ppm), Mn (0.5–17.0 ppm) and Zn (0.04–0.252 ppm) in individual deposits, when compared to all the groups studied. Scheelite from oxidized and reduced skarn deposits displays several types of chondrite-normalized pattern: (1) LREE-enriched with a positive or negative Eu anomaly, (2) Bell-shaped REE patterns with negative or without Eu anomaly, and (3) Flat REE patterns with a negative Eu anomaly. Scheelite from oxidized and reduced skarn deposits is commonly zoned and mostly bluish under UV light.

Key words: scheelite, gold deposits, skarns, greisen-type deposits, Bohemian Massif.

INTRODUCTION

Laser Ablation Inductively Plasma Coupled Mass Spectrometry (LA-ICP-MS) spot analysis and mapping have been successfully used to document and interpret trends of trace element distribution in sulphides such as pyrite, arsenopyrite, chalcopyrite, sphalerite, molybdenite and others (e.g., Cook et al., 2009, 2013; Large et al., 2009, 2014; Sung et al., 2009; Lin et al., 2011; Thomas et al., 2011; Winderbaum et al., 2012; Pašava et al., 2013, 2017; George et al., 2015; Caraballo et al., 2023a, b). Cathodoluminescene (CL) imaging has proved to be an effective technique for revealing internal texture, zoning and trace element distribution in scheelite (Gaft et al., 1999; Brugger et al., 2002; Poulin et al., 2016; Ding et al., 2018; Zhang et al., 2018; Sciuba et al., 2020).

Scheelite ($CaWO_4$) is a common accessory mineral that occurs in different types of ore deposits and, on the basis of study of REE and other trace element distribution, it has been proposed as an important indicator mineral for targeting Au (polymetallic), W and skarn-type deposits (Malec, 1985; Štemprok and Mašková, 1992; Ghaderi et al., 1999; Dostal et al., 2009; Chowdhury et al., 2011; Poulin et al., 2016; Fu et al., 2017; McClenaghan et al., 2017; Manéglia et al., 2018; Zhao et al., 2018; Yuan et al., 2019; Sciuba et al., 2020; Miranda et al., 2022, 2024).

* Corresponding author, e-mail: jan.pasava@geology.cz

Received: April 16, 2025; accepted: June 25, 2025; first published online: August 29, 2025

Scheelite is also a major mineral in greisen and skarn-type deposits (Xiong et al., 2006; Ren et al., 2010; Song et al., 2014; Guo et al., 2016; Poulin, 2016; Poulin et al., 2016, 2018) and an accessory mineral in aplite, pegmatite and metamorphosed sedimentary exhalative Fe-Mn (Brugger et al., 1998; Uspensky et al., 1998) and volcanogenic massive sulphide deposits (Poulin, 2016; Poulin et al., 2016, 2018).

Scheelite and powellite ($CaMoO_4$) form a partial solid solution where Mo^{6+} substitutes for W^{6+} (Tysonet al., 1988). Replacement of W by Mo and Ca by Sr, Pb, Fe, Mn, Ba and REE have been reported (Cottrant, 1981; Raimbault et al., 1993; Ghaderi et al., 1999) and contents of Na, V, Nb, Ta, S, As, Pb, U, Th, Mn, Fe, Au, Ba, B, Co, Cr, K, Ni, Sb Sc, Bi, Cu, Sn, Zn, Li, Ti and Rb have been measured in various amounts in scheelite in different types of deposits (Anglin, 1996; Eichhorn et al.1997; Zhigang et al., 1998; Ghaderi et al., 1999; Brugger et al., 2000a, b; Brugger et al., 2002; Xiong et al., 2006; Liu Yan et al., 2007; Dostal et al., 2009; Graupner et al., 2010; Peng et al., 2010; Ren et al., 2010; Song et al., 2014; Hazarika et al., 2016; Poulin, 2016; Poulin et al., 2016; Fu et al., 2017; Sun and Chen, 2017, Sciuba et al., 2020; Miranda et al., 2022, 2024). The REE distribution patterns and total REE concentrations in scheelite play an important role in investigating their precipitation processes. Europium anomalies identified in many deposits can be used to indicate the temperature of scheelite crystallization, the elemental substitution mechanism, and Na activity during scheelite crystallization as well as the redox state (Ghaderi et al., 1999; Brugger et al., 2000a, 2008; Song et al., 2014). Anomalies in Eu values can reflect the degree of magma differentiation, and are also closely related to the pH of the fluid (Guo, Z. et al., 2016; Fu et al., 2017; Ding et al., 2018; Zhang et al., 2018; Yuan et al., 2019; Sciuba et al., 2020). In hydrothermal fluids, Sverjensky (1984) showed that Eu^{2+} predominates at temperatures above 250°C. The high REE concentrations (~10–5000 ppm; Uspensky et al., 1998) in scheelite have been used for Sm-Nd geochronology to date gold mineralization (Anglin et al., 1996; Frei et al., 1998; Uspensky et al., 1998; Kempe et al., 2001; Roberts et al., 2006) whereas the Sr and Nd isotopic compositions have been used to constrain the sources and pathways of auriferous hydrothermal fluids (Bell et al.,1989; Kent et al., 1995; Darbyshire et al., 1996; Frei et al., 1998).

Analysis of bulk mineral chemical composition of different types of scheelite from the Bohemian Massif using instrumental neutron activation analysis (INAA) was done by Malec (1985). On the basis of his collection we provide new *in situ* LA-ICP-MS data on the distribution of REE and other trace elements in scheelite from the Bohemian Massif, from greisen, orogenic gold, reduced intrusion related gold system (RIRGS), and oxidized and reduced skarn associations, and also scheelite from other associations that are not related to any of the previous groups. We also document how different the trace element chemical composition of scheelite can be within a specific type of mineralization, this variation being a function of the origin, composition and physico-chemical conditions of the hydrothermal fluids from which it precipitates. It can also be significantly influenced by the distribution of REE and other trace elements within co-existing mineral phases. We provide further evidence that scheelite chemical composition can be used to fingerprint indicator mineral provenance in exploration and mineral assessment surveys.

CHARACTERISTICS OF SELECTED TYPES OF MINERAL DEPOSITS, SCHEELITE TEXTURE AND MINERAL ASSEMBLAGE

Basic characteristics of the scheelite occurrences studied from the Bohemian Massif, representing greisen/quartz-vein-, orogenic gold-, Au-RIRGS- and oxidized and reduced skarn associations are summarized in Table 1 and their location shown on Figure 1. Major deposits are briefly described in the following text.

SN-W-BEARING GREISENIZED GRANITE AND RELATED QUARTZ VEINS

The Sn-W-(Li) greisen deposits are mostly formed by cassiterite, wolframite and zinnwaldite, and are related to strongly fractionated Variscan S and A type granite affinities within the Saxothuringian Unit along the Czech–German boundary (Erzgebirge). Scheelite is widespread in Sn-W deposits at Cínovec, Horní Slavkov-Krásno-Huber and other localities (Seltman and Štemprok, 1995). Brief characteristics of these sites, including Horní Babákov, Ovesná Lhota and Cetoraz, are given in Table 1.

The Cínovec deposit (Fig. 1) had been exploited since the 14th century. The deposit is genetically linked to a late Variscan highly fractionated A-type granitic intrusion forming the latest evolutionary stage of the volcano-plutonic system of the Teplice caldera. The ore-bearing albite-zinnwaldite granite forms a mostly hidden cupola-like body with an elliptical N–S elongated outcrop (1.4   0.3 km). Its upper part, up to a depth of 750 m, is formed by albite-zinnwaldite granites, while the deeper part consists of biotite granites. In the uppermost part of the pluton (the "canopy") up to a depth of ~300 m, the granite is altered, crosscut with planar quartz-zinnwaldite veins and partly greisenized. Stockscheider (marginal pegmatite) forms a several dm- to 2.5 m-thick layer at the contact between the granite cupola and the surrounding rhyolite (Breiter et al., 2017a).

Tin and tungsten mineralization is spatially associated with a cupola of lithium-albite granite, separated from the enclosing Teplice rhyolite by a continuous pegmatite rim (Stockscheider et al., 2017a). The main minerals forming the Li-Sn-W mineralization are quartz, wolframite, zinnwaldite, topaz, cassiterite, fluorite, feldspar, hydromuscovite and scheelite, while sulphides are represented by arsenopyrite, stanine sphalerite, galena, Bi and Cu minerals (including native bismuth, bismuthinite, chalcopyrite), pyrite and other minerals (Štemprok, 1965; Breiter et al., 2017b). On the Czech side, total geological resources were calculated at ~ 564 10^6 t of Li-Sn-W ore averaging 0.057% Sn, 0.016% W and 0.2% Li (Newall, 2015). Apart from this, the Cínovec deposit also has significant contents of Nb, Ta and especially Sc (Hreus et al., 2021), and hence differs distinctly from the greisen ores in the western part of the Krušné hory Mts. (Štemprok et al., 1995; Breiter et al., 2017a).

We studied two types of scheelite: (a) greyish-white large grains from massive greisen (SCH-47) and (b) reddish-brown large grains from vein greisen (SCH-48).

The Krásno-Huber deposit, yielded 10–12 000 t of metallic Sn during its 600 year mining history until it was abandoned in 1987. Sn-W-Li ores occur within quartz veins and stocks in greisen. The main minerals include zinnwaldite, topaz, cassiterite, wolframite, chalcopyrite, sphalerite and arsenopyrite, ac-

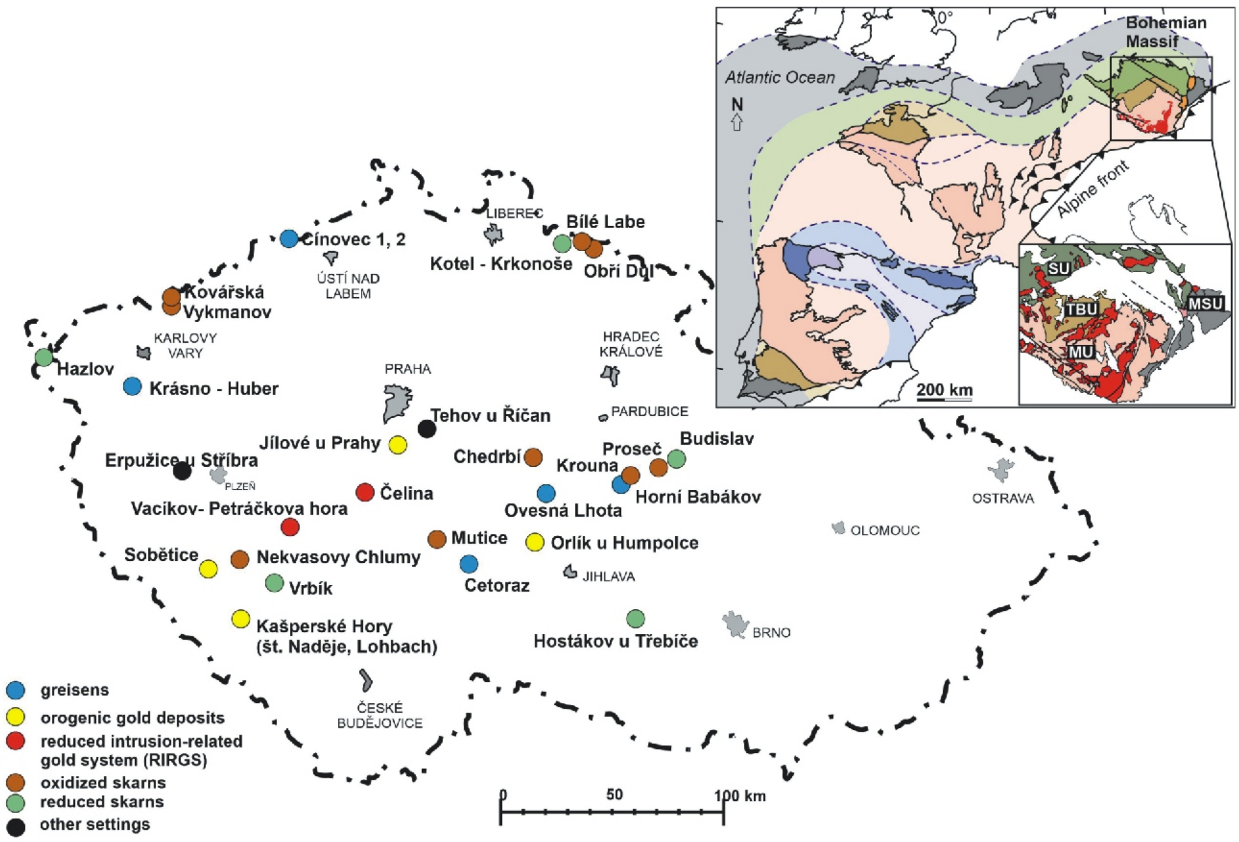

Fig. 1. Distribution of the scheelite localities studied in the Czech Republic

TBU – Teplá-Barrandian Unit, SU – Saxothuringian Unit, MU – Moldanubian Unit, MSU – Moravo-Silesian Unit, adapted from Ackerman et al. (2017)

companied by less frequent molybdenite, stannite, bornite, covellite and rare scheelite (Beran and Sejkora, 2006). The ore grade decreased from 1.5–1.7% Sn close to the surface, in the year 1540, to 0.2–0.4% Sn at depth in the 18th century. It is a typical greisen-type deposit, spatially and genetically linked to the younger intrusive complex of S-type acidic intrusions and especially with their Li-F rich members. This was supported by Re-Os dating of molybdenite at 323.3 ±1.6 (Ackerman et al., 2017), indicating close temporal relationship with granites of the Eibenstock–Nejdek pluton.

We studied two 1-mm grains from greisen (SCH-43), which were very light blue and homogeneous in cathodoluminiscence (CL). Scheelite is associated with chalcopyrite and wolframite.

OROGENIC AU DEPOSITS

In the Bohemian Massif, scheelite is commonly found in orogenic gold deposits (e.g., Jílové deposit, Kašperské Hory deposit) and prospects (Sobětice and Orlík u Humpolce – see Table 1 for more information; Morávek, 1995a).

THE JÍLOVÉ AU DEPOSIT

The Jílové deposit (Morávek, 1971; Morávek, 1995b, 1996) is located in the central part of the Bohemian Massif and represents a vein to stockwork type of orogenic gold deposit (Zachariáš et al., 2013). It was the most important mine in the former Bohemian Kingdom during the medieval times. It is estimated that about 6 to 10 t of gold was mined from the Jílové deposit in the past; remaining resources are estimated to be between 13 and 17 t of Au. On the basis of the ^{40}Ar/^{39}Ar age of hydrothermal muscovite, the formation of the gold-bearing quartz veins hosted by reverse faults in the Jílové deposit occurred at 339 ±1.5 Ma. The mineralization is essentially coeval with the late intrusive phases of the Central Bohemian Plutonic Complex and with late-orogenic large-scale tectonic movements at the boundary between two crustal terranes (Teplá-Barrandian and Moldanubian). Morávek (1971) identified six stages of Variscan gold-bearing mineralization in the Jílové deposit. Scheelite-bearing assemblages (stages 2–3) precipitated at 292 ±8°C from a low-salinity fluid with calculated values: $^{18}O_{SMOW}$ = +4.2 ±0.5‰ and $^{13}C_{PDB}$ = –11 ±1‰. Some veins in the southern part of the Jílové district contain scheelite in association with dolomite and/or quartz.

The orange scheelite grain, up to 0.5 cm across (SCH-41-generally homogeneous and showing pale yellow luminiscence), from a quartz vein several cm thick, comes from the third level of the Pepř mine. The quartz vein is hosted in metavolcanic rocks of the Jílové Belt (Morávek, 1971). Scheelite in the vein is locally cut by a system of tiny carbonate veinlets. According to Morávek (1971) the scheelite is younger than the main quartz matrix and locally crystallization of both quartz and scheelite was contemporaneous. The scheelite is younger than the molybdenite and older than the gold (Morávek, 1971).

Table 1

Summary of the main geological characteristics of scheelite-bearing samples

Deposit	Major metal	Mineral association**	Intrusion	Host rock	Geotectonic Unit	Age
Quartz vein/greisen deposits						
Cínovec/ Zinnwald	Sn-W-Li	Qz+Znw+Sch (We studied two types of scheelite: 1. greyish white large grains from massive greisen (SCH-47) and (2) reddish-brown large grains of scheelite from vein greisen (SCH-48).	Cínovec-Zinnwald granite (cupola) intrusion to paleorhyolite	quartz veins in strongly fractionated and slightly peraluminous rare metal A-type granites	Saxothurin-gicum	311–321.5 Ma
Krásno-Huber	Sn(W)	Qz+Sch (We studied two 1 mm grains from greisen (SCH-43), showing weak light blue and homogeneous texture in cathodoluminiscence (CL). Scheelite is associated with chalcopyrite and wolframite	Carlsbad plutonic intrusion	quartz veins in lithium - topaz granite	Saxothurin-gicum	320–330 Ma
Cetoraz		Qz+Ms+Kfs+Ghn+Py+Wf+Sch	Pacov Orthogneiss	quartz veins in orthogneiss		494–485 Ma
Ovesná Lhota	Sn-W	Qz+Ms+Tur+Cst+Wf+Sch	small adamellite intrusions related to Moldanubian Pluton	quartz veins in migmatites	Moldanubi-cum	Variscan
Horní Babákov	W	Qz+Ms+Brl+Flr+Feb+Sch	Nasavrky pluton - biotite granodiorite	quartz veins inside granodiorite body	Bohemicum	Variscan
Oxidized skarns						
Obří Důl	Fe-Cu-As-W	Grt+Cpx+Amp+Sch	Krkonoše-Jizera Massif	dolomite marble in contact zone of I-type porphyric biotite granite	Saxothurin-gicum	312 Ma
Kovářská	F-Be-W	Kfs+Cpx+Czo+Amp+Bvn+ Sch	no observable relation to granite intrusion	crystalline rocks of amphibolite facies (paragneiss, mica schist)	Saxothurin-gicum	Variscan
Vykmanov u Kovářské	W-Pb-Zn	Cpx+Flr+Sph+Sch	no observable relation to granitoid intrusion	crystalline rocks of amphibolite facies (paragneiss, mica schist)	Saxothurin-gicum	Variscan
Mutice u Mladé Vožice	W	Cpx+Plg+Sch	no observable relation to granitoid intrusion	paragneiss and migmatites	Moldanubi-cum	pre-Variscan
Nekvasovy-Chlumy	W	Cpx+Plg+Sch	Central Bohemian Massif - Chanovice apophyse (granodiorite)	skarn in cordierite-biotite migmatites	Moldanubi-cum	Variscan
Proseč	W	Grs+Di+Qtz±Ttn+Sch	Budislav Pluton in Polička crystalline unit	skarn-marble xenoliths in tonalite to granodiorite	Bohemicum	Variscan
Krouna	W	Grs+Di+Qtz±Ttn+Sch	no observable relation to granitoid intrusion	skarn-like calc-slicate rocks of Svratka crystalline unit	Bohemicum	Variscan
Chedrbí	W	Amp+Kfs+Cpx+Grt+Sch	no observable relation to granitoid intrusion	amphibolite	Kutná Hora-Svratka crystallini-cum	pre-Variscan
Bílé Labe	Cu-W	Plg+Qz+Sch	Krkonoše-Jizera Massif	impregnations in metasomatized	Saxothurin-gicum	Variscan

Tabl. 1 cont.

				biotite granite and quartz veins		
Reduced skarns						
Budislav u Litomyšle	W	Cpx+Plg+Wol+Sch	quartz diorite-tonalite-granodiorite Budislav Massif	xenoliths of skarnized marbles and skarn in tonalite	Bohemicum	Variscan
Kotel (Krkonoše)	Cu	Grt+Cpx+Act+Ep+Sch	Krkonoše-Jizera Massif	dolomite marble in contact zone of porphyric biotite granite	Saxothurin-gicum	Variscan
Hostákov u Třebíče	W	Cpx+Grt+Ves+Flr+Qz+Sch	Třebíč porphyritic amphibole-biotite melasyenite (durbachite) Massif	xenoliths of biotite paragniess in amphibole-biotite melasyenite (durbachite)	Moldanubi-cum	Variscan
Hazlov u Chebu	W	Grt+Ves+Wol+Plg+Ep+Sch	Smrčiny granite Massif	skarn xenoliths in granite	Saxothurin-gicum	Variscan
Vrbík u Horažďovic	W	Grt+Cpx+Scp+Sch	Central Bohemian Massif - amphibole-biotitic granodiorite	skarnized dolomite xenolith in granodiorite	Moldanubi-cum	Variscan
Reduced Intrusion Related Gold System (RIRGS)						
Vacíkov-Petráčkova hora	Au	Qz+Po+Ccp+Py+Sch+Mol	Central Bohemian Massif	sheeted arrays of quartz veins and veinlets hosted by the Petráčkova hora granodiorite stock		342.1–348.5 Ma
Čelina	Au - W	Cpx-Amp-Bt-Sch (We studied scheelite sample SCH-3) from bedding parallel quartz vein associated with calc-silicate hornfels in amphibolite. It forms small anhedral grains (0.1–0.7 mm) mostly enclosed in amphibole and locally in association with plagioclase.)	Central Bohemian Massif – tonalite	amphibolite		345–358 Ma
Orogenic Gold Deposits						
Kašperské Hory	Au-W	Qz+Sulp+Sch (We studied two types of scheelite: 1. scheelite from thin quartz vein crosscutting finely banded calc-silicate hornfels (rocks) (SCH5) which was sampled in the Naděje gallery at the Kašperské Hory deposit. Scheelite forms up to 0.8 mm subhedral grains in white-grey quartz matrix and is accompanied by arsenopyrite (up to 0.9 mm. 2. – Scheelite (SCH-6) is from the heavy mineral concentrate from the Lohbach brook, which contains abundant ilmenite, garnet, lesser magnetite, rutile, sillimanite and clinozoisite and rare monazite, spinel, pyrite, arsenopyrite, apatite and native gold. Scheelite (up to 3 mm in size) is intergrown with quartz, biotite, sericite, sillimanite (with inclusions of Ti minerals and apatite), garnet, pyrite and limonite. Locally, scheelite contains inclusions of apatite and pyrrhotite. The mineral assemblage of the heavy mineral concentrate indicates several	no observable relation to granitoid intrusion	biotite, sillimanite-biotite,±cordierite, muskovite, garnet paragneiss	Moldanubi-cum	344 Ma (Au veins)

Tabl. 1 cont.

		sources: (a) sillimanite-biotite gneiss, (b) quartz veins with gold and (c) skarn.				
Sobětice	Au-Ag	Qz+Au+Sulph+Sch	exocontact of Klatovy granodirite apophyse of the Central Bohemian Massif	coincident quartz lodes in marble at the contact with paragneiss	Moldanubi-cum	Variscan
Jílové u Prahy	Au	Qz+ Cal+Au+Sulph+Sch (We studied a. 0.5 cm orange scheelite grain (SCH-41 – rather homogeneously looking and showing low yellow luminiscence) in quartz vein (several cm thick) coming from the third level of the Pepř mine.			Bohemicum	339.0 ±1.5
Orlík u Humpolce	Au	Qz+Plg+Cpx+Amp+Sulph+Sch+Au	no observable relation to granitoid intrusion	quartz veins in paragneiss with calc-silica rocks and quartzites associated with migmatites	Moldanubi-cum	pre-Variscan

Deposit	Deposit size	Temperature and salinity of the fluids	Reference
Quartz vein/greisen deposits			
Cínovec/ Zinnwald	564 Mt 0.057% Sn, 0.016 % W*, 0.2% Li – total geological resources	384–439°C (topaz); 2.4–9.5wt.% NaCl eq.	Seifert et al. (2011), Seifert and Pavlova (2016), Ackerman et al. (2017), Breiter et al. (2017a, b), Zhang et al. (2017), Starý (2019)
Krásno-Huber	13.8 Mt 0.224% Sn, 0.032%W* – indicated resources	low-greisenization related to low-salinity (0–7 wt.% NaCl eq.) aqueous fluids with low amount of CO_2, CH_4, and N_2 (≤10 mol% in total) at temperatures of ~350–400°C and pressures of 300–530 bar (quartz, topaz, cassiterite)	Suček et al. (1995), Dolníček et al. (2012), Ackerman et al. (2016)
Cetoraz	83 kt 0.61%W – inferred resources	P-T conditions of 720 ±75 °C at 0.65 ±0.29 GPa calculated from mineral chemistry of muscovite, biotite, quartz, K-feldspar, plagioclase, sillimanite and garnet by THERMOCALC 3.33 software for orthogneiss host rock	Němec and Tenčík (1976), Šponar et al. (1985), Jurák et al. (1986), Losertová et al. (2013), Buřivalová and Losos (2018), Buriánek et al. (2020)
Ovesná Lhota	occurrence	not available data	Tenčík (1970), Losertová et al. (2014)
Horní Babákov	occurrence	not available data	Hájek (1971)
Oxidized skarns			
Obří Důl	0.1 Mt 0.43–0.47% W, 0.8 Mt 0.41–0.43 % Cu, 0.19–0.49% Sn – indicated resources	clinopyroxene showed homogenization temperatures (Th) in the range of 387–424°C and only secondary fluid inclusions (Th 228–262°C, salinity up to 8 wt.% NaCl equiv.) were found in garnet (grossular)	Ackerman et al. (2017), Veselovský et al. (2018)
Kovářská	2.8 Mt, 0.25% W – potencial resources	not available data	Roos and Veselovský (1985)
Vykmanov u Kovářské	indication	not available data	
Mutice u Mladé Vožice	showing	not available data	Malec (1985)
Nekvasovy-Chlumy	4 kt 1.67% W – inferred resources	not available data	Hujsl (1988)
Proseč	occurrence	not available data	Buriánek (2009)
Krouna	occurrence	500–600°C, 6–15 kbar, based on Fe^{2+}/Mg ion exchange in garnet/clinopyroxen system	Bubal (2013)
Chedrbí	occurrence	not available data	Malec (1985)

Tabl. 1 cont.

Bílé Labe	occurrence		not available data	Tuček (1970)
Reduced skarns				
Budislav u Litomyšle	occurrence		550–520°C	Buriánek (2009)
Kotel (Krkonoše)	occurrence			Žáček (2008)
Hostákov u Třebíče	14.8 kt 0.46% W		not available data	Holub and Páša (2004)
Hazlov u Chebu	700 kt 0.3% W - inferred resources		not available data	Štemprok (1985)
Vrbík u Horažďovic	4.8 kt 3.6 % W - mined out		not available data	Hujsl et al. (1987)
Reduced Intrusion Related Gold System (RIRGS)				
Vacíkov - Petráčkova hora		30.7 Mt 1.08 g/t – inferred resources	Polyphase fluid inclusions hosted by igneous quartz of the Petračkova hora granodiorite indicate minimum trapping conditions of about 3 kbar and 550°C. The gold-rich Q1 toQ4 veins may have formed along a quasi-isobaric cooling path at 2.5 to 1.5 kbar and 590 to 400°C. The salinity of primary aqueous inclusions falls into ranges 6 to 23 and 33 to 41 equiv. wt% NaCl; in igneous quartz, populations in salinity were observed between 5 to 16, 35 to 40 and 62 to 70 equiv. wt% NaCl.	Studničný (1994), Zachariáš et al. (2001)
Čelina		7.9 Mt 1.58 g/t Au, 0.285 %W – indicated resources	Corresponding fluids belong to the C-H-O-N system and probably resulted from fluid–rock interactions within the metamorphic series at high P-T conditions (T ≈ 450–550°C and P ≈ 250–400 Mpa). Maximum (550°C calculated from Al, Ca and Na contens in plagioclase and amphibole, minimum based on coexisting biotite-chlorite boundary	Malec (1985), Kovář and Mandík (1993), Boiron et al. (2001), Ackerman et al. (2017)
Orogenic Gold Deposits				
Kašperské Hory		11.7 Mt 4.71 g/t Au; 3.1 Mt 1.32% W – indicated resources	The corresponding fluids of Stages I and II belong to the C-H-O-N system. The P-T conditions correspond to 590–520°C and to 0.44–0.25 GPa for Stage I and 480–390°C and ~0.2 GPa for Stage II; calculated from izotopic equilibrium temperatures for Qz-Ms coexisting pair (stage I) respectively for Qz-Sch coexisting pair(stage II);	Punčochář (1992), Strnad et al. (2012), Ackerman et al. (2019)
Sobětice		old workings	low salinity (1–2.2 wt%NaCl eq.) H_2O-CO_2 fluids in Q1 (ore bearing), estimated T ~350°C, P ~ 400 Mpa; based on H_2O-CO_2 isochores calculated from fluid inclusions in quartz	Černý and Litochleb (1983), Hemalová (2010)
Jílové u Prahy		3.3 Mt 3.0 g/t Au – geological resources	216–238°C 3.5 wt.% eq. NaCl; scheelite originated from low saline H_2O type fluid at stable T ~ 298°C, characterized by a more evolved Sr isotopic composition (87Sr/ 86 Sr = 0.7087–0.7105; associated with scheelite).	Zachariáš et al. (2013)
Orlík u Humpolce		old workings	360–380°C, 0.6–0.8 kbar calculated from primary inclussions in ore-bearing quartz and in scheelite	Ďurišová et al. (1992), Buřival and Losertová (2015)

* – wolframite is the W ore; ** – mineral abbreviations after Whitney and Evans (2010)

THE KAŠPERSKÉ HORY DEPOSIT

Exploration in the 1980s, and until 1999, resulted in estimation of a total resource of 50 t of Au (Punčochář, 1992). The Kašperské Hory gold deposit is located close to the tectonic boundary between the monotonous and varied units of a regional shear zone of Moldanubicum (Fig. 1). The predominant host rock is variably migmatized biotite or biotite–sillimanite paragneiss with minor layers of quartzite, quartz–feldspar gneiss, calc-silicate rocks, amphibolite and marble, accompanied by two bodies of orthogneiss. Variscan magmatic rocks form small intrusions of granitic lithologies belonging to the Moldanubian Batholith (MB) and the Central Bohemian Plutonic Complex (CBPC) accompanied by granodiorite porphyry and small pegmatite bodies. Four stages of mineralization were identified (Strnad et al., 2012). Stages I–II are represented by three different quartz vein generations formed at ~390–590°C, containing variable amounts of arsenopyrite, scheelite, pyrite, and invisible gold hosted mainly by arsenopyrite. Economic gold mineralization is bound to stage III, characterized by the formation of quartz, galena, native gold and Bi–Te minerals at lower T conditions (180–290°C; Strnad et al., 2012). The gold mineralization forms stratabound bodies bound by layers of calc-silicate rocks (Morávek and Punčochář, 1983) or disseminations related to stage II mineralization. The gold is typically associated with pyrite, pyrrhotite, arsenopyrite, löllingite, molybdenite, Bi–Te minerals, chlorite, scapolite and albite (Pertold and Punčochář, 1996).

Ackerman et al. (2019) concluded, on the basis of arsenopyrite and molybdenite Re/Os (~341 and 333 Ma, respectively) and Ar-Ar geochronological data on silicate minerals (~332 to 325 Ma), that this Au deposit is younger than the gold deposits spatially associated with the CBPC (~ 349–339 Ma), indicating instead a temporal relationship to the nearby MB.

The scheelite studied comes from two locations:

(1) Scheelite from a thin quartz vein cross-cutting finely banded calc-silicate hornfels (SCH5) was sampled in the Naděje gallery in the Kašperské Hory deposit. Scheelite forms subhedral grains, up to 0.8 mm across, in white-grey quartz matrix and is accompanied by arsenopyrite (up to 0.9 mm). Malec (1985) concluded that this scheelite was remobilized from an earlier scheelite phase disseminated in a stratiform layer in calc-silicate hornfels, during the formation of Au-W mineralization.

(2) Sample SCH-6 is from a heavy mineral concentrate from the Lohbach brook, which contains abundant ilmenite, garnet, lesser magnetite, rutile, sillimanite, clinozoisite, rare monazite, spinel, pyrite, arsenopyrite, apatite and native gold. Scheelite (up to 3 mm in size) is intergrown with quartz, biotite, sericite, sillimanite (with inclusions of Ti minerals and apatite), garnet, pyrite and limonite. Locally, scheelite contains inclusions of apatite and pyrrhotite. The mineral assemblage of the heavy mineral concentrate indicates several sources: (a) sillimanite-biotite gneiss, (b) quartz veins with gold and (c) skarn.

REDUCED INTRUSION-RELATED GOLD SYSTEMS (RIRGS)

Scheelite is also a common mineral in RIRGS of the Bohemian Massif (e.g., Mokrsko and Čelina deposit, Vacíkov-Petráčkova Hora deposit – see Table 1 for more information; Morávek, 1996).

The Mokrsko and Čelina deposits show low-grade (1.5–2.5 g/t Au) mineralization and share features of both orogenic and RIRGS (Zachariáš et al., 2014; Fig. 1). They belong to the Psí Hory gold-bearing district with a long history of gold mining, since Celtic times (the 3rd to 1st centuries B.C.). The deposits are mainly hosted by tonalite of the calc-alkaline Sázava tonalite suite (~354 Ma, Janoušek et al., 2004) of the CBPC. Gold dominantly occurs in quartz veins (<1 mm to 1 m thick) and stockworks with up to 1% arsenopyrite at Mokrsko, whereas pyrite and pyrrhotite are dominant at Čelina (Morávek 1995a), with relatively abundant scheelite accompanied by native bismuth, native gold, maldonite [Au_2Bi], aurostibite [$AuSb_2$], joséite-B [Bi_4Te_2S], pilsenite [Bi_4Te_3], tetradymite [Bi_2Te_2S], Bi_2Te, bismuthinite [Bi_2S_3] and other phases (Zachariáš et al., 2014). Molybdenite has yielded Re-Os age values of 342.9 ±1.4 Ma (Zachariáš and Stein, 2001) and 342.6 ±2.2 Ma (Ackerman et al., 2017), indicating close relationship of gold deposition with the end of intrusive activity (345–358 Ma, Janoušek et al., 2004, 2010). Chalcopyrite, galena, sphalerite, loellingite, cubanite, tetrahedrite and ullmanite occur as accessory minerals. With total gold resources of 100–140 tonnes, the Psí Hory district belongs among the most important gold districts in Europe (Morávek, 1996).

The scheelite sample (SCH-3) is from a bedding-parallel quartz vein associated with calc-silicate hornfels in amphibolite. It forms small anhedral grains (0.1–0.7 mm) mostly enclosed in amphibole and locally in association with plagioclase.

SKARN

We follow the classification of skarn deposits into oxidized and reduced on the basis of the mineral assemblage and scheelite composition after Miranda et al. (2022). Oxidized skarns are closely associated with magnetite-series intrusions emplaced at shallow crustal levels (<2 kbar; Newberry, 1983; Newberry and Swanson, 1986; Chang et al., 2019) and developed in impure carbonates and/or hematite-rich metasedimentary host rocks (Newberry, 1983; Newberry and Swanson, 1986). In general, reduced skarns are hosted in pure limestone and are associated with ilmenite-series intrusions (Ishihara, 1977), emplaced at greater depth (>2 kbar; Newberry and Swanson, 1986; Chang et al., 2019). Reduced skarns are characterized predominantly by clinopyroxene, amphibole and sulphides with minor garnet, whereas oxidized skarns consist mainly of garnet, clinopyroxene, amphibole and oxides.

OXIDIZED SKARN

We provide new data on scheelite from W occurrences (e.g., Mutice, Krouna, Nekvasovy Chlumy, Chedrbí, Proseč, and Bílé Labe), see more detailed description in Table 1.

The Obří důl polymetallic deposit is located in the Krkonoše mountains of North Bohemia and has been classified as a polymetallic skarn (Fe-Cu-Zn-As) in the exocontact of the Variscan Krkonoše-Jizera pluton (Veselovský et al., 2018; Fig. 1) with Re-Os ages obtained from molybdenite (312 ±1.4 Ma, Ackerman et al., 2017) and arsenopyrite (307.5 ±5.6 Ma, Veselovský et al., 2018). The deposit was mined in the past for As and Cu, with resources estimated at ~100,000 t at 0.43–0.47% W and 856,000 t at 0.41–0.43% Cu and 0.19–0.49% Sn. The orebody consists of two lenses, their thicknesses varying from 1 to 12 m. The deposit is formed by pyroxene-garnet skarn hosting polymetallic mineralization represented by irregular clusters, impregnations, and rare veinlets of pyrrhotite, chalcopyrite and arsenopyrite with minor pyrite, sphalerite, molybdenite, cassiterite, stannite, scheelite, malayaite, bismuthinite and other ore minerals (Šrein and Šreinová, 2000; Pašava et al., 2016). Ore is localized in pyroxene-garnet skarn and altered dolomite. Scheelite is present in two associations: (a) with prehnite, pumpellyite and calcite in younger quartz veins (alpine-type) cross-cutting scheelite-bearing contact skarn and (b) in association with ore minerals in contact metamorphosed skarn (Malec, 1985). Most of the scheelite samples came from contact-metamorphosed skarn and were described by Miranda et al. (2024).

REDUCED SKARN

Typical examples of reduced skarn deposits with scheelite in the Bohemian Massif are the Vrbík and Kotel deposits for which scheelite compositions were reported by Miranda et al. (2024). We provide new data for scheelite from Budislav (see Table 1 for more detailed description).

Vrbík deposit at Horažďovice. This small scheelite deposit is characterized by a lense-shaped diopside skarn (~50 19 m with a thickness of ~1.8 m) which is in fact a xenolith sitting in the Variscan granitoids of the Central Bohemian Plutonic Complex (CBPC; Hujsl et al., 1987; Fig. 1). Euhedral whitish, greyish or slightly yellowish grains are up to 2 cm in size and, locally, scheelite concentrations reached ~40% (Hujsl et al., 1987).

The Kotel polymetallic deposit (Krkonoše Mts.) is a polymetallic contact skarn, belonging to the Krkonoše-Jizera metamorphic complex, close to the contact with the Variscan Krkonoše-Jizera Granite Pluton. The skarn was briefly exploited in the 19th century (Malásek, 1957). Šrein et al. (1998) reported Cu 0.64 wt.%, Pb 0.032 wt.%, Zn 0.037 wt.% in average ore samples. Greyish-white scheelite grains (up to 4 mm) with white to bluish white CL zones are dispersed in the rock matrix, not intergrown with sulphides. The mineral paragenesis is represented by calcite, quartz, plagioclase, grossular, diopside, vesuvian, epidote, actinolite, chlorite, K-feldspar, titanite, fluorite, fluorapatite and zircon. The ore minerals are pyrite, chalcopyrite, arsenopyrite, sphalerite, minor scheelite and Ag-Cu-Fe sulphide (Šrein et al., 1998; Žáček, 2008).

OTHER SETTINGS

We studied scheelite in quartz veins hosted in Neoproterozoic volcano-sedimentary rocks at Erpužice u Stříbra and Tehov u Říčan.

Erpružice u Stříbra

Scheelite (SCH-14) was taken from an abandoned quarry of Neoproterozoic amphibolite schist (metabasalt), part of the Teplá Barrandian Unit. Scheelite forms rare fine-grained impregnations in a limonitized quartz-veinlet (Malec ,1985).

Tehov u Říčan

Scheelite (SCH-36) is associated with arsenopyrite and cassiterite in quartz-feldspar-tourmaline veinlets and tourmalinized parts of contact metamorphosed schists/hornfels at the contact of the Říčany Variscan granite (Bernard et al., 1981). The scheelite is commonly intergrown with plagioclase but rarely replaces plagioclase and quartz (Malec, 1985).

SAMPLES AND METHODS

Twenty-six polished sections from 26 sites representing five major association types from the Bohemian Massif (greisen-, orogenic gold and RIRGS-, oxidized and reduced skarn deposits, Table 1) were studied. Major and minor element composition (n = 368 analysis, including those partly published by Miranda et al., 2024) and cathodoluminescence (CL) images of scheelite were obtained by electron probe micro-analyzer (EPMA) at Université Laval by use of a *CAMECA SX-100* instrument equipped with five wavelength-dispersive spectrometers (WDS) and a CL detector (see Appendix 3). The analytical conditions for CL images were using an accelerating voltage set at 15 kV and the beam current at 20 nA with a working distance of 2 mm.The analyses were performed using a 10-µm-diameter beam. Analytical conditions for major element analyses (CaO and WO_3) were 20 nA for beam current and 15 kV for accelerating voltage, with a counting time of 20 s at the peak and 10 s in the background. For minor elements (Na, Sr, Mo, Y and Fe), the analytical conditions were 100 nA beam current, 15 kV of accelerating voltage, and counting times of 120 s at the peak and 30 s in the background. Metal tungsten (W), metal molybdenum (Mo), diopside (Ca), celestite (Sr), YPO_4 (Y), magnetite (Fe) and albite (Na) were used as standards. For CL investigation, the accelerating voltage was set at 15 kV, the beam current at 20 nA, with a working distance of 2 mm. The dwell time of each pixel was 0.03 ms. The CL images were recorded in grey-scale in order to document texture and zonation patterns in the scheelite prior to micro-analyses (EPMA and LA-ICP-MS).

The concentration and distribution of the minor and trace elements in the scheelite (n = 368 analyses) were determined by LA-ICP-MS at the LabMaTer, Université du Québec ŕ Chicoutimi (UQAC) by use of an Excimer 193 nm RESOlution M-50 laser ablation system (Australian Scientific Instrument) equipped with a double volume cell S-155 (Laurin Technic) and coupled with an Agilent 7900 mass spectrometer. The LA-ICP-MS tuning parameters were a laser frequency of 15 Hz, a fluence of 3 J/cm^2, and scanning speed of 10ěm/s for the line scans. Spots across the surface of scheelite grains were made with beam sizes of 33 and 55 µm, depending on grain size. Given the distinct textures in scheelite, the spots were performed in all distinct CL zones to obtain as much variance as possible in the scheelite composition. Data reduction was carried out by use of Iolite v3 running in Igor Pro 6.37 (Paton et al., 2011). ^{44}Ca was used for internal standardization for scheelite on the basis of EPMA results (Appendix 1). Synthetic glass reference material NIST-610 was used as an external standard for all elements by use of preferred values from the GeoReM database (Jochum et al., 2005). The basalt glasses GSE-1g, GSD-1g and Gprobe6-A and the NIST-612 (synthetic glass) were used as secondary reference materials for quality control. The reference materials were analyzed at the beginning, throughout and the end of each analytical session, to monitor potential instrumental drift. The results obtained for the monitors allowed for standard deviations on the working values (Appendix 4). The following isotopes were measured: ^{23}Na, ^{24}Mg, ^{39}K, ^{44}Ca, ^{49}Ti, ^{51}V, ^{55}Mn, ^{57}Fe, ^{61}Ni, ^{63}Cu, ^{66}Zn, ^{75}As, ^{88}Sr, ^{89}Y, ^{93}Nb, ^{95}Mo, ^{107}Ag, ^{118}Sn, ^{137}Ba, ^{139}La, ^{140}Ce, ^{141}Pr, ^{146}Nd, ^{147}Sm, ^{153}Eu, ^{157}Gd, ^{159}Tb, ^{163}Dy, ^{165}Ho, ^{166}Er, ^{169}Tm, ^{172}Yb, ^{175}Lu, ^{181}Ta, ^{182}W, ^{183}W, ^{208}Pb, ^{209}Bi, ^{232}Th and ^{238}U. Silicon and S were also monitored to identify possible silicate and sulphide inclusions, respectively. Analyses affected by inclusions were discarded.

Pearson and Spearman correlation coefficients and their significance at levels of confidence p = 0.001; 0.01 and 0.05 corresponding to 99.9, 99 and 95% confidence, respectively, were calculated (Holčín and Komenda, 2015) and used for the evaluation of monotonic relationships between the elements analysed in scheelite from different types of deposit/mineralization.

RESULTS

CATHODOLUMINESCENCE AND TRACE ELEMENT VARIATIONS

GREISEN-RELATED SCHEELITE

Scheelite from greisen-type deposits shows a homogeneous texture (Fig. 2A) or two generations (Fig. 2B). We studied two types of scheelite from Cínovec. Scheelite from massive greisen (Cínovec 1, SCH-47) is heterogeneous, showing brighter CL at grain edges, while the darker central part is more homogenous (Fig. 2C). Reddish-brown grains of scheelite (Cínovec 2, SCH-48) from vein-type greisen are more homogeneous under CL. Under UV light, scheelite from Sn-W deposits displays variable colours from whitish (H. Babákov) via yellowish (Cínovec) to bluish (H. Slavkov-Huber).

Chemical composition

Scheelite from greisens shows variable chemical composition (Appendicies 1 and 2 and Table 2) and REE patterns (Fig. 3). Scheelite from Horní Babákov (SCH-37) shows maximum median values of Y (465 ppm), LREE (2295 ppm) and HREE (633 ppm) while scheelite from Krásno-Huber (SCH-43) displays the lowest median concentrations of As (bdl), Y (0.1 ppm), Nb (7.8 ppm), Mo (0.4 ppm), LREE (1 ppm) and HREE (0.1 ppm) of all the scheelite studied from the greisen-type association. The highest median values of Sr (567 ppm), Nb (244 ppm) in the greisen group were found in scheelite from Cetoraz. Scheelite from Ovesná Lhota has median Sr (240 ppm), Nb (30 ppm), Y (357 ppm) and Mo (1.7 ppm) values close to those of Horní Babákov whereas LREE (739 ppm) and HREE (143 ppm) are lower.

Scheelite from massive greisen (Cínovec 1, SCH-47) at Cínovec shows the highest median concentrations of Zn (59 ppm), As (11370 ppm), Ag (9.3 ppm), Sn (8 ppm), Pb (3704 ppm), Bi (940 ppm) and Th (223 ppm) of all greisen-associated scheelite (Appendix 1). Scheelite from vein greisen at Cínovec (Cínovec 2, SCH-48) displays high median values of Mo (7478 ppm) and U (2996 ppm) which are comparable with those of scheelite from the massive greisen at Cínovec.

REE patterns

Scheelite from greisens displays the following REE patterns (Fig. 3): (1) LREE-enriched with a positive Eu anomaly (Cetoraz) (2) HREE-enriched with negative Eu and Ce anomalies (Cínovec 2, SCH-48), (3) Bell-shaped REE patterns with a negative Eu anomaly (Cínovec 1, SCH-47), (4) Flat and bell-shaped REE patterns without a Eu anomaly (Ovesná Lhota), (5) Flat REE patterns with a positive Eu anomaly (Ovesná Lhota and Cetoraz).

Scheelite from massive greisen (Cínovec 1, SCH-47) shows LREE-depleted and bell-type patterns, both with a Eu negative anomaly (Fig. 3A). Scheelite with a LREE-depleted pattern shows enrichment in Sb (67-fold), Bi (6-fold), Y (5-fold), Hf (4-fold), REE (3-fold) and Mo (1.5-fold). Scheelite from vein greisen at Cínovec (Cínovec 2, SCH-48) is dominantly characterized by a HREE-enriched pattern with negative Eu and Ce anomalies (Fig. 3A).

Scheelite from massive greisen at Krásno-Huber shows irregular REE patterns (mostly with a positive Eu anomaly, Fig. 3C), often with the values below detection limits.

Scheelite from Horní Babákov shows bell-shaped REE chondrite-normalized patterns with a Eu positive anomaly (Fig. 3D). In general, scheelite from H. Babákov shows comparable a trace element distribution to scheelite from Krásno-Huber except for enrichment in Y and REE, which is also much higher than in scheelite from other greisen localities.

Scheelite from Cetoraz shows LREE-enriched patterns with a positive or without a Eu anomaly or flat REE patterns showing a positive Eu anomaly (Fig. 3E). It is enriched in Na (like that of H. Babákov), Mn and Sr (the highest median values among all the greisen samples). Median values of Y, LREE and HREE are comparable with those of H. Babákov and significantly higher than those of Cínovec and Krásno-Huber.

Scheelite from Ovesná Lhota shows flat REE patterns with or without a positive Eu anomaly (Fig. 3F).

OROGENIC GOLD SCHEELITE

Scheelite CL from the orogenic gold deposits is predominantly homogeneous (Fig. 2D). Only scheelite from the Jílové deposit shows oscillatory zoning (Fig. 2E). Under UV, scheelite from this setting is dominantly bluish.

Chemical composition

Scheelite from Jílové shows the highest median values of Na (84 ppm), As (15 ppm), Y (466 ppm), LREE (1032 ppm) and HREE (188 ppm) and low Mo median values (23 ppm) when compared to scheelite from other orogenic gold locations in the Bohemian Massif (Appendix 1). Scheelite from Kašperské hory – Naděje and Kašperské hory – Lohbach has peak median Mo values of 113 and 106 ppm, respectively, while scheelite from Orlík is characterized by the highest median Sr value (2118 ppm, Appendix 1).

REE patterns

Scheelite from orogenic gold settings displays bell-shaped REE patterns with a positive Eu anomaly and flat REE patterns with a positive, or small negative, Eu anomaly. REE patterns for the Jílové, Sobětice, Kašperské hory-Naděje, Kašperské Hory Lohbach and Orlík u Humpolce deposits are shown on Figure 4A–E.

At Jílové, oscillatory-zoned scheelite has flat and bell-shaped REE patterns in the same scheelite grain (Figs. 2E and 4A). Scheelite with a flat REE pattern and positive Eu anomaly is characterized by higher Ni (20-times), Mg (5-times), Th (3-times) and U (2-times) values, compared to scheelite with a bell-shaped pattern with a positive Eu anomaly, which has significantly higher V (5-times), Na (4-times), REE (3-times), and Y (2-times) concentrations.

At Sobětice, scheelite with a bell-shaped pattern and small negative Eu anomaly is characterized by higher V (4-times), Y (2-times), and REE (2-times) values compared to scheelite with a flat REE pattern and positive Eu anomaly, which shows significantly higher U (30-times) and Sb (4-times) values.

AU RIRGS SCHEELITE

Scheelite from RIRGS is predominantly homogeneous (e.g., Čelina SCH-3; Fig. 2F) under CL and displays creamy white (Vacíkov) to bluish (Čelina) colour under UV light.

Chemical composition

Scheelite from Vacíkov (SCH-1) is characterized by significantly higher median values of Na (113 ppm), Sr (155 ppm), LREE (919 ppm) and similar median concentrations of K, Ti, Mn, As, Nb, Mo and HREE when compared to scheelite from the Čelina deposit (SCH-3) (Appendix 1).

Scheelite from this setting is characterized by the highest median values of Na (54 ppm), K (13.1 ppm), Mg (10 ppm), As (12.3 ppm), V (0.8 ppm) and Cu (1 ppm) of all the groups of mineral deposits studied (Table 2). In comparison with scheelite from orogenic gold deposits, it typically shows significantly higher Nb and Mo median values and lower Sr, LREE and HREE median values (Table 2).

REE patterns

Scheelite from RIRGS displays a bell-shaped REE pattern with a negative Eu anomaly while scheelite from Vacíkov has steep LREE-enriched patterns with a negative Eu anomaly (Fig. 4F, G).

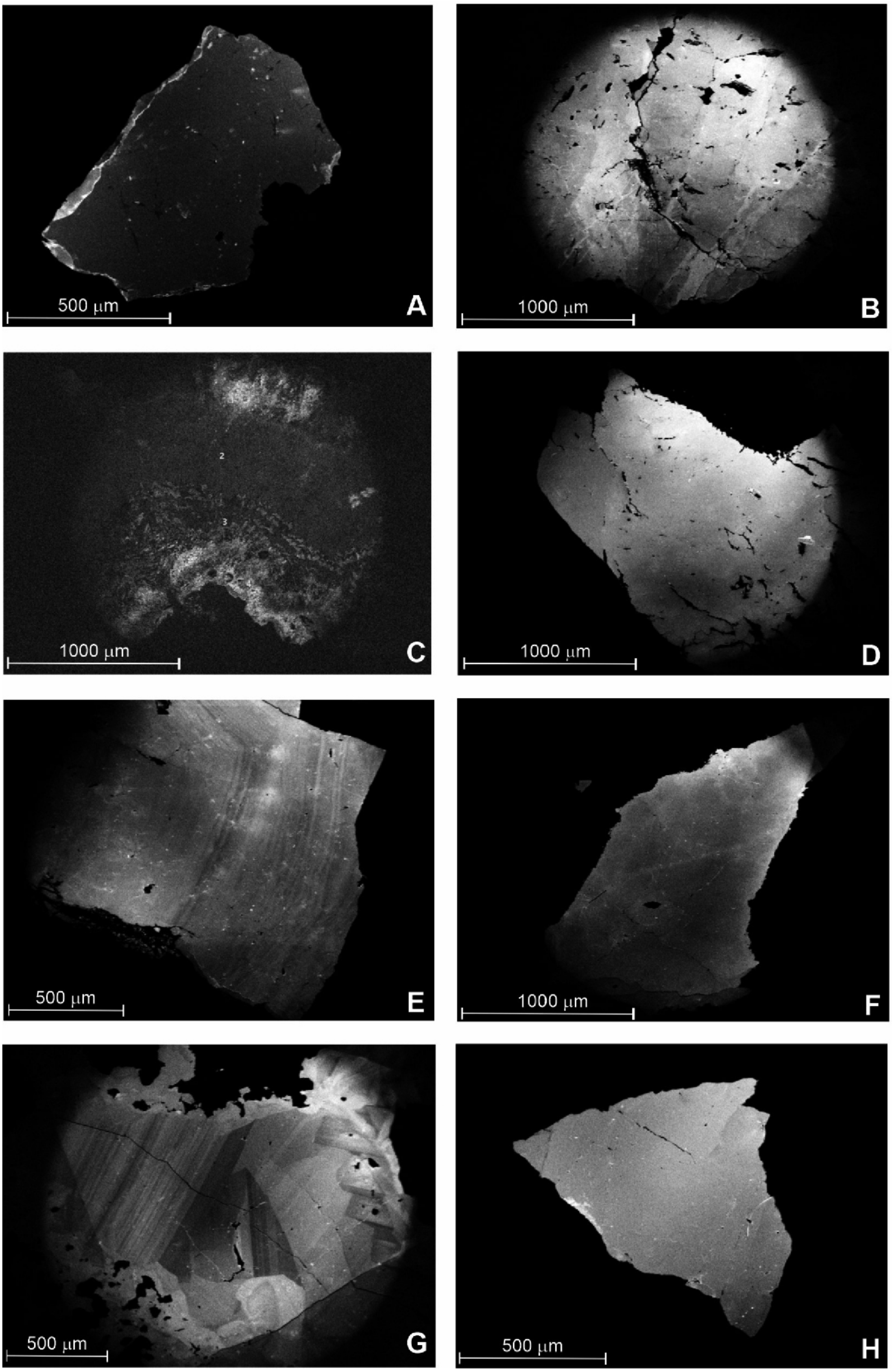

Fig. 2. Cathodoluminiscence (CL) images of scheelite grains from different types of mineralization in the Bohemian Massif

A – homogeneous scheelite grain from Krásno-Huber greisen deposit; **B** – oscillatory zoning/two generations of scheelite from a Ovesná Lhota quartz-cassiterite-wolframite vein; **C** – inhomogeneous (brighter) marginal part of grain with more homogeneous (darker) central part of scheelite grain from massive greisen at the Cínovec deposit; **D** – homogeneous scheelite from the Kašperské Hory (Naděje gallery) orogenic Au deposit; **E** – oscillatory zoned scheelite from the Jílové orogenic Au deposit; **F** – homogeneous scheelite from the Čelina – RIRGS Au deposit; **G** – scheelite with oscillatory zoning from oxidized skarn at Mutice; **H** – homogeneous scheelite from reduced skarn at Hostákov

Table 2

Summary of scheelite chemical composition in different deposit/mineralization types from the Bohemian Massif (in situ LA-ICP-MS data)

Greisen-related		Na	Mg	Si	K	Ti	V	Mn	Ni	Cu	Zn	As	Sr	Y	Nb	Mo	Ag	Sn	Sb	Ba
n = 61	**Minimum**	bdl	3.2	bdl	6.7	bdl	bdl	bdl	bdl	bdl	bdl	bdl	158	bdl	2	bdl	bdl	bdl	bdl	bdl
	Maximum	792	318	321	19	17	10	481.5	44	33	74	14442	1494	1081	361	13886	16	35	1.6	6.5
	Median	38	8.5	63	10	1.9	0.1	69.5	0.2	0.2	0.2	8.3	281	88	27	12	0.03	0.4	0.01	0.1
	Mean	142	63	68	11	3.1	1.0	85.8	3.0	4.7	15	2770	350	239	57	2063	1.8	2.9	0.2	0.8
	STD	182	107	66	3.3	3.4	2.1	107.1	9.0	8.2	23	4360	203	278	80	3408	4.0	6.3	0.4	1.5
Au-orogenic-related																				
n = 60	**Minimum**	bdl	bdl	bdl	bdl	bdl	bdl	2.2	bdl	bdl	bdl	0.3	31	0.8	1.3	0.5	bdl	bdl	bdl	bdl
	Maximum	153	253	2558	38	7.4	1.4	67.0	40	35	70	64	3600	653	16	310	0.5	0.7	25.4	16
	Median	21	3.1	9.0	11	1.0	0.04	6.2	0.2	0.1	0.1	1.7	190	47	3.0	22				0.2
	Mean	32	9.8	81	12.0	1.2	0.2	11.7	3.2	2.9	4.0	6.4	577	123	4.7	58	0.1	0.1	0.7	0.6
	STD	31	32	330	7.8	1.3	0.3	14.0	8.0	6.5	14	11	947	166	3.5	77	0.1	0.1	3.5	2.0
Au-RIRGS-related																				
n = 24	**Minimum**	10	bdl	bdl	4.6	bdl	bdl	6.4	bdl	bdl	bdl	4.7	20	31	8.9	1036	bdl	bdl	bdl	0.1
	Maximum	153	263	973	32	6.0	2.1	27.2	63	46	69.5	39	181	240	66	6199	2.1	1.4	4.4	0.7
	Median	54	10	107	13	1.2	0.8	8.4	0.2	1.0	0.05	12	37	66	27	2382	0.003	0.03	0.1	0.2
	Mean	68	41	168	13	1.5	0.8	10.1	6.7	10	11	14	89	80	30	2470	0.1	0.1	0.3	0.3
	STD	43	65	216	5.8	1.3	0.6	4.7	16	13	22	6.9	65	48	14	1050	0.4	0.3	0.9	0.2
Oxidized skarn-related																				
n = 165	**Minimum**	bdl	bdl	bdl	bdl	bdl	bdl	bdl	bdl	bdl	bdl	bdl	23	0.1	1.2	91	bdl	bdl	bdl	bdl
	Maximum	306	550	941	82	18.1	6.1	107.0	125	86	97	69	320	1476	1168	53932	4.3	7.0	1.7	49
	Median	32	3	58	12	1.8	0.3	11.6	0.2	0.1	0.2	5.4	47	63	77	2494	0.01	0.1	0.02	0.2
	Mean	65	16	117	15	2.5	0.6	18.2	3.6	3.9	2.5	8.7	59	146	126	5416	0.1	0.3	0.1	0.6
	STD	74	57	182	13	2.5	0.8	21.8	13	11	10	11	35	214	167	8274	0.5	0.8	0.2	3.8
Reduced skarn-related																				
n = 58	**Minimum**	bdl	bdl	bdl	bdl	bdl	bdl	0.3	bdl	bdl	bdl	0.3	36	0.4	1.4	72	bdl	bdl	bdl	bdl
	Maximum	74	539	1612	125	19.5	7.0	107.0	56	83	97	18	3600	209	361	3197	4.3	7.4	1.0	49
	Median	6.2	5.4	39	9.7	1.3	0.02	5.9	0.2	0.1	0.02	1.5	98	8.2	19	245	0.01	0.1	0.01	0.3
	Mean	10.3	20.5	93	11	1.7	0.2	6.3	3.3	5.7	17	1.7	391	9.2	33	490	0.1	0.1	0.2	0.3
	STD	15.3	75.7	215	7.1	1.7	0.4	6.3	10	14	82	1.2	590	8.3	40	495	0.5	0.2	0.5	0.3

Greisen-related		La	Ce	Pr	Nd	Sm	Eu	Gd	Tb	Dy	Ho	Er	Tm	Yb	Lu	Hf	Ta	Pb	Bi	Th	U	LREE	HREE	ΣREE
n = 61	**Minimum**	bdl	bdl	bdl	bdl	bdl	bdl	bdl	bdl	bdl	bdl	bdl	bdl	bdl	bdl	bdl	0.4	bdl	bdl	bdl	bdl			
	Maximum	257	824	113	899	325	90	381	52	443	63	182	18	114	12	4.5	7.9	14859	11662	445	6908	2470	882	3775
	Median	19	33	5.2	26	11	7.9	14	2.7	22	3.5	14	3.1	34	4.1	0.1	1.3	9	0.9	0.2	0.3	129	91	199
	Mean	53	234	34	232	81	16	90	12	94	13	39	4.6	37	3.8	0.4	2.0	986	540	36	1079	741	205	945
	STD	66	282	42	322	119	21	137	18	133	18	49	4.7	30	2.9	0.8	1.8	3016	2029	93	1677	932	249	1245
Au-orogenic-related																								
n = 60	**Minimum**	1.9	1.5	0.1	0.4	0.1	0.4	0.1	bdl	0.1	bdl	0.1	bdl	0.1	bdl	bdl	0.3	1.4	bdl	bdl	bdl	4.4	0.4	4.8
	Maximum	138	261	44	370	179	450	239	33	204	25	51	4.3	31	3.8	0.1	0.6	47	0.8	4.8	25	1233	331	1559
	Median	10	25	3.3	18	5.1	12	6.2	0.9	7.9	1.3	4.5	0.6	5.2	0.6	0.01	0.4	9.2		0.1	0.1	78	20	101
	Mean	21	67	9.5	62	25	54	32	4.5	31	4.2	10	1.2	8.9	0.9	0.02	0.5	11	0.1	0.5	1.8	269	61	330
	STD	25	79	12	97	47	94	63	8.8	55	6.7	13	1.2	8.5	1.0	0.03	0.1	8.0	0.2	1.1	4.2	370	89	455
Au-RIRGS-related																								
n = 24	**Minimum**	2.1	7.3	1.7	18.3	8.6	1.8	15.5	1.5	8.6	1.3	3.5	0.4	1.7	0.1	bdl	0.4	0.5	bdl	bdl	bdl	63	18	95
	Maximum	403	623	52	247	51	4.2	48	4.8	33	7.2	22	2.0	10	0.8	0.02	1.4	8.4	0.6	0.5	2.3	1335	80	1368
	Median	7.7	27.4	5.1	47.3	18.8	2.7	21.9	2.2	15.9	2.7	7.2	0.6	3.3	0.3	0.01	0.6	2.5				141	33	206
	Mean	109	205	19	97	19	2.7	24	2.5	17	3.0	8.0	0.7	3.8	0.4	0.01	0.6	4.2	0.1	bdl	0.2	477	35	512
	STD	129	220	18	78	10	0.5	8.0	0.9	6.7	1.4	4.2	0.3	1.7	0.1	0.005	0.2	2.6	0.1	0.1	0.5	452	15	446
Oxidized skarn-related																								
n = 165	**Minimum**	0.01	0.03	0.008	0.056	0.04	bdl	0.061	bdl	0.070	0.005	0.008	0.001	bdl	bdl	bdl	0.3	0.4	bdl	bdl	bdl	0.2	0.1	0.4
	Maximum	330	698	86	509	227	12	286	45	320	57	167	20	133	15	0.2	35	236	56	6.4	7.9	1566	757	2232
	Median	27	84	12	69	19	2.0	21	2.4	17	2.8	8.0	0.8	4.9	0.4	0.01	0.7	5.9		0.1	0.1	234	36	274
	Mean	47	149	20	114	31	2.6	32	4.2	30	5.2	16	2.0	14	1.6	0.02	1.9	10	1.4	0.3	0.3	395	74	468
	STD	65	176	21	119	36	2.2	38	5.8	42	7.4	23	2.9	22	2.6	0.02	3.9	21	5.4	0.7	0.8	425	105	514
Reduced skarn-related																								
n = 58	**Minimum**	0.01	0.1	0.02	0.1	0.04	0.005	0.1	bdl	bdl	bdl	0.1	bdl	0.1	0.01	bdl	0.3	0.8	bdl	bdl	bdl	0.5	0.2	0.8
	Maximum	49	116	24	195	63	29	86	11	65	9.7	24	2.3	15	1.2	0.05	5.9	21	3.5	2.9	10	491	115	689
	Median	2.0	6.4	0.8	3.4	1.3	0.8	2.5	0.3	2.5	0.4	0.8	0.1	0.4	0.0	0.001	0.5	2.2			0.1	26	5.2	31
	Mean	8.2	17	2.3	14	3.2	1.3	3.2	0.3	2.3	0.4	1.1	0.1	0.7	0.1	0.0	1.0	7.0	0.1	0.2	0.3	49	5.0	54
	STD	12	24	3.3	19.9	4.1	1.6	3.1	0.3	2.1	0.4	1.0	0.1	0.7	0.1	0.0	1.3	17	0.1	0.5	0.5	65	4.4	66

bdl – below detection limit

SCHEELITE FROM OXIDIZED AND REDUCED SKARN DEPOSITS

Scheelite from oxidized and reduced skarn deposits is commonly zoned (Fig. 2G) although some samples are homogeneous (Fig. 2H) and are mostly bluish under UV light. Only scheelite from Bílé Labe shows a yellowish colour while that from Chedrbí is pinkish.

Chemical composition

Oxidized skarns

Among oxidized skarns, scheelite from Obří důl is characterized by the highest median values of Mo (7214 ppm) and As (11 ppm), while scheelite from Bílé Labe shows the highest median values of Na (244 ppm), V (0.96 ppm – close to Obří důl), Mn (90 ppm), Pb (26 ppm), Bi (0.6 ppm – close to Vykmanov), Y (529 ppm), LREE (1376 ppm) and HREE (250 ppm) (Appendix 1). Changes in chemical composition of selected elements (Mo, Nb, Sr and Y) within one scheelite grain from Obří důl (SCH-24) and Mutice (SCH-10) skarns are shown on Figure 5A, B. At Obří důl, under cathodoluminiscence, the darker part is enriched in REE, Y, Mo and Nb at similar Sr concentration. At Mutice, an oscillatory-zoned scheelite grain shows Mo and Sr enriched in the darker parts while Nb peak concentration coincides with the highest REE concentrations. Scheelite from Nekvasovy Chlumy has the highest median values of Sr (116 ppm) and has a comparable Mo content (558 ppm) to scheelite from Proseč, Krouna and Mutice (Appendix 1). Scheelite from Mutice displays the highest median values of Nb (215 ppm), Cu (1.9 ppm) and U (0.6 ppm) and comparable levels of Y, LREE and HREE concentrations to Obří důl (Appendix 1).

Scheelite from Kovářská has the highest median content of K (44.5 ppm) and very low median concentrations of Mn (2.8 ppm – comparable to Chedrbí), As and Nb (0.5 and 1.5 ppm, respectively – comparable to Vykmanov and Chedrbí), Y (4.2 ppm – comparable to Vykmanov), REE (4.1 ppm – comparable to Vykmanov) within the group of oxidized skarns (Appendix 1).

Of all mineral deposit types, scheelite from oxidized skarns is characterized by the highest median Mo (2494 ppm), REE (274 ppm), LREE (234 ppm) and Nb (77 ppm). Compared to scheelite from reduced skarns, it has significantly higher Y, Mo, LREE and HREE (Table 2).

Reduced skarns

Among this group, scheelite from Hostákov u Třebíče shows the highest median values of Nb (108 ppm), LREE (171 ppm) and REE (178 ppm). The molybdenum content (598 ppm) is high and close to that of scheelite from Vrbík (880 ppm; Appendix 1). Scheelite from Budislav displays the highest median values of Mn (17 ppm), Na (16.3 ppm), Y (41.2 ppm) and HREE (23.3 ppm; Appendix 1).

Scheelite from the reduced skarns is characterized by the lowest median values of Y (8.2 ppm) and Mn (5.9 ppm – close to orogenic gold scheelite) of all the mineral deposit groups studied. The similarly low median As value (1.5 ppm) is close to that of the orogenic gold setting (Table 2).

REE patterns

Scheelite from oxidized and reduced skarn deposits displays the following REE patterns: (1) LREE-enriched with a positive or negative Eu

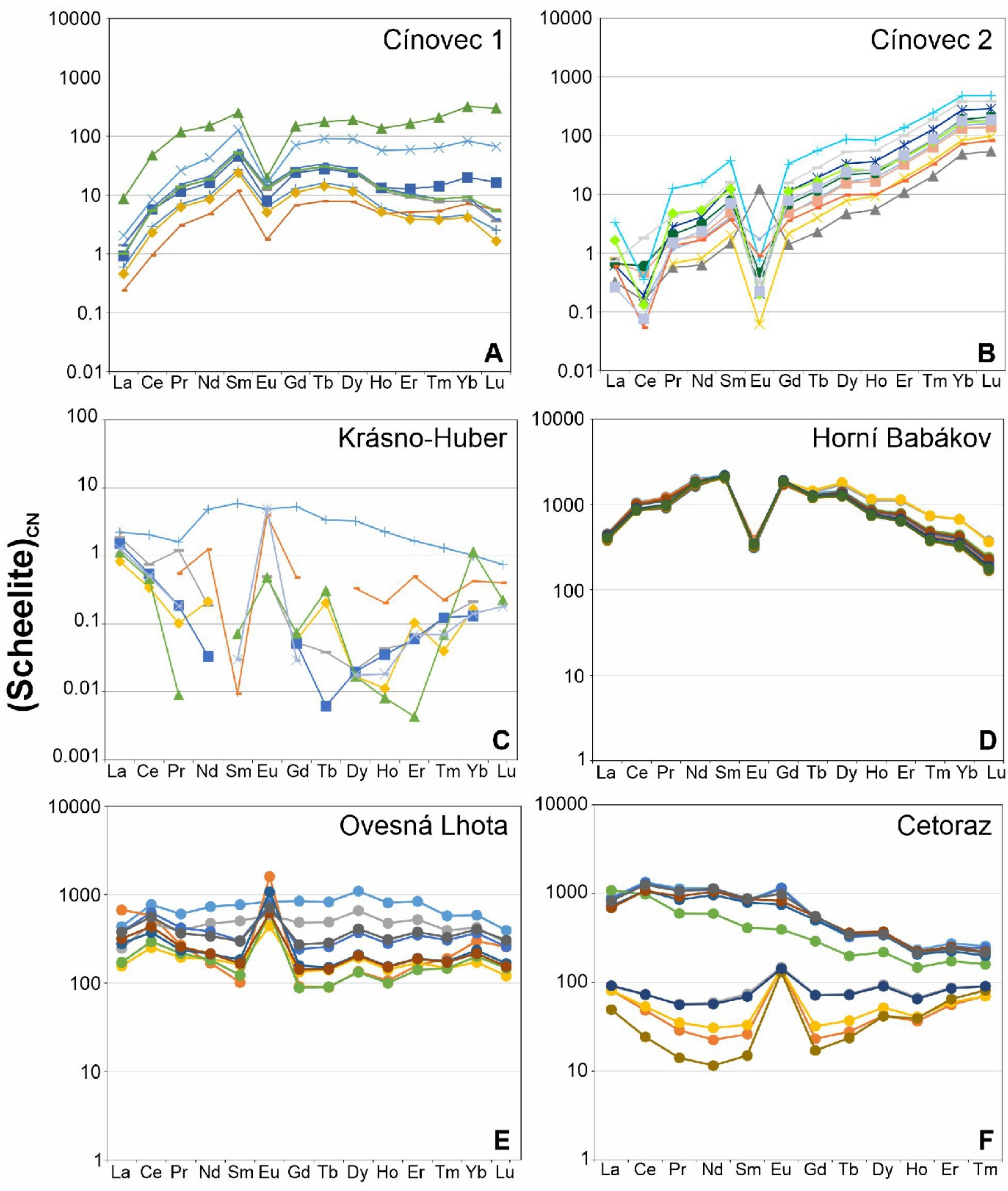

Fig. 3. Rare earth element patterns in scheelite from individual greisen and quartz-cassiterite-wolframite vein localities (Bohemian Massif)

A – Cínovec 1 (massive greisen), **B** – Cínovec 2 (vein-type greisen), **C** – Krásno-Huber deposit, **D** – Horní Babákov deposit (greisen), **E** – Ovesná Lhota (quartz-cassiterite-wolframite vein), **F** – Cetoraz (quartz-wolframite vein)

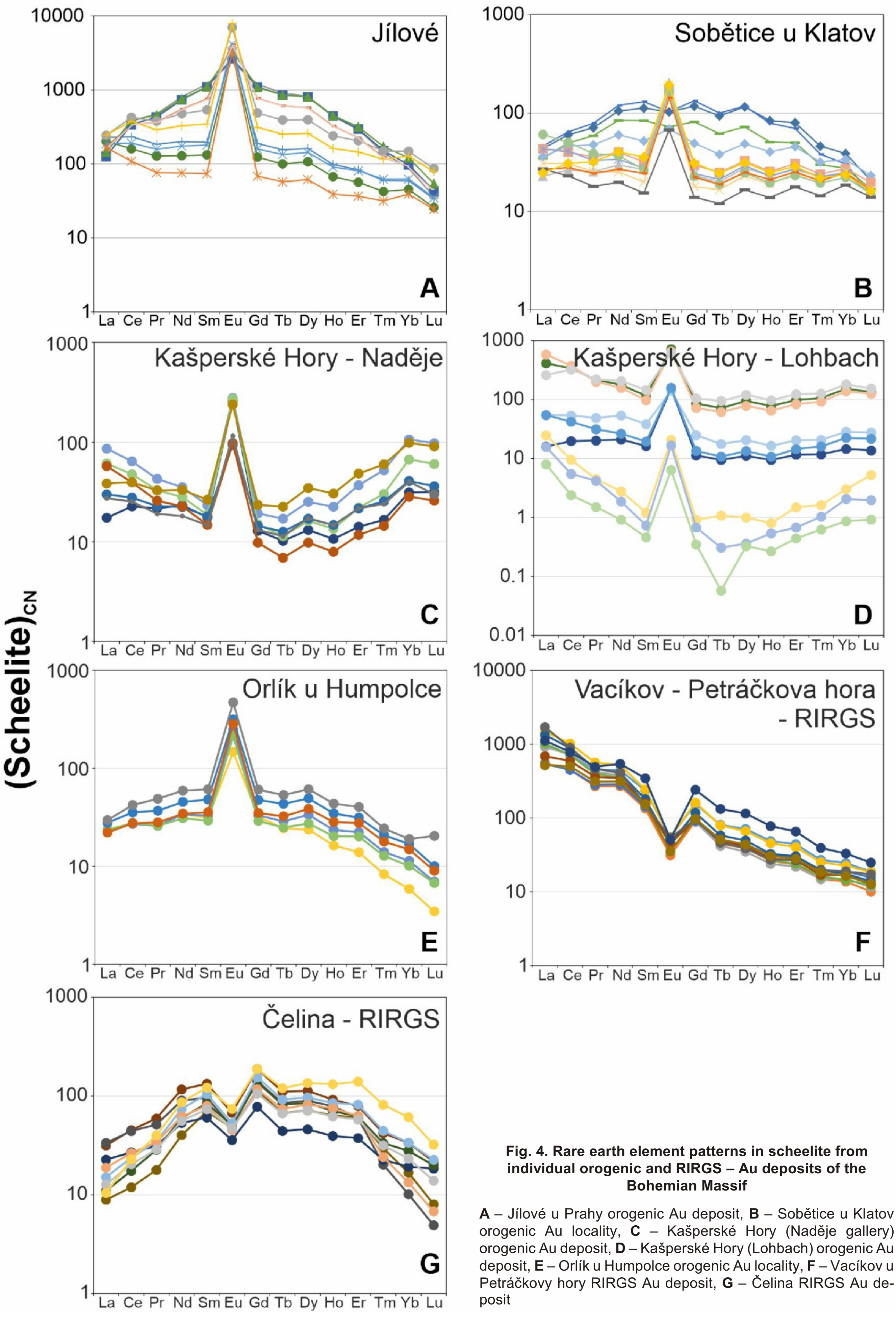

Fig. 4. Rare earth element patterns in scheelite from individual orogenic and RIRGS – Au deposits of the Bohemian Massif

A – Jílové u Prahy orogenic Au deposit, **B** – Sobětice u Klatov orogenic Au locality, **C** – Kašperské Hory (Naděje gallery) orogenic Au deposit, **D** – Kašperské Hory (Lohbach) orogenic Au deposit, **E** – Orlík u Humpolce orogenic Au locality, **F** – Vacíkov u Petráčkovy hory RIRGS Au deposit, **G** – Čelina RIRGS Au deposit

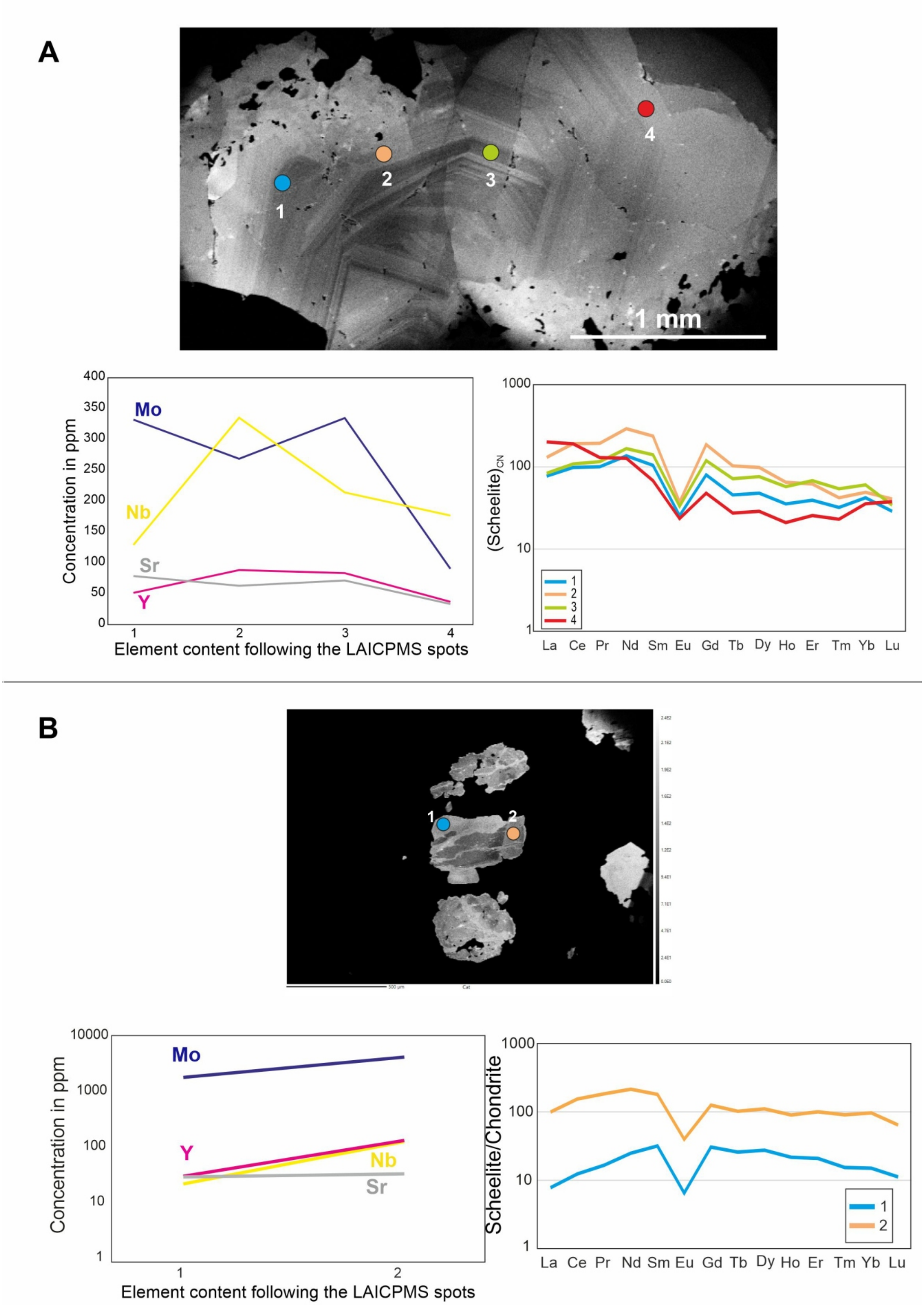

Fig. 5. Changes in chemical composition (Mo, Nb, Sr, Y and REE) in scheelite with oscillatory zoning from oxidized skarn at Mutice (A) and Obří důl (B)

anomaly, (2) Bell-shaped REE patterns with a negative or absent Eu anomaly, (3) Flat REE patterns with a negative Eu anomaly (Figs. 6 and 7). REE patterns of scheelite from oxidized skarn deposits (Bílé Labe, Krouna u Poličky, Proseč u Litomyšle, Nekvasovy Chlumy, and Chedrbí) are shown on Figure 7A–E, respectively. REE patterns of scheelite from reduced skarn at Budislav u Litomyšle are shown on Figure 7F.

SCHEELITE FROM THE OTHER SETTINGS

Both scheelite grains studied are homogeneous under CL and show a bluish colour under UV light. They also show very similar distributions of trace and REE contents except for higher Mo and Sr values in scheelite from Tehov u Říčan (Appendix 1). The chondrite-normalized REE patterns are flat with a positive Eu anomaly (Fig. 8). Their chemical signature is similar to that of scheelite from orogenic gold deposits (Fig. 4).

CORRELATION ANALYSIS

Pearson and Spearman correlation coefficients and their significance at levels of confidence p = 0.001; 0.01 and 0.05 were calculated for individual groups of scheelite samples analysed. In the following text we list only the highest correlations at the level of confidence 99.9%.

SCHEELITE FROM GRESISEN

Pearson correlation coefficients: **REE** and Na, Mg, Y; **Mo** and U, As, Sn, Hf; **Th** and V, Ag, Bi; **U** and Mo, As, Zn; **Sr** and Nb, Mn; **Sn** and V, As, Mo, Ag; **Bi** and Pb, Hf, V, Th, Sn, Ag, Sb, Ta, As. Molybdenum shows negative correlation with REE, Y and W.

Spearman correlation coefficients: **REE** and Na, Y; **Mo** and U, As, Sn, Hf, Bi, Zn, Cu, Ti; **Th** and Pb, Bi, Ta, Ag, As, Sn, Nb, Cu, Ti, V, Mn; **Sr** and U; **Mn** and LREE, Pb, Nb, Th, Y, Na, Ti.

SCHEELITE FROM OROGENIC GOLD DEPOSITS

Pearson correlation coefficients: **REE** and Y, Hf, Na; **Mo** and Nb; **Th** and Mn, U, Nb; **Sr** and Ta; **As** and Hf, Y, REE, Na, K.

Spearman correlation coefficients: **REE** and Y, Hf, Na, As; **Mo** and Mn, Nb, Th; **Th** and U, Mn, Mo, Ba; **Sr** and As, K, Ta; **Pb** and Y, HREE.

SCHEELITE FROM AU-RIRGS

Pearson correlation coefficients: **LREE** and Na, Sr, Ta, Pb; **HREE** and Y; **Sr** and Pb, LREE; **U** and As, V; **Th** and Sn, Zn.

Spearman correlation coefficients: **LREE** and Ta,Na, Nb, U; **HREE** and Y; **Sr** and Pb, U, Ta.

SCHEELITE FROM OXIDIZED SKARNS

Pearson correlation coefficients: **REE** and Y, Na, Nb, Ta, V, Mn; **Mo** and As.

Spearman correlation coefficients: **REE** and Y, Na, Nb, V, Hf, Ta, Th, U, As, Mn; **Mo** and As, Ti, Na, Ta, Ti, K, Bi, LREE, Pb, Th; **Nb** and LREE, HREE, Y, Hf, Th, Na, V, Ta, U, Sn, As, Mn.

SCHEELITE FROM REDUCED SKARNS

Pearson correlation coefficients: **HREE** and Y; **LREE** and Ta, Nb; **Mo** and Sn; **Sr** and Au, B; Mn and Si.

Spearman correlation coefficients: **HREE** and Pb, W; **LREE** and Y; **Mo** and Y, Ti, Pb; **Y** and LREE, Th, Nb, Mo.

DISCUSSION

DISTRIBUTION OF TRACE ELEMENTS AND TYPES OF REE PATTERNS

Several studies show that the chemical composition of scheelite is strongly influenced by the composition and physicochemical conditions of the hydrothermal fluids from which it precipitates, the composition of the host rock, crystallographic control and the partition coefficients between fluids, scheelite and co-precipitating minerals (Ghaderi et al., 1999; Brugger et al., 2008; Song et al., 2014; Poulin et al., 2018; Sciuba et al., 2020; Miranda et al., 2022; Altenberger et al., 2024; Haupt et al., 2025).

Several authors (Hsu and Galli, 1973; Hsu, 1977; Tyson et al., 1988) showed that Mo^{6+} replaces W^{6+} at moderate to high fO_2 and that Nb^{5+}, Ta^{5+}, As^{5+} and V^{5+} substitute for W^{6+}, whereas divalent cations (Sr^{2+}, Eu^{2+}, Mn^{2+}, Pb^{2+} and Mg^{2+}) are readily incorporated into the Ca-site due their similarities to Ca^{2+} (Ghaderi et al., 1999). Additionally, scheelite may contain significant amounts of REE^{3+} and Y^{3+} that substitute for Ca^{2+}. In hydrothermal fluids, the temperature, pH and oxidation state of the fluids will control the relative abundance of Ce^{4+} and Eu^{2+} (Sverjensky, 1984; Brugger et al., 2008; Pattan et al., 2008).

Miranda et al. (2022) reported that scheelite from magmatic-hydrothermal deposits has higher Mo, Nb, and Mn and lower Sr contents and predominantly negative Eu anomalies when compared to those formed dominantly by metamorphic fluids in orogenic settings. These authors also concluded that Ti, V, Mn, As, Y, Nb, U and Eu anomaly are the most important variables for discrimination of different types of magmatic-hydrothermal deposits.

GREISEN-RELATED SCHEELITE

Miranda et al. (2024) showed that quartz-vein/greisen Sn-W scheelite is characterized by high Th, U, Ta, Y and Pb contents, which differs from oxidized skarns and RIRGS. By comparison with other types of mineral deposit in the Bohemian Massif, scheelite from the greisen association displays high Y, U and Th and the highest median values of Sr, Mn, Bi, Sn, Zn, Hf and HREE. Our data, however show significant differences in the distribution of most of these elements (Mo, Nb, As, Y, U, Th, Mn, Zn, HREE) in scheelite from individual greisens of the Bohemian Massif (Appendix 1). For example, we note low median concentrations of Y and REE at Krásno-Huber and Cínovec, two major greisen-type deposits, and more than three orders of magnitude higher Pb, Bi, As, Th and U in scheelite in greisen from Cínovec (the latter most likely reflecting the presence of different nano-/micro inclusions/impurities). This scheelite is also significantly enriched in Mo, Nb, consistent with the observations of Breiter et al. (2016) and also in Sn. On the other hand, with the exception of scheelite from Cínovec, consistently high Sr at a roughly similar range of As contents and also elevated Sn accompanied by lower Mo values make them distinguishable from most oxidized and reduced skarns and also from RIRGS (Fig. 9A, B). Most outliers with increased Sn values in the group of oxidized skarns are represented by spots measured in scheelite from the Obří důl deposit from which the presence of Sn-bearing phases was described by Šrein and Šreinová (2000). Higher Nb at a much lower range of Sr and at a higher range of Mo values make them distinct from scheelite of the orogenic gold deposits whereas scheelite from oxidized and reduced skarns is typical of higher Sr and lower Mo values (except for the Cínovec deposit with high Mo values; Fig. 9C, D). Interestingly, the primitive chemical composition of rock without Mo, Nb and Ta is typical of Horní Babákov and Ovesná Lhota and yet, the contents of these elements in schee-

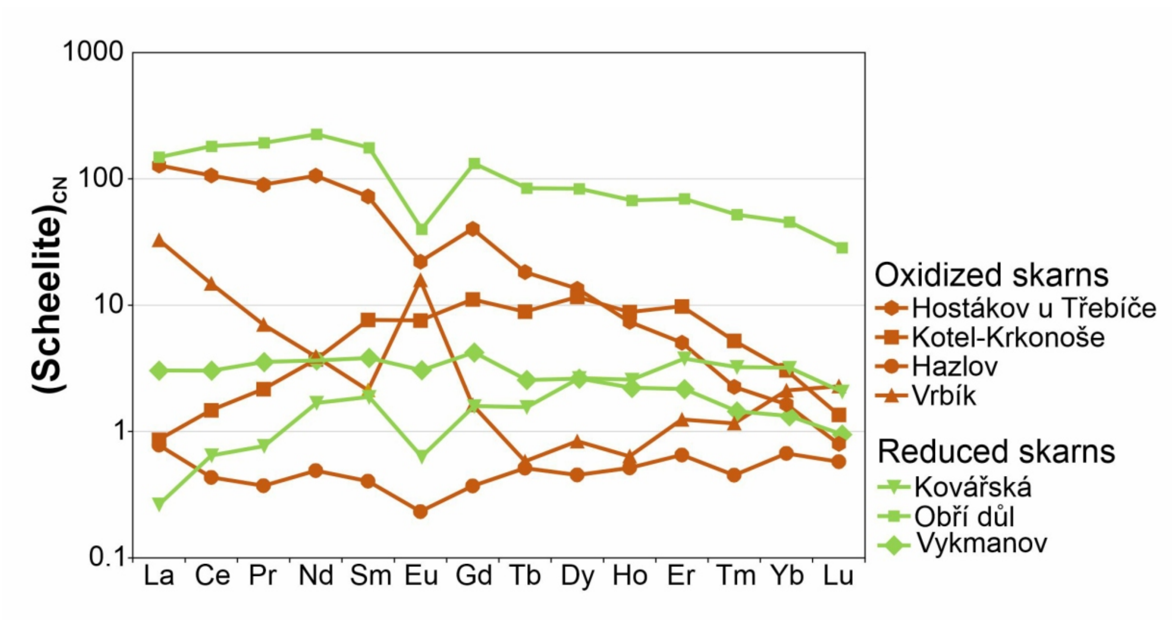

Fig. 6. Rare earth element patterns in scheelite from oxidized and reduced skarns of the Bohemian Massif (on the basis of median values for every locality)

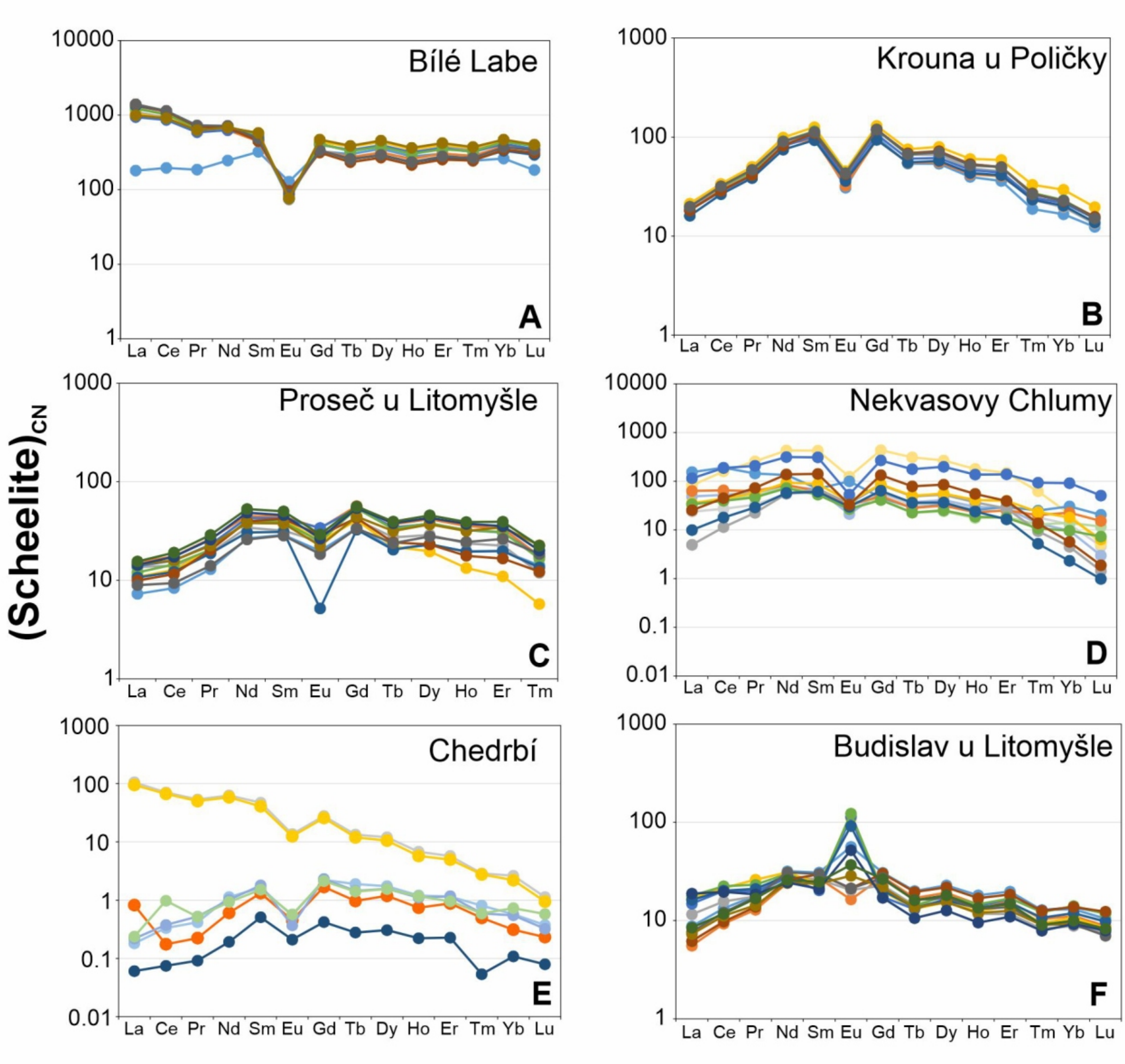

Fig. 7. Rare earth element patterns in scheelite from individual oxidized and reduced skarn deposits/showings of the Bohemian Massif

A – Bílé Labe oxidized skarn, **B** – Krouna u Poličky oxidized skarn, **C** – Proseč u Litomyšle oxidized skarn, **D** – Nekvasovy Chlumy oxidized skarn, **E** – Chedrbí oxidized skarn, **F** – Budislav u Litomyšle reduced skarn

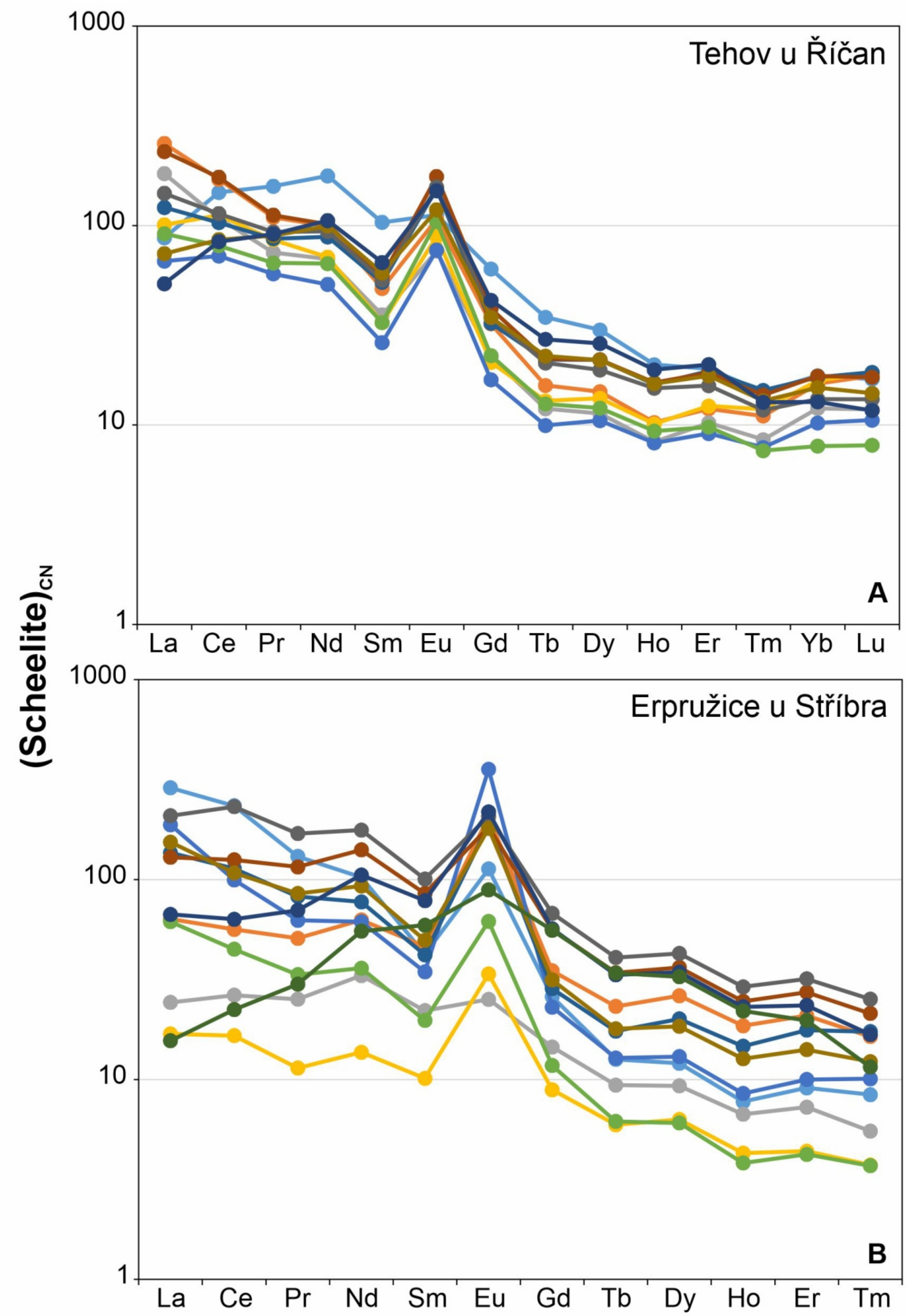

Fig. 8. Rare earth element patterns in scheelite from other individual localities of the Bohemian Massif

A – Tehov u Říčan, **B** – Erpružice u Stříbra

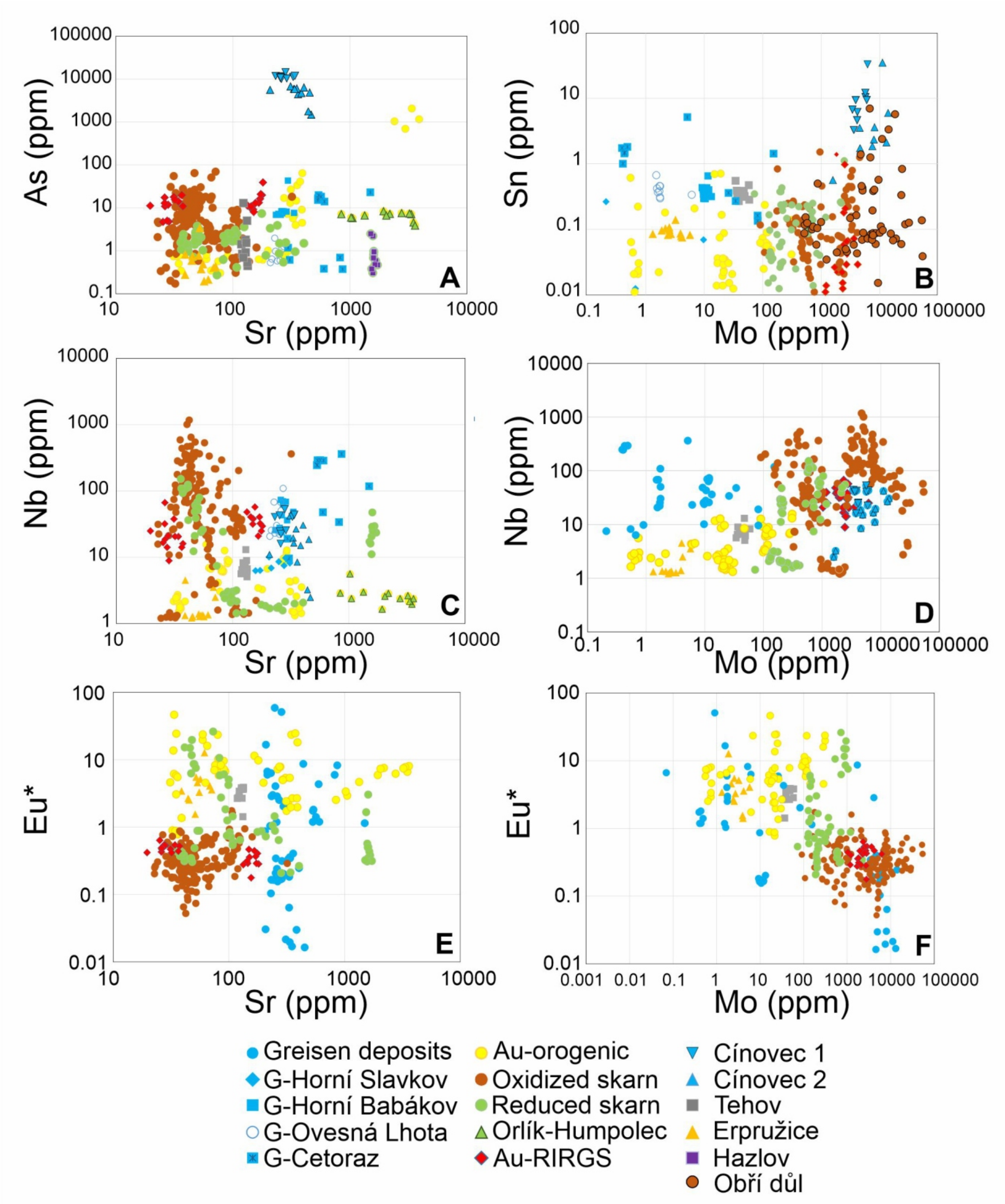

Fig. 9. Binary plots of the minor and trace element composition of the scheelite

A – Sr *versus* As, **B** – Mo *versus* Sn, **C** – Sr *versus* Nb, **D** – Mo *versus* Nb, **E** – Sr *versus* Eu anomaly, **F** – Mo *versus* Eu anomaly lite are similar to those of Mo-rich greisens in the Krušné hory Mts. More information is needed to explain this situation. For example, quartz-cassiterite-wolframite veins at Ovesná Lhota are associated with a small adamelite intrusion which is a part of the Moldanubian Pluton. Morávek (1992) described these veins as only weakly gold-bearing. We can only speculate whether elevated Nb values and a positive Eu anomaly (Fig. 3) could be related to the processes associated with gold enrichment.

Different types of REE pattern and Eu anomaly in scheelite from greisen and related quartz veins of the Bohemian Massif (Fig. 3) reflect different sources of fluids and processes (e.g., Song et al. 2014). The negative Ce anomaly at Cinovec 2 (Fig. 3B) suggests more reduced fluid conditions (Pattan et al., 2005). The shape of the chondrite-normalized REE pattern (typical of a pronounced Eu negative anomaly) from the massive greisen at Cínovec reflects REE distribution in greisen (hostrock) and also other granitic rocks from Cínovec (cf. Breiter et al., 2017a; Fig. 11). This is apparently not the case of scheelite from Krásno-Huber, which is typically of very low REE concentrations and a sharp positive Eu anomaly while the local host rock shows almost two order magnitude higher REE values and a pronounced Eu negative anomaly (Fig. 11). In addition, the shape of the REE pattern in scheelite from Horní Babákov and Cetoraz does not correspond to that of their host rock (Fig. 11) which may indicate that the mineralizing fluids forming that scheelite was not formed by magmatic fluids exsolved from these intrusions. Scheelite from Horní Babákov and Čelina (RIRGS) shows a uniform REE pattern suggesting a homogeneous source of fluids, while scheelite grains from Cetoraz and Ovesná Lhota are characterized by different REE patterns, indicating variable conditions of scheelite formation. Scheelite from the greisen quartz vein at Ovesná Lhota has a similar REE pattern to a group of orogenic Au deposits with a sharp positive Eu anomaly.

A wide range of Eu* at restricted Sr values characterizes scheelite from the greisen-type association from other groups (Fig. 9E), whereas in the Eu* vs Mo diagram greisen-type scheelite shows a more scattered picture (Fig. 9F). The correlation between REE + Y and Na in scheelite from greisen-type, oxidized skarn and orogenic Au and RIRGS associations (at the deposit-type level; Fig. 10A) indicates a coupled substitution after the following equation: $2Ca^{2+} = (REE, Y)^{3+} + Na^{+}$ (Nassau, 1963; Nassau and Loiacono, 1963; Cottrant, 1981; Burt, 1989; Raimbault et al., 1993; Brugger et al., 2000a). This type of substitution is considered a major substitution in scheelite (Nassau and Loiacono, 1963; Cottrant, 1981; Burt, 1989; Raimbault et al., 1993; Brugger et al., 2002). However, looking in more detail at the REE+Y vs. Na relationship in scheelite from individual deposits from the Bohemian Massif, no positive correlation between these variables at Cínovec and Krásno-Huber (greisen-type), Chedrbí and Vykmanov (oxidized skarn-type) and Sobětice (orogenic Au-type) is visible (Fig. 10B).

OROGENIC AU-RELATED SCHEELITE

On the basis of a study of 25 representative orogenic gold deposits worldwide, Sciuba et al. (2020) reported that scheelite from deposits hosted in low and moderate metamorphic facies rocks commonly have higher REE (median 334 ppm and 632 ppm, respectively) and Y (median 145 ppm and 253 ppm, respectively), Sr, and Na, and low Mn and Nb contents, whereas scheelite from deposits hosted in high metamorphic facies rocks commonly have low REE (median 101 ppm) and Y (median 37 ppm), Sr, and Na, and high Mn and Nb contents. The chemical composition of scheelite from Jílové (lower metamorphic grade) and of Sobětice, Kašperské Hory and Orlík u Humpolce (high metamorphic grade) is in support of this observation (Appendix 1). The only exception is that scheelite from Orlík u Humpolce shows anomalously high Sr (and low Mn and Nb) content, which likely reflects its close association with the sedimentary (calc-silicate) host rock and scheelite from Sobětice displays low Nb, reflecting its low concentration in the host rock (silicified marble).

The bell-shaped and flat patterns with dominant positive Eu anomaly described from many orogenic Au deposits worldwide (Ghaderi et al., 1999; Brugger et al., 2000b; Roberts et al., 2006; Sciuba et al., 2020) are also typical for the Bohemian orogenic gold scheelite (Fig. 4A–E). REE patterns in scheelite from Jílové, Kašperské Hory-Naděje and Orlík (Fig. 4A, C, E) reflect a homogeneous fluid source, locally with variable redox conditions (e.g., oscillatory zonation of scheelite at Jílové; Fig. 2E; Ďurišová and Sztacho, 1986; Strnad et al., 2012; Zachariáš et al., 2013) or fluctuations in pH from fluid- to rock-buffered conditions, as proposed by Brugger et al. (2008) or even a changing rate of crystallization combined with processes of chemical diffusion (Shore and Fowler, 1996).

Scheelite from Jílové and Kašperské Hory-Naděje, Kašperské Hory-Lohbach and Orlík is typified by a positive correlation between Na and REE+Y (Fig. 10B), reflecting most likely coupled substitution. Scheelite from Sobětice shows a negative correlation between Na and REE+Y (Fig. 10B) and a slightly positive relationship between Na and Eu* (Fig. 10C), similar to scheelite from the Nevoria Au deposit, Australia (Sciuba et al., 2020), which was ascribed as of both Au skarn (Mueller et al., 2004) and orogenic Au (Goldfarb et al., 2005) type.

Sciuba et al. (2020) reported a negative correlation of Na with Eu* in scheelite from selected world orogenic Au deposits which is consistent with that of the Jílové, Kašperské Hory-Lohbach and Kašperské Hory-Naděje deposits, while scheelite from Orlík show the opposite trend (Fig. 10C). Sciuba et al. (2020) also noted that the Na content is higher in scheelite from deposits hosted in felsic to intermediate rocks (median 120 ppm and 194 ppm, respectively), and lower in scheelite from deposits hosted in sedimentary rocks (median 53 ppm). Scheelite from our orogenic Au deposits has a much lower median Na value of 21 ppm.

Sciuba et al. (2020) concluded that scheelite from orogenic gold deposits have distinct Sr, Mo, Eu, As, and Sr/Mo, but indistinguishable REE, signatures, compared to scheelite from other deposit types. We show that scheelite from this type of setting in the Bohemian Massif has in general higher REE concentrations when compared to that of reduced skarn (Table 2). Miranda et al. (2024) proposed that orogenic Au deposits and metamorphic scheelite are characterized by low Mo, Nb and Mn, high Sr and Na contents, with commonly positive Eu anomalies. The low Mo content (median value of 21 ppm) and dominant positive Eu anomaly in scheelite from orogenic settings from the Bohemian Massif suggests relatively reduced metamorphic-derived fluids (Song et al., 2014; Poulin et al., 2018; Sciuba et al., 2020). From all the mineral deposit-types studied in the Bohemian Massif, scheelite from orogenic Au deposits shows the lowest median Nb value, which supports this observation. The low (but not lowest) median Mo value is comparable with that of the greisen-type association while the low median Mn value is close to that of RIRGS and reduced skarns. The higher Sr median values were found in the greisen-type association while those of Na were observed in the greisen-type association, RIRGS and oxidized skarns.

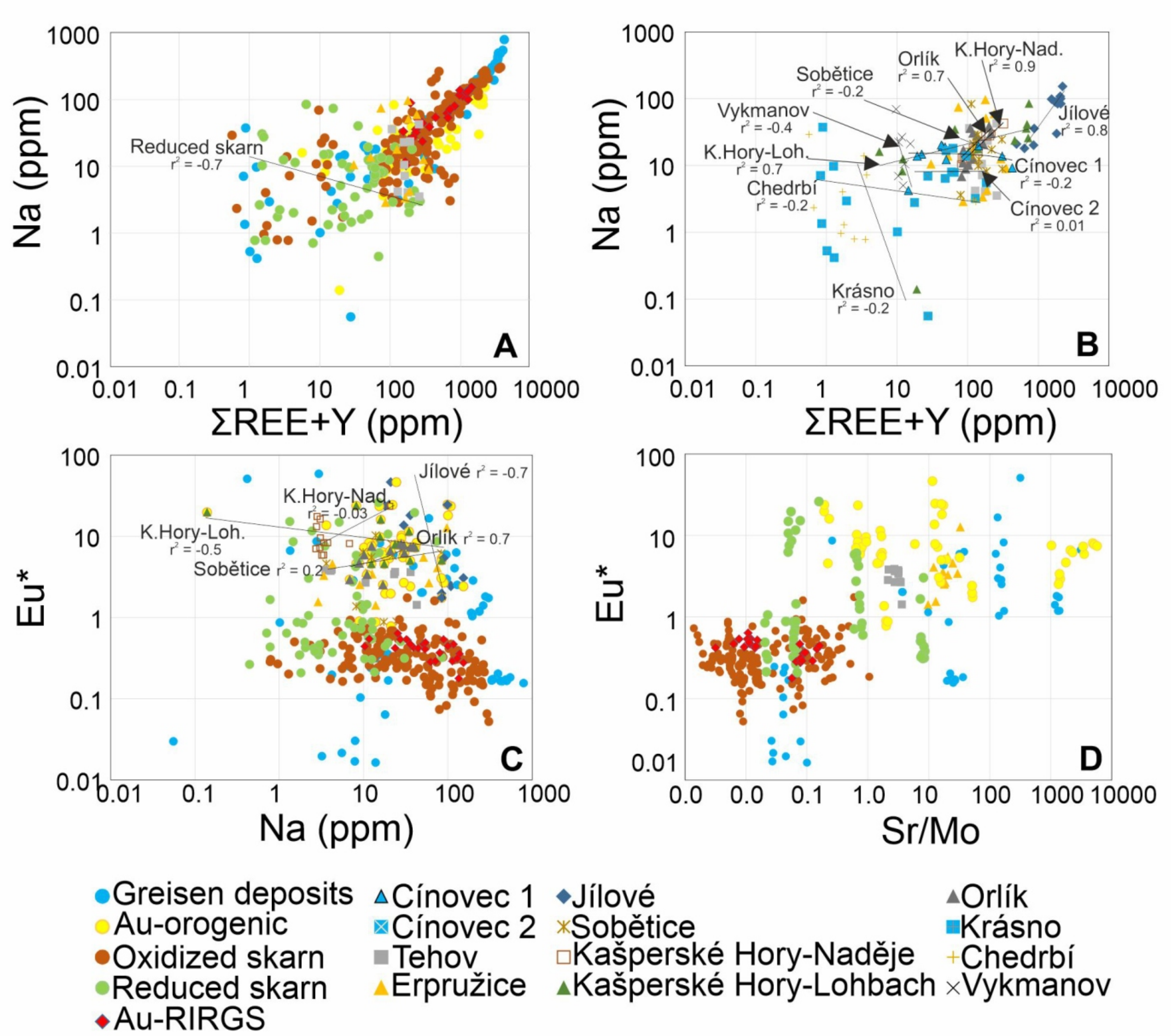

Fig. 10. Binary plots of chemical composition of the scheelite

A – REE + Y *versus* Na (basic trends), **B** – REE + Y *versus* Na (selected deposit trends), **C** – Na *versus* Eu anomaly (selected deposit trends), **D** – Sr/Mo *versus* Eu anomaly. The values of correlation coefficients (r^2) are shown for selected deposits/mineralizations

Scheelite from orogenic Au deposits can be distinguished from that of oxidized and reduced skarns by higher Sr/Mo values and positive Eu anomalies (Fig. 10D). Scheelite from other settings (quartz veins at Tehov and Erpružice) plots close to that of orogenic Au deposits. Similarly, orogenic Au scheelite shows mostly lower Mo and Nb values when compared to those from oxidized and reduced skarns and RIRGS, and lower Nb values than the group of greisen-related scheelite (Fig. 9D). Scheelite from quartz veins at Tehov and Erpružice again plots close to Au orogenic scheelite. Scheelite from orogenic Au settings can be discriminated from other mineral deposit types in a Sr vs Nb plot (Fig. 9C) and from oxidized skarns by a higher Eu anomaly, lower Mo and larger range of Sr values (see Fig. 9E, F).

RIRGS-RELATED SCHEELITE

Miranda et al. (2024) showed that scheelite from Čelina displays similar REE patterns to that of the felsic intrusions related to the mineralization, suggesting that the exsolved mineralizing fluid REE patterns are controlled by the chemical composition of the ore-related intrusions and might be reflected by the REE concentrations of scheelite grains. Our new data also show that in comparison with scheelite from orogenic Au settings, scheelite from RIRGS-type mineralizations (Čelina and Vacíkov) is significantly enriched in Mo and Nb, moderately in As and shows similar contents of Mn, Zn, Y and REE. Scheelite from the orogenic Au association contains higher concentrations of Sr, Pb, Th and U. In most of elemental diagrams, scheelite from RIRGS plots close to the field of oxidized skarns (e.g., Fig. 9A–F). From reduced skarns they can be discriminated in a Mo/Sn plot (Fig. 9B).

Scheelite from Vacíkov-Petráčkova hora displays a homogeneous chemical composition and a typical REE pattern with a negative Eu anomaly (Fig. 4F), which is similar to that from Dublin Gulch (intrusion-hosted sheeted quartz veins – not shown, Miranda et al. 2024), consistent with the origin of scheelite from reduced-type fluids (Zachariáš et al., 2001). A predominantly negative Eu anomaly in scheelite from RIRGS results from a different magma composition, salinity and co-genetic REE-bearing minerals (Miranda et al., 2024).

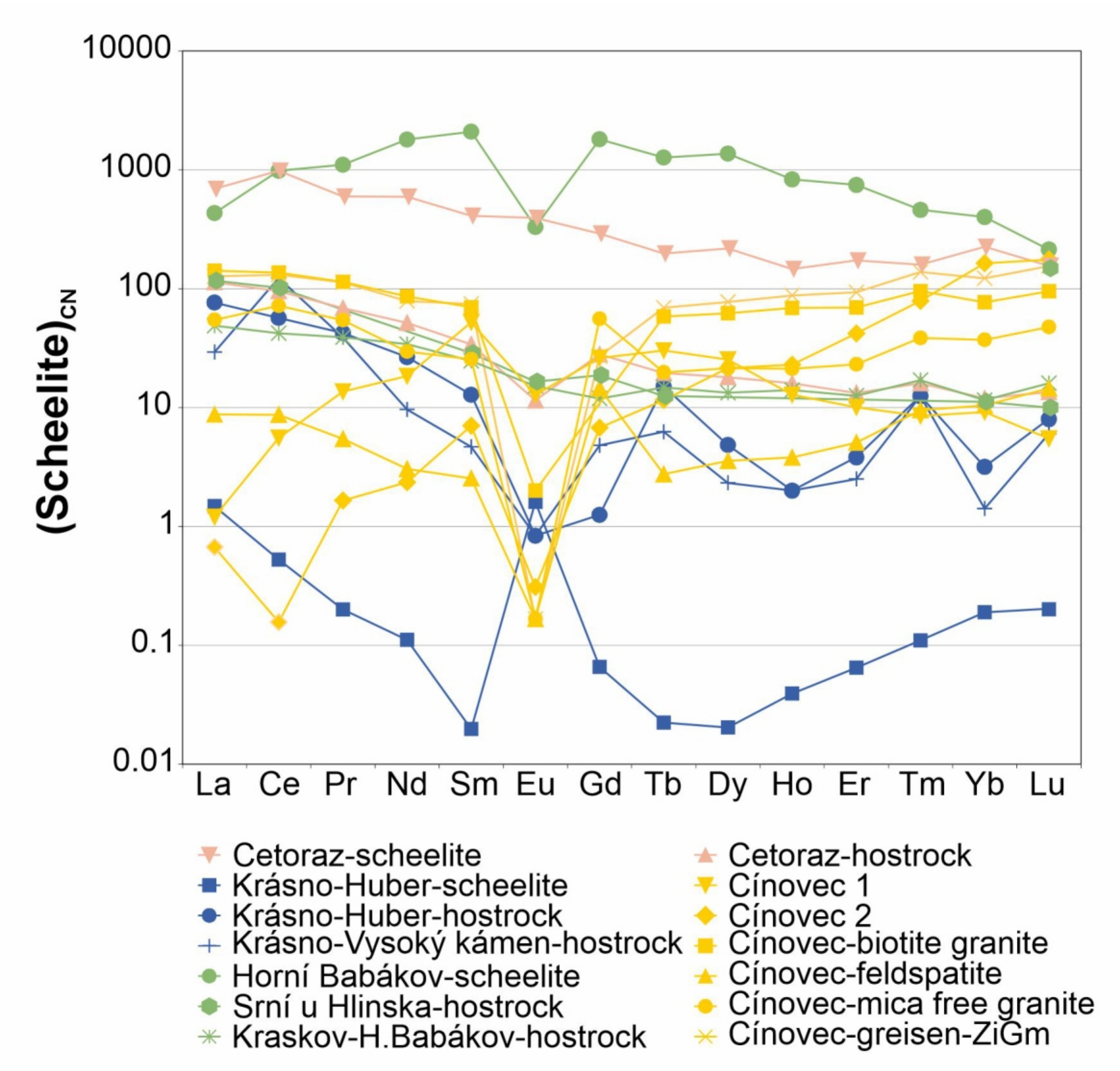

Fig. 11. Rare earth element patterns in selected scheelite (this work) and host rock

Data for Cínovec lithology from Breiter et al. (2017a) and for other hostrocks from the Geochemical Database of the Czech Geological Survey

OXIDIZED AND REDUCED SKARN-RELATED SCHEELITE

On the basis of the study of trace element composition of scheelite from 19 well-documented reduced and oxidized skarn systems, Miranda et al. (2022) concluded that scheelite from reduced and oxidized skarns can be discriminated from those of orogenic and intrusion-related gold deposits due to their lower Sr and higher Mo, Ta, and Nb concentrations. Our study confirmed the highest median Mo, Nb, REE and LREE values in scheelite from oxidized skarn systems of all the mineral deposits/showings studied in the Bohemian Massif. Scheelite from reduced skarns is characterized by the lowest median values of Y and also Mn and As, which are close to those of the orogenic gold setting.

Scheelite from oxidized and reduced skarns is dominated by REE patterns with a negative anomaly, which is consistent with crystallization of plagioclase in their magmatic source rock (Banks et al., 1994; Barker et al., 2004). On the other hand, a combination of increased (high) Sr values with smaller negative Eu anomalies, as documented in scheelite from the Hazlov and Kotel-Krkonoše reduced skarns by Miranda et al. (2024), might indicate release of Sr and Eu from Ca-bearing phases during alteration, consistent with observations by Yuan et al. (2019). Large Eu anomalies coupled with low Sr values in scheelite from the reduced skarns at Vrbík and Budislav are somewhat similar to some orogenic Au deposits (Fig. 9E).

The very homogeneous composition of the scheelites is reflected in REE patterns with a negative Eu anomaly from oxidized skarns at Krouna, Proseč and Bílé Labe, and the only slightly inhomogeneous scheelite composition from oxidized skarns at Mutice and Nekvasovy Chlumy is consistent with the findings of Banks et al. (1994), Barker et al. (2004), Miranda et al. (2022) and points to magmatic fluid sources. A change in the shape of REE patterns from LREE-enriched with a negative Eu anomaly (accompanied by significantly higher Y and Nb and lower Mo contents in the scheelite) to flat-/bell-shaped with a negative Eu anomaly in oxidized skarn scheelite at Chedrbí documents most likely differences in co-precipitating minerals and in the salinity of the magmatic fluids as reported by Miranda et al. (2022).

On the basis of the comparison of the REE patterns in scheelite grains and host rock at Obří důl (oxidized skarn), Miranda et al. (2024) proposed that the scheelite chemical composition directly reflects, to some degree, the composition of the mineralizing fluids and host rocks (regardless of the substitution mechanism controlling the REE incorporation in scheelite). They also proposed that the more fractionated REE patterns, such as the steep negative slope at Obří důl, reflect co-precipitation of other mineral phases, types of ligands, and salinity, rather than the original magmatic source.

Primary scheelite from reduced skarns were studied by electron microprobe by Žaludková et al. (2010) who reported higher Mo (up to 2.12 wt.% MoO_3) and low Fe (up to 0.08 wt.% FeO) contents in scheelite from Staré Podhradí and Boží hora u Žulové (Žulovský massif) relative to that from Hostákov and Slavice (Třebíčský massif – up to 0.35 wt.% MoO_3 , and up to 0.05 wt.% FeO). They concluded that the chemical composition of the scheelite reflects different chemical compositions of the source fluids and host rock. Miranda et al. (2024) reported a range of 569–2469 ppm Mo (mean 1022 ppm, LA-ICP-MS data) in scheelite from Hostákov. Scheelite from Staré Podhradí showed a high Mo median value (1126 ppm) and low REE (17.5 ppm) and a LREE-enriched pattern with a negative Eu anomaly (this study).

SCHEELITE FROM OTHER SETTINGS

Scheelite from quartz veins at Tehov and Erpružice, characterized by low Mo, Nb, Y, and LREE >HREE, shows many similarities with scheelite from orogenic Au settings (e.g., Fig. 9) and also similar REE patterns (LREE-enriched with positive Eu*).

CONCLUSIONS

The study of chemical composition of scheelite from five major types of deposit within the mineralization of the Bohemian Massif (greisens and related quartz veins, Au-orogenic and Au-RIRGS, oxidized and reduced skarns) can be summarized as follows:

1. Scheelite can display both homogeneous and inhomogeneous chemical compositions within one grain and/or deposit type.
2. Both homogeneous and zoned scheelite seen by cathodoluminescence from greisens and related quartz veins show the highest median values of Sr (281 ppm), Y (88 ppm), Mn (70 ppm), Bi (0.9 ppm), Sn (0.4 ppm), U (0.3 ppm), Th and Zn (0.2 ppm), Hf (0.1 ppm) and HREE (91 ppm) among all the groups studied. Five different types of chondrite-normalized REE pattern in this scheelite reflect different sources and types of fluids and processes. For example, the REE patterns from the massive greisen at Cínovec reflect the REE distribution in the host rock. Scheelites from Cetoraz and Ovesná Lhota are characterized by different REE patterns, indicating changes in fluid chemical composition, whereas scheelite from H. Babákov is typical of a very homogeneous source of fluid.
3. Predominantly homogeneous in CL, scheelite from the Au orogenic setting is typical of the highest median value of Pb (9.2 ppm) and very low median value of Mg (3.1 ppm) comparable to scheelite from oxidized skarns (3.3 ppm) and a low median Mo value (22 ppm) which is close to that of greisen-type scheelite (11.6 ppm). It also shows the lowest median value of Nb (3 ppm) of all the groups studied. Scheelite from orogenic gold settings displays mostly bell-shaped chondrite-normalized REE patterns and flat REE patterns, both with a positive Eu anomaly.
4. Predominantly homogeneous in CL, scheelite from RIRGS has the highest median values of Si (168 ppm), Mg (10 ppm), As (12 ppm), V (0.8 ppm) and Cu (1 ppm) of all the groups studied. It is, compared to scheelite from orogenic gold deposits, typical of significantly higher Nb and Mo median values and lower Sr, LREE and HREE median values. Scheelite from RIRGS displays mostly bell-shaped normalized REE patterns with a negative Eu anomaly.
5. Predominantly zoned in CL, scheelite from oxidized skarn has the highest median Mo (2494 ppm), REE (274 ppm), LREE (234 ppm) and Nb (77 ppm). Compared to scheelite from reduced skarns, it has significantly higher Y, Mo, LREE and HREE.
6. Predominantly homogeneous in CL, scheelite from reduced skarns is characterized by the lowest median values of Nb (19 ppm), Y (8.2 ppm), Mn (5.9 ppm), and Zn (0.2 ppm) of all the groups studied. A similarly low median As value (1.5 ppm) is close to that of the orogenic gold setting.
7. Scheelite from oxidized and reduced skarns displays five types of chondrite-normalized REE patterns: (1) LREE-enriched with a positive or negative Eu anomaly, (2) Bell-shaped REE patterns with a negative Eu anomaly or without an Eu anomaly, (3) Flat REE patterns with a negative Eu anomaly.
8. Scheelite from other settings (Erpružice u Stříbra and Tehov u Říčan) shows many similarities with that of Au orogenic settings.
9. We suggest that Mo vs. Sn and Nb and Eu* binary plots seem to be suitable, with some exceptions, for determination of scheelite origin from different ore deposit types.

Acknowledgements. We would like to thank Marc Choquette (Université Laval), Dany Savard and Audrey Lavoie (Université du Quebec à Chicoutimi) for their assistance with EPMA and LA-ICP-MS analyses and Markéta Štěpánová (Czech Geological Survey, Prague) for help with finalizing figures. It is a contribution to the RENS project (TAČR SS02030023) and also to the Strategic Research Plan of the Czech Geological Survey (DKRVO 2023-2027). We thank the Natural Science and Engineering Research Council of Canada for its support. The authors would like to thank the anonymous reviewers for their valuable comments, which helped to improve this manuscript. We also thank Tadeusz M. Peryt and Stanislaw Z. Mikulski for their efficient editorial handling and Jan Zalasiewicz for language improvement.

REFERENCES

Ackerman, L., Haluzová, E., Creaser, R.A., Pašava, J., Veselovský, F., Breiter, K., Erban, V., Drábek, M., 2017. Temporal evolution of mineralization events in the Bohemian Massif inferred from the Re-Os geochronology of molybdenite. Mineralium Deposita, **52**: 651–662; https://doi.org/10.1007/s00126-016-0685-5

Ackerman, L., Žák, K., Haluzová, E., Creaser, R.A., Svojtka, M., Pašava, J., Veselovský, F., 2019. Chronology of the Kašperské Hory orogenic gold deposit, Bohemian Massif, Czech Republic. Mineralium Deposita, **54**: 473–484; https://doi.org/10.1007/s00126-018-0822-4

Altenberger, F., Krause, J., Wintzer, N.E., Iglseder, C., Berndt, J., Bachmann, K., Raith, J.G., 2024. Polyphase stratabound scheelite-ferberite mineralization at Mallnock, Eastern Alps, Austria. Mineralium Deposita, **59:** 1109–1132; https://doi.org/10.1007/s00126-024-01250-x

Anglin, C.D., Jonasson, I.R., Franklin, J., 1996. Sm-Nd dating of scheelite and tourmaline: implications for the genesis of Archean gold deposits, Val d'Or, Canada. Economic Geology, **91**: 1372–1382; https://doi.org/10.2113/gsecongeo.91.8.1372

Banks, D.A., Yardley, B.W.D., Campbell, A.R., Jarvis, K.E., 1994. REE composition of an aqueous magmatic fluid: A fluid inclusion study from the Capitan Pluton, New Mexico, U.S.A., Chemical Geology, **113:** 259–272; https://doi.org/10.1016/0009-2541(94)90070-1

Bell, K., Anglin, C.D., Franklin, J.M., 1989. Sm-Nd and Rb-Sr isotope systematics of scheelites: possible implications for the age and genesis of vein-hosted gold deposits. Geology, **17**: 500–509; https://doi.org/10.1130/0091-7613(1989)017%3C0500:SNARSI%3E2.3.CO;2

Beran, P., Sejkora, J., 2006. The Krásno Sn-W ore district near Horní Slavkov: mining history, geological and mineralogical characteristics. Journal of Geosciences, **51**: 3–42; http://doi.org/10.3190/JCGS.987

Bernard, J.H., Čech, F., Dávidová Š., Dudek, A., Fediuk, F., Hovorka, D., Kettner, R., Koděra, M., Kopecký, L., Němec, D., Paděra K., Petránek, J., Sekanina, J., Staněk, J., Šímová, M., 1981. Mineralogie Československa. 2 vydání, Academia Praha.

Boiron, M.Ch., Bakarat, A., Cathelineau, M., Banks, D.A., Ďurišová, J., Morávek, P., 2001. Geometry and P-V-T-X conditions of microfissural ore fluid migration: the Mokrsko gold deposit Bohemia. Chemichal Geology, **173**: 207–225; https://doi.org/10.1016/S0009-2541(00)00276-X

Breiter, K., Korbelová, Z., Šešulka, V., Honig, S., 2016. New rock and mineral data from the Li (Sn, W, Nb, Ta)-deposit Cínovec-jih (in Czech with English summary). Zprávy o geologických výzkumech, **49**: 113–121; https://doi.org/10.3140/zpravy.geol.2016.41

Breiter, K., Ďurišová, J., Hrstka, T., Korbelová, Z., Vaňková, M.H., Galiová, M. V., Kanický, V., Rambousek, P., Knésl, I., Dobeš, P., Dosbaba, M., 2017a. Assessment of magmatic vs. metasomatic processes in rare-metal granites: A case study of the Cínovec/Zinnwald Sn-W-Li deposit, Central Europe. Lithos, **292–293**: 198–217; https://doi.org/10.1016/j.lithos.2017.08.015

Breiter, K., Korbelová, Z., Chládek, Š., Uher, P., Knésl, I., Rambousek, P., Honig, S., Šešulka, V., 2017b. Diversity of Ti-Sn-W-Nb-Ta oxide minerals in the classic granite-related magmatic-hydrothermal Cínovec/Zinnwald Sn-W-Li deposit (Czech Republic). European Journal of Mineralogy, **29**: 727–738; https://doi.org/10.1127/ejm/2017/0029-2650

Brugger, J., Giere, R., Grobety, B., Uspensky, E., 1998. Scheelite-powellite and paraniite-(Y) from the Fe-Mn deposit at Fianel, Eastern Swiss Alps. American Mineralogist, **83**: 1100–1110; http://minsocam.org/MSA/AmMin/toc/Articles_Free/1998/Brugger_p1100-1110_98.pdf

Brugger, J., Bettiol, A.A., Costa, S., Lahaye, Y., Bateman, R., Lambert, D.D., Jamieson, D.N., 2000a. Mapping REE distribution in scheelite using luminescence. Mineralogical Magazine, **64**: 891–903; https://doi.org/10.1180/002646100549724

Brugger, J., Lahaye, Y., Costa, S., Lambert, D., Bateman, R., 2000b. Inhomogeneous distribution of REE in scheelite and dynamics of Archaean hydrothermal systems (Mt. Charlotte and Drysdale gold deposits, Western Australia). Contributions to Mineralogy and Petrology, **139**: 251–264; https://doi.org/10.1007/s004100000135

Brugger, J., Maas, R., Lahaye, Y., McRae, C., Ghaderi, M., Costa, S., Lambert, D., Bateman, R., Prince, K., 2002. Origins of Nd-Sr-Pb isotopic variations in single scheelite grains from Archaean gold deposits, Western Australia. Chemical Geology, **182**: 203–225; https://doi.org/10.1016/S0009-2541(01)00290-X

Brugger, J., Etschmann, B., Pownceby, M., Liu, W., Grundler, P., Brewe, D., 2008. Oxidation state of europium in scheelite: Tracking fluid–rock interaction in gold deposits. Chemical Geology, **257**: 26–33; https://doi.org/10.1016/j.chemgeo.2008.08.003

Bubal, J., 2013. Geochemie a vznik skarnů Českého masívu (in Czech). Diploma Thesis, PřfUK Praha.

Buriánek, D., 2009. Petrography of the Polička crystalline complex (in Czech with English summary). Acta Musei Moraviae, Scientiae Geologicae, **94**: 3–46.

Buriánek, D., Buřivalová, L., Houzar, S., Losos, Z., Míková, J., 2020. Geochronology and petrogenesis of orthogneisses from the Pacov body: implications for the subdivision of the Cambro-Ordovician peraluminous magmatism and related mineralizations in the Monotonous and Varied units of the Moldanubian Zone (Bohemian Massif). Mineralogy and Petrology, **114**: 175–197; https://doi.org/10.1007/s00710-020-00699-8

Burt, D., 1989. Compositional and phase relations among rare earth elements. Reviews in Mineralogy, **21**: 259–307; https://doi.org/10.1515/9781501509032-013

Buřival, Z., Losertová, L., 2015. Metamorphosed gold deposit from Orlik near Humpolec, Czech Republic. In: Proceeding of the 13th Biennial SGA Meeting, 24–27 August 2015, Nancy, France, **2**: 687–690.

Buřivalová, L., Losos, Z., 2018. Tungsten mineralization in quartz veins at the Cetoraz deposit, Czech Republic. In: Joint 5th Central-European Mineralogical Conference and 7th Mineral Sciences in the Carpathians Conference. Book of Contributions and Abstracts, p. 12, Comenius University Bratislava.

Caraballo, E., Dare, S., Beaudoin, G., 2023a. Variation of trace elements in chalcopyrite from worldwide Ni-Cu sulfide and Reef-type PGE deposits: implications for mineral exploration. Mineralium Deposita, **57**: 1293–1321; https://doi.org/10.1007/s00126-021-01091-y

Caraballo, E., Beaudoin, G., Dare, S., Genna, D., Petersen, S., Relvas, J.M.R.S., Piercey, S.J., 2023b. Trace Element Composition of Chalcopyrite from Volcanogenic Massive Sulfide Deposits: Variation and Implications for Provenance Recognition. Economic Geology, **118**: 1923–1958; https://doi.org/10.5382/econgeo.5020

Chang, Z., Shu, Q., Meinert, L., 2019. Skarn deposits of China. Special Publications of the Society of Economic Geologists, **22**: 189–234; https://doi.org/10.5382/SP.22.06

Chowdhury, S., Lentz, D.R., 2011. Mineralogical and geochemical characteristics of scheelite-bearing skarns, and genetic relations between skarn mineralization and petrogenesis of the associated granitoid pluton at Sargipali, Sundergarh District, Eastern India. Journal of Geochemical Exploration, **108**: 39–61; http://dx.doi.org/10.1016/j.gexplo.2010.07.005

Cook, N.J., Ciobanu, C.L., Mao, J., 2009. Textural controls on gold distribution in As-free pyrite from the Dongping, Huangtuliang and Hougou gold deposits, North China Craton (Hebei Province, China). Chemical Geology, **264**: 101–121; https://doi.org/10.1016/j.chemgeo.2009.02.020

Cook, N.J., Ciobanu, C.L., Meria, D., Silcock, D., Wade, B., 2013. Arsenopyrite–pyrite association in an orogenic gold ore: tracing mineralization history from textures and trace elements. Economic Geology, **108**: 1273–1283; https://doi.org/10.2113/econgeo.108.6.1273

Cottrant, J., 1981. Cristallochimie et geochimie des terres rares dans la scheelite: application ŕ quelques gisements français. Ph.D. Thesis, Université Pierre et Marie Curie.

Černý, P., Litochleb, J., 1983. Mineralogie zlatonosného zrudnění ze Sobětic u Klatov (in Czech). Časopis Národního muzea, **153**: 150–158;

https://publikace.nm.cz/en/periodicals/jotnmpnhs/153-1-4/mineralogie-zlatonosneho-zrudneni-ze-sobetic-u-klatov

Darbyshire, D.P.F., Pitfield, P.E.J., Campbell, S.D.G., 1996. Late Archean and Early Proterozoic gold-tungsten mineralization in the Zimbabwe Archean craton: Rb-Sr and Sm-Nd isotope constraints. Geology, 24: 19–22; https://doi.org/10.1130/0091-7613(1996)024%3C0019:LAAEPG%3E2.3.CO;2

Ding, T., Ma, D., Lu, J., Zhang, R., 2018. Garnet and scheelite as indicators of multi-stage tungsten mineralization in the Huangshaping deposit, southern Hunan province, China. Ore Geology Reviews, **94**: 193–211; https://doi.org/ 10.1016/j.oregeorev.2018.01.029

Dolníček, Z., René, M., Prochaska, W., Kovář, M., 2012. Fluid evolution of the Hub Stock, Horní Slavkov-Krásno Sn-W ore district, Bohemian Massif, Czech Republic. Mineralium Deposita, **47**: 821–833; https://doi.org/10.1007/s00126-012-0400-0

Dostál, J., Kontak, D., Chatterjee, A.K., 2009. Trace element geochemistry of scheelite and rutile from metaturbidite-hosted quartz vein gold deposits, Meguma Terrane, Nova Scotia, Canada: genetic implications. Mineralogy and Petrology, **97**: 95–109; https://doi.org/10.1007/s00710-009-0067-0

Ďurišová, J., Sztacho, P., 1986. Fluid inclusion study in minerals of scheelite-bearing parageneses along the northern contact of the Moldanubian pluton (in Czech). MS Geofond Praha.

Ďurišová, J., Sztacho, P., Dubessy, J., 1992. A fluid inclusion study of Au-W stratiform mineralization at Orlik near Humpolec, Czechoslovakia. European Journal of Mineralogy, **4**: 965–976; https://doi.org/10.1127/ejm/4/5/0965

Eichhorn, R., Höll, R., Jagout, E., Schärer, U., 1997. Dating scheelite stages: a strontium, neodymium, lead approach from the Felhertal tungsten deposit, CentralAlps, Austria. Geochimica et Cosmochimica Acta, **61**: 5005–5022; https://doi.org/10.1016/S0016-7037(97)00349-9

Frei, R., Nägler, T.F., Schönberg, R., Kramers, J.D., 1998. Re-Os, Sm-Nd, U-Pb,and stepwise lead leaching isotope systematics in shear-zone hosted gold mineralization: genetic tracing and age constraints of crustal hydrothermal activity. Geochimica et Cosmochimica Acta, **62**: 1925–1936; https://doi.org/10.1016/S0016-7037(98)00111-2

Fu, Y., Hollings, P., Zhou, H., Lin, H., Jiang, L., Yang, T., 2017. In-situ LA-ICP-MS trace elements analysis of scheelites from the giant Beiya gold–polymetallic deposit in Yunnan Province, Southwest China and its metallogenic implications. Ore Geology Reviews, **80**: 828–837; https://doi.org/10.1016/J.OREGEOREV.2016.08.030

Gaft, M., Panczer, G., Uspensky, E., Reisfeld, R., 1999. Laser-induced time-resolved luminescence of rare-earth elements in scheelite. Mineralogical Magazine, **63**:199–210; https://doi.org/10.1180/002646199548439

George, L., Cook, N.J., Ciobanu, C.L., Wade, B.P., 2015. Trace and minor elements in galena: A reconnaissance LA-ICP-MS study. American Mineralogist, **100**: 548–569; https://doi.org/10.2138/am-2015-4862

Ghaderi, M., Palin, J.M., Campbell, I.H., Sylvester, P.J., 1999. Rare earth element systematics in scheelite from hydrothermal gold deposits in the Kalgoorlie-Norseman region, Western Australia. Economic Geology, **94**: 423–437; https://doi.org/10.2113/gsecongeo.94.3.423

Goldfarb, R.J., Baker, T., Dube, B., Groves, D.I., Hart, C.J.R., Gosselin, P., 2005. Distribution, character, and genesis of gold deposits in metamorphic terranes. Economic Geology, **100**: 407–450; https://doi.org/10.5382/AV100.14

Graupner, T., Niedermann, S., Rhede, D., Kempe, U., Seltmann, R., Williams, C., Klemd, R., 2010. Multiple sources for mineralizing fluids in the Charmitan gold(-tungsten) mineralization (Uzbekistan). Mineralium Deposita, **45**: 667–682; https://doi.org/10.1007/s00126-010-0299-2

Guo, S., Chen, Y., Liu, C.Z., Wang, J.G., Su, B., Gao, Y.J., Wu, F.Y., Sein, K., Yang, H., Mao, Q., 2016. Scheelite and coexisting F-rich zoned garnet, vesuvianite, fluorite, and apatite in calc-silicate rocks from the Mogok metamorphic belt, Myanmar: Implications for metasomatism in marble and the role of halogens in W mobilization and mineralization. Journal of Asian Earth Sciences, **117**: 82–106; https://doi.org/10.1016/j.jseaes.2015.12.004

Guo, Z., Li, J., Xu, X., Song, Z., Dong, X., Tian, J., Yang, Y., She, H., Xiang, A., Kang, Y., 2016. Sm/Nd dating and REE composition of scheelite for the Honghuaerji scheelite deposit, Inner Mongolia, Northeast China. Lithos, **261**: 307–321; https://doi.org/10.1016/j.lithos.2016.03.006

Hájek, J., 1971. Tungsten mineralization in greisen at Horní Babákov near Hlinsko in Bohemia (in Czech with English summary). Sborník geologických věd, Řada Ložisková geologie **14**: 127–148.

Haupt, C.P., Krause, J., Schulz, B., Götze, J., Chischi, J., Berndt, J., Klemme, K., Schmidt, S., Aupers, K., Reinhardt, N., 2025. New insights on the formation of the polymetamorphic Felbertal tungsten deposit (Austria, Eastern Alps) revealed by CL, EPMA, and LA-ICP-MS investigation. Mineralium Deposita, **60**: 631–652; https://doi.org/10.1007/s00126-024-01284-1

Hazarika, P., Mishra, B., Pruseth, K.L., 2016. Scheelite, apatite, calcite and tourmaline compositions from the late Archean Hutti orogenic gold deposit: implications for analogous two stage ore fluids. Ore Geology Reviews, **72**: 989–1003; https://doi.org/10.1016/j.oregeorev.2015.09.004

Hemalová, K., 2010. Fluid inclusions in Au-quartz veins from Padr and Sobětice localities (in Czech with English summary). Diploma Thesis, Faculty of Science, Charles University, Prague.

Holčík, J., Komenda, M. (eds.), 2015. Matematická biologie: e-learningová učebnice (in Czech). Masarykova univerzita, Brno; https://portal.matematickabiologie.cz

Holub, M., Páša, J., 2004. Přehodnocení zásob malých ložisek scheelitových rud (W), stav ke dni 30.11.2004, závěrečná zpráva (in Czech). Unpublished report, MS CGS Geofond FZ006767.

Hreus, S., Výravský, J., Cempírek, J., Breiter, K., Galiová, M.V., Krátký, O., Šešulka, V., Škoda, R., 2021. Scandium distribution in the world-class Li-Sn-W Cínovec greisen-type deposit: Result of a complex magmatic to hydrothermal evolution, implications for scandium valorization. Ore Geology Reviews, **139**, 104433; https://doi.org/10.1016/j.oregeorev.2021.104433

Hsu, L., 1977. Effects of oxygen and sulfur fugacities on the scheelite tungstenite and powellite-molybdenite stability relations. Economic Geology, **72**: 664–670.

Hsu, L.C., Galli, P.E., 1973. Origin of the scheelite-powellite series of minerals. Economic Geology, **68:** 681–696.

Hujsl, J., 1988. Horažďovicko – Scheelity – vyhledávací průzkum (in Czech). Unpublished report, MS CGS Geofond P068156.

Hujsl, J., Blüml, A., Holub, F., Kořán, J., Macourek, K., Morvicová, L., Slačík, J., 1987. Dílčí závěrečná zpráva úkolu Wolfram – moldanubikum. Lokalita: Vrbík. Surovina: W rudy. Etapa průzkumu: vyhledávací (in Czech). Unpublished report, MS CGS Geofond Praha, P 056551.

Ishihara, S., 1977. The Magnetite-Series and Ilmenite-Series Granitic Rocks. Mining Geology, **27**: 293–305.

Janoušek, V., Braithwaite, C.J.R., Bowes, D.R., Gerdes, A., 2004. Magma mixing in the genesis of Hercynian calc-alkaline granitoids: an integrated petrographic and geochemical study of the Sázava intrusion, Central Bohemian Pluton, Czech Republic. Lithos, **78**: 67–99; https://doi.org/10.1016/j.lithos.2004.04.046

Janoušek, V., Wiegand, B.A., Žák, J., 2010. Dating the onset of Variscan crustal exhumation in the core of the Bohemian Massif: new U-Pb single zircon ages from the high-K calc-alkaline granodiorites of the Blatná suite, Central Bohemian Plutonic Complex. Journal of the Geological Society: **167**: 347–360; https://doi.org/10.1016/j.lithos.2004.04.046

Jochum, K.P., Nohl, U., Herwig, K., Lammel, E., Stoll, B., Hofmann, A.W., 2005. GeoReM: a new geochemical database for reference materials and isotopic standards. Geostandards and Geoanalytical Research, **29**: 333–338; https://doi.org/10.1111/j.1751-908X.2005.tb00904.x

Jurák, L., Hranáč, P., Anft, A., Novosad, I., Páša, J., Procházka, J., 1986. Dílčí závěrečná zpráva úkolu Wolfram - moldanubikum. Lokalita: Cetoraz. Surovina: W rudy. Etapa průzkumu: vyhledávací (in Czech). Unpublished report, MS CGS Geofond Praha, P 057675.

Kempe, U., Belyatsky, B., Krymsky, R., Kremenetsky, A.A., Ivanov, P.A., 2001. Sm-Nd and Sr isotope systematics of scheelite from the giant Au(-W) deposit Muruntau (Uzbekistan): implications for the age and sources of Au mineralization. Mineralium Deposita, **36**: 379–392; https://doi.org/10.1007/s001260100156

Kent, A.J.R., Campbell, I.H., Mcculloch, M.T., 1995. Sm-Nd systematics of hydrothermal scheelite from the Mount Charlotte Mine, Kalgoorlie, Western Australia; an isotopic link between gold mineralization and komatiites. Economic Geology, **90**: 2329–2335; https://doi.org/10.2113/gsecongeo.90.8.2329

Kovář, J., Mandík, L., 1993. Závěrečná zpráva ložiska Čelina (in Czech). Unpublished report. MS CGS Geofong FZ006626.

Large, R.R., Danyushevsky, L., Hollit, C., Maslennikov, V., Meffre, S., Gilbert, S., Bull, S., Scott, R., Emsbo, P., Thomas, H., Singh, B., Foster, J., 2009. Gold and trace element zonation in pyrite using a laser imaging technique: implications for the timing of gold in orogenic and Carlin-style sediment-hosted deposits. Economic Geology, **104**: 635–668; https://doi.org/10.2113/gsecongeo.104.5.635

Large, R.R., Halpin, J.A., Danyushevsky, L.V.,, Maslennikov, V.V., Bull, S.W., Long, J.A., Gregory, D.D., Lounejeva, E., Lyons, T.W., Sack, P.J., McGoldrick, P.J., Calver, C.R., 2014. Trace element content of sedimentary pyrite as a new proxy for deep-time ocean–atmosphere evolution. Earth and Planetary Science Letters, **389**: 209–220; https://doi.org/10.1016/j.epsl.2013.12.020

Lin, Y.E., Cook, N.J., Ciobanu, C.L., Liu, Y.P., Zhang, Q., Liu, T.G., Gao, W., Yang, Y.L., Danyushevskiy, L.V., 2011 Trace and minor elements in sphalerite from base metal deposits in South China: a LA-ICPMS study. Ore Geology Reviews, **39**: 188–217; https://doi.org/10.1016/j.oregeorev.2011.03.001

Liu, Y., Deng, J., Li, C., Shi, G., Zheng, A., 2007. REE composition in scheelite and scheelite Sm-Nd dating for the Xuebaoding W-Sn-Be deposit in Sichuan. Chinese Science Bulletin, **52**: 2543–2550; https://doi.org/10.1007/s11434-007-0355-1

Losertová, L., 2011. Mineralogie rudních výskytů v okolí Humpolce (in Czech). MS, Bc. Thesis. PřMU Brno.

Losertová, L., Buřival, Z., Losos, Z., Houzar, S., 2013. Mineral assemblage and chemical composition of Mg-wolframite and scheelite from Cetoraz by Pacov, Czech Republic (in Czech with English summary). Acta Musei Moraviae, Scientiae Geologicae, **98**: 41–48.

Losertová, L., Buřival, Z., Losos, Z., 2014. Mineral assemblage of Sn-W ores from Ovesná Lhota near Světlá nad Sázavou, Czech Republic (in Czech with English summary). Acta Musei Moraviae, Scientiae Geologicae , **99**: 69–76.

Malásek, F., 1957. Výroční zpráva o prospekčních pracích z r. 1956 (in Czech). MS, Geofond Praha.

Malec, J., 1985. Scheelite genesis on selected localities (in Czech). MS, Geofond Praha.

Manéglia, N., Beaudoin, G., Simard, M., 2018. Indicator minerals of the Meliadine orogenic gold deposits, Nunavut (Canada), and application to till surveys. Geochemistry Exploration Environmental Analyses, **18**: 241–251; https://doi.org/10.1144/geochem2017-036

McClenaghan, M., Parkhill, M., Pronk, A., Seaman, A., McCurdy, M., Leybourne, M., 2017. Indicator mineral and geochemical signatures associated with the Sisson W-Mo deposit, New Brunswick, Canada. Geochemistry Exploration Environmental Analysis, **17**: 297–313; https://doi.org/10.1144/geochem2015-396

Miranda, A.C.R., Beaudoin, G., Rottier, B., 2022. Scheelite chemistry from skarn systems: implications for ore-forming processes and mineral exploration. Mineralium Deposita, **57**: 1469–1497; https://doi.org/10.1007/s00126-022-01118-y

Miranda, A.C.R., Beaudoin, G., Rottier, B., Pašava, J., Bohdálek, P., Malec, J., 2024. Trace element signatures in scheelite associated with various deposit types: a tool for mineral targeting. Journal of Geochemical Exploration, **266**, 107555; https://doi.org/10.1016/j.gexplo.2024.107555

Morávek, P., 1971. Ore-deposits structure and mineralization of the Jílové gold-mining district. Sborník Geologických Věd ložisková Geologie, **13**: 7–170.

Moravek, P. (ed.), 1992. Gold in the Bohemian Massif (in Czech). Czech Geological Survey, Praha.

Morávek, P. (ed.), 1995a. Gold Deposits of the Central and SW Part of the Bohemian Massif. Excursion Guide, Third Biennial SGA Meeting Mineral Deposits: from Their Origin to Their Environmental Impacts, Prague, August 28–31, 1995. Czech Geological Survey.

Morávek, P., 1995b. Gold metallogeny of Central and Western European Variscides. In: Mineral Deposits from Their Origin to Their Environmental Impacts (eds. J. Pašava, B. Kříbek and K. Žák): 67–70. AA Balkema, Rotterdam.

Morávek, P. (ed.), 1996. Gold deposits in Bohemia. Czech Geological Survey, Prague.

Morávek, P., Punčochář, K., 1983. A new perspective type of a metamorphogenic Au-W mineralization in the Kašperské hory district (in Czech). Geologický Průzkum, **25**: 193–196.

Mueller, A.G., Nemchin, A.A., Frei, R., 2004. The Nevoria gold skarn deposit, southern cross greenstone belt, Western Australia; II, pressuretemperature-time path and relationship to postorogenic granites. Economic Geology, **99**: 453–478; https://doi.org/10.2113/gsecongeo99.3.453

Nassau, K., 1963. Calcium tungstate – IV: the theory of coupled substitution. Journal of Physics and Chemistry of Solids, **24**: 1511–2151.

Nassau, K., Loiacono, G.M., 1963. Calcium tungstate—III: trivalent rare earth substitution. Journal of Physics and Chemistry of Solids, **24**: 1503–1510.

Němec, D., Tenčík, I., 1976. Regionally metamorphosed greisens at Cetoraz, the Bohemian-Moravian Heights (Českomoravská vrchovina), Czechoslovakia. Mineralium Deposita, **11**: 210–217.

Newall, P., 2015. Competent person's report on the Cinovec – lithium project, Czech Republic. Wardell Armstrong International for European Metals Holding. Wardel Armstrong International, Truro, UK.

Newberry, R., 1983. The formation of subcalcic garnet in scheelite bearing skarns. Canadiam Mineralogist, **21**: 529–544.

Newberry, R., Swanson, S., 1986. Scheelite Skarn Granitoids: An evaluation of the roles of magmatic source and process. Ore Geology Reviews, **1**: 57–81; https://doi.org/10.1016/0169-1368(86)90005-3

Pašava, J., Frimmel, H., Vymazalová, A., Dobeš, P., Jukov, A.V., Koneev, R., 2013. A two stage evolution model for the Amantaytau orogenic-type gold deposit in Uzbekistan. Mineralium Deposita, **48**: 825–840; https://doi.org/10.1007/s00126-013-0461-8

Pašava, J., Svojtka, M., Veselovský, F., Ďurišová, J., Ackerman, L., Pour, O., Drábek, M., Halodová, P., Haluzová, E., 2016. Laser ablation ICP-MS study of trace element chemistry in molybdenite—an important tool for identification of different types of mineralization. Ore Geology Reviews, **72**: 874–895; https://doi.org/10.1016/j.oregeorev.2015.09.007

Pašava, J., Ackerman, L., Halodová, P., Pour, O., Ďurišová, J., Zaccarini, F., Aiglsperger, T., Vymazalová, A., 2017. Concentrations of platinum-group elements (PGE), Re and Au in arsenian pyrite and millerite from Mo-Ni-PGE-Au black shales (Zunyi region, Guizhou Province, south China): results from LA-ICPMS study. European Journal of Mineralogy, **29**: 623–633; https://doi.org/https://doi.org/10.1127/ejm/2017/0029-2640

Paton, C., Hellstrom, J., Paul, B., Woodhead, J., Hergt, J., 2011. Iolite: freeware for the visualization and processing of mass spectrometric data. Journal of Analytical Atomic Spectrometry, **26**: 2508–2518; https://doi.org/10.1039/c1ja10172b

Pattan, J.N., Pearce, N.J.G., Mislankar, P.G., 2005. Constraints in using Cerium-anomaly of bulk sediments as an indicator of paleo bottom water redox environment: A case study from the Central Indian Ocean Basin. Chemical Geology, **221**: 260–278; https://doi.org/10.1016/j.chemgeo.2005.06.009

Peng, J., Zhang, D., Hu, R., Wu, M., Lin, Y., 2010. Sm/Nd and Sr isotope geochemistry of hydrothermal scheelite from the Zhazixi W-Sb deposit, western Hunan (in Chinese with English summary). Acta Geologica Sinica, **82**: 1514–1521.

Pertold, Z., Punčochář, M., 1996. The Kašperské Hory ore district. In: Gold Deposits in Bohemia (ed. P. Morávek): 79–96. Czech Geological Survey, Prague.

Poulin, R.S., 2016. A Study of the Crystal Chemistry, Cathodoluminescene, Geochemistry and Oxygen Isotopes in Scheelite: Application towards Discriminating among Diering Ore-Deposit Systems. Ph.D. Thesis, Laurentian University, Sudbury, ON, Canada.

Poulin, R.S., McDonald, A.M., Kontak, D.J., McClenaghan, M.B., 2016. On the relationship between cathodoluminescence and the chemical composition of scheelite from geologically diverse ore-deposit environments. Canadian Mineralogist, **54**: 1147–1173; https://doi.org/10.3749/canmin.1500023

Poulin, R.S., Kontak, D.J., McDonald, A., McClenaghan, M.B., 2018. Assessing scheelite as an ore-deposit discriminator using its trace element and REE chemistry. Canadian Mineralogist, **56**: 265–302; https://doi.org/10.3749/canmin.1800005

Punčochář, M., 1992. Závěrečná zpráva úkolu Kašperské hory. Surovina Au a W rudy. Etapa: vyhledávací (in Czech). Unpublished report, Geofond Praha FZ006375.

Raimbault, L., Baumer, A., Dubru, M., Benkerrou, C., Croze, V., Zahm, A., 1993. REE fractionation between scheelite and apatite in hydrothermal conditions. American Mineralogist, **78**: 1275–1285.

Ren, Y.S., Zhao, H.L., Lei, E., Wang, H., Ju, N., Wu, C.Z., 2010. Trace element and rare earth element geochemistry of the scheelite and ore genesis of the Yangjingou large scheelite deposit in Yanbian area, northeastern China. China Acta Petrologica Sinica, **26**: 3720–3726.

Roberts, S., Palmer, M.R., Waller, L., 2006. Sm-Nd and REE characteristics of tourmaline and scheelite from the Bjorkdal gold deposit, northern Sweden: evidence of an intrusion-related gold deposit? Economic Geology, **101**: 1415–1425; https://doi.org/10.2113/gsecongeo.101.7.14

Roos, E., Veselovský, F., 1985. Ložiskové zhodnocení scheelitových indicií ve středních Krušných horách. MS CGS Geofond Praha, P049200.

Sciuba, M., Beaudoin, G., Grzela, D., Makvandi, S., 2020. Trace element composition of scheelite in orogenic gold deposits. Mineralium Deposita, **55**: 1149–1172; https://doi.org/10.1007/s00126-019-00913-4

Seifert, T., Atanasova, P., Gutzmer, J., Pfänder, J., 2011. Mineralogy, geochemistry and age of greisen mineralization in the Li-Rb-Cs-Sn-W deposit Zinnwald, Erzgebirge, Germany Goldschmidt Conference Abstracts: 1833.

Seifert, T., Pavlova, G.G., 2016. New ^{40}Ar/ ^{39}Ar ages of Sn- and W-polymetallic mineralization in the Erzgebirge / Krušné hory (DE, CZ). Goldschmidt Conference Abstracts: 2792.

Seltmann, R., Štemprok, M., 1995 Metallogenic overview of the Krušné hory Mts. (Erzgebirge) region. Excursion Guide. Ore Mineralizations of the Krušné hory Mts. (Erzgebirge). Czech Geological Survey, Prague.

Shore, M., Fowler, A.D., 1996. Oscillatory zoning in minerals: A common phenomenon. Canadian Mineralogist, **34**: 1111–1126.

Song, G., Qin, K., Li, G., Evans, N.J., Chen, L., 2014. Scheelite elemental and isotopic signatures; implications for the genesis of skarn-type W-Mo deposits in the Chizhou area, Anhui Province, eastern China. American Mineralogist, **99**: 303–317; https://doi.org/10.2138/am.2014.4431

Starý, J., 2019. Ložiskově-geologická studie revíru Cínovec – ložiska Cínovec-Jih, Cínovec-Severozápad a Cínovec-Východ (úkol č.3 pro naplnění Usnesení vlády ČR č.713/2017) (in Czech). Unpublished report, Geofond Praha P000076/2019.

Strnad, L., Goliáš, V., Mihaljevič, M., Pudilová, M., 2012. The Variscan orogenic gold deposit, Bohemian Massif, Czech Republic. Ore Geology Reviews, **48**: 428–441; https://doi.org/10.1016/j.oregeorev.2012.06.001

Studničný, I., 1994. Závěrečná zpráva úkolu Vacíkov. Surovina: zlato (Cu, W). Etapa průzkumu: vyhledávací. Stav ke dni: 31.4.1994 (in Czech). Unpublished report. Geofond Praha FZ006423.

Suček, P., Beran, P., Farka, O., Holub, M., Jangl, L., Kozubek, P., Ludvík, V., Majer, J., Osvald, P., Pavlů, D., 1995. Závěrečná likvidační zpráva závodu Stannum Horní Slavkov (in Czech). Unpublished report, Geofond Praha FZ006630.

Sun, K., Chen, B., 2017. Trace elements and Sr-Nd isotopes of scheelite; implications for the W-Cu-Mo polymetallic mineralization of the Shimensi Deposit, south China. American Mineralogist, **102**: 1114–1128; https://doi.org/10.2138/am-2017-5654

Sung, Y.H., Brugger, J., Ciobanu, C.L., Pring, A., Skinner, W., Danyushevsky, L.V., Nugus, M., 2009. Invisible gold in arsenian pyrite and arsenopyrite from a multistage Archean gold deposit: Sunrise Dam, Eastern Goldfields Province, Western Australia. Mineralium Deposita, **44**: 765–791; https://doi.org/10.1007/s00126-009-0244-4

Sverjensky, D.M., 1984. Europium redox equilibrium in aqueous solutions. Earth and Planetary Science Letters, **67**: 70–78; https://doi.org/10.1016/0012-821X(84)90039-6

Šponar, P., Páša, J., Komínek, E., Procházka, Z., Doležalová, J., Hošek, M., Příhodová, A., Hranáč, P., Luna, P., Tenčík, I., 1985 Revize šlichových anomálií. Etapa: vyhledávací (in Czech). Unpublished report, MS CGS Geofond P047303.

Šrein, V., Litochleb, J., Šreinová, B., 1998. Selected skarn and associated metamorphogenic mineralizations of the Bohemian Massif (in Czech with English summary). Bulletin mineralogicko-petrologického oddělení Národního muzea v Praze, **6:** 132–146.

Šrein, V., Šreinová, B., 2000. Mineralogy of the skarns of the Bohemian part of the western and central Krušné hory Mountains. Acta Montana, **A17**: 67–108.

Štemprok, M., 1965. Petrology and the vertical extent of mineralization in the Cínovec (Zinnwald) granite cupola (in Czech with English summary). Sborník geologických Věd, ložisková Geologie Mineralogie, **5**: 7–106.

Štemprok, M., 1985. Zhodnocení ložiskového významu kontaktního skarnu u Hazlova (in Czech). Unpublished, MS CGS Geofond Praha, P049329.

Štemprok, M., Mašková, A., 1992. Scheelite mineralization of the Bohemian Massif. Zentralblatt für Geologie und Paläontologie, Teil **1/2**: 117–129.

Štemprok, M., Seltmann, R., Breiter, K., 1995. The Cinovec/Zinnwald Sn-W-Li deposit. Excursion Guide. Ore Mineralizations of the Krušné hory Mts. (Erzgebirge). Czech Geological Survey, Prague.

Thomas, H.V., Large, R.R., Bull, S.W., Maslennikov, V., Berry, R.F., Fraser, R., Froud, S., Moye, R., 2011. Pyrite and pyrrhotite textures and composition in sediments laminated quartz veins, and reefs at Bendigo Gold Mine, Australia: insights for ore genesis. Economic Geology, **106**: 1–31; https://doi.org/10.2113/econgeo.106.1.1

Tuček, K., 1970. Naleziště českých nerostů a jejich literature (in Czech). Academia, Praha.

Tyson, R.M., Hemphill, W.R., Theisen, A.R., 1988. Effect of the W:Mo ratio on the shift of excitation and emission spectra in the scheelite-powellite series. American Mineralogist, **73**: 1145–1154.

Uspensky, E., Brugger, J., Graeser, S., 1998. REE geochemistry systematics of scheelite from the Alps using luminescence spectroscopy: from global regularities to facies control. Schweizerische Mineralogische und Petrographische Mitteilungen, **78**: 33–56.

Veselovský, F., Ackerman, L., Pašava, J., Žák, K., Haluzová, E., Creaser, R.A., Dobeš, P., Erban, V., Tásler, R., 2018. Multiphase formation of the Obří důl polymetallic skarn deposit, West Sudetes, Bohemian Massif: geochemistry and Re-Os dating of sulfide mineralization. Mineralium Deposita, **53**: 665–682; https://doi.org/10.1007/s00126-017-0766-0

Whitney, D.L., Evans, B.W., 2010. Abbreviations for names of rock-forming minerals. American Mineralogist, **95**: 185–187; https://doi.org/10.2138/am.2010.3371

Winderbaum, L., Ciobanu, C.L., Cook, N.J., Paul, M., Metcalfe, A., Gilbert, S., 2012. Multivariate analysis of a LA–ICP-MS trace element dataset for pyrite. Mathematical Geosciences, **44**: 823–842; https://doi.org/10.1007/s11004-012-9418-1

Xiong, D.X., Sun, X.M., Shi, G.Y., Wang, S.W., Gao, J.F., Xue, T., 2006. Trace elements, rare earth elements (REE) and Nd-Sr isotopic compositions in scheelites and their implications for the mineralization in Daping gold mine in Yunnan province, China. China Acta Petrologica Sinica, **22**: 733–741.

Yuan, L., Chi, G., Wang, M., Li, Z., Xu, D., Deng, T., Geng, J., Hu, M., Zhang, L., 2019. Characteristics of REEs and trace elements in scheelite from the Zhuxi W deposit, South China: Implications for the ore-forming conditions and processes. Ore Geology Reviews, **109**: 585–597; https://doi.org/10.1016/j.oregeorev.2019.05.003

Zachariáš, J., Stein, H.J., 2001. Re-Os ages of Variscan hydrothermal gold mineralisations, Central Bohemian metallogenic zone, Czech Republic. In: Mineral Deposits at the Beginning of the 21st century (ed. A. Piestrzynski): 851–854. Balkema, Lisse.

Zachariáš, J., Pertold, Z., Pudilová, M., Žák, K., Pertoldová, J., Stein, H., Markey, R., 2001. Geology and genesis of Variscan porphyry-style gold mineralization, Petráčkova hora deposit, Bohemian Massif, Czech Republic. Mineralium Deposita, **36**: 517–541; https://doi.org/10.1007/s001260100187

Zachariáš, J., Žák, K., Pudilová, M., Snee, L.W., 2013. Multiple fluid sources/pathways and severe thermal gradients during formation of the Jílové orogenic gold deposit, Bohemian Massif, Czech Republic. Ore Geology Reviews, **54**: 81–109; https://doi.org/10.1016/j.oregeorev.2013.02.012

Zachariáš, J., Morávek, P., Gadas, P., Pertoldová, J., 2014. The Mokrsko-West gold deposit, Bohemian Massif, Czech Republic: mineralogy, deposit setting and classification. Ore Geology Reviews, **58**: 238–263; https://doi.org/10.1016/j.oregeorev.2013.11.005

Zhang, R., Lehmann, B., Seltmann, R., Sun, W., Li, C., 2017. Cassiterite U-Pb geochronology constrains magmatic-hydrothermal evolution in complex evolved granite systems: the classic Erzgebirge tin province (Saxony and Bohemia). Geology, **45**: 1095–1098; https://doi.org/10.1130/G39634.1

Zhang, Q., Zhang, R.Q., Gao, J.F. Lu, J.J., Wu, J.W., 2018. In-situ LA-ICP-MS trace element analyses of scheelite and wolframite: Constraints on the genesis of veinlet-disseminated and vein-type tungsten deposits, South China. Ore Geology Reviews, **99**: 166–179; https://doi.org/10.1016/j.oregeorev.2018.06.004

Zhao, W.W., Zhou, M.F., Williams-Jones, A.E., Zhao, Z., 2018. Constraints on the uptake of REE by scheelite in the Baoshan tungsten skarn deposit, South China. Chemical Geology, **477**: 123–136; https://doi.org/10.1016/j.chemgeo.2017.12.020

Zhigang, Z., Chaoyang, L., Yuping, L., Guangzhi, T., 1998. REE geochemistry of scheelite of two genetic types from Nanyangtian, southeastern Yunnan, China. Geology Geochemistry, **26**: 34–38.

Žáček, V., 2008. Cu-skarn in Kotel, Krkonoše Mts. (Czech Republic) (in Czech with English summary). Bulletin mineralogicko-petrologického oddělení Národního muzea v Praze, **16/2**: 230–237; https://publikace.nm.cz/periodicke-publikace/bmpholnrhmvp/16-2/cu-skarn-v-kotli-v-krkonosich-ceska-republika

Žaludková, K., Losos, Z., Večeřa, J., 2010. Scheelite mineralisation of the Ca-skarns in Žulová Batholith and Třebíč Batholith (Czech Republic) (in Czech with English summary). Acta rerum naturalium, **8**: 1–16.

APPENDIX 1

Basic statistical data on LA-ICP-MS trace element distribution in scheelite in individual deposits within the mineral deposit groups studied

Source file	Category	Na (ppm)	Mg (ppm)	Si (ppm)	K (ppm)	Ti (ppm)	V (ppm)	Mn (ppm)	Ni (ppm)	Cu (ppm)	Zn (ppm)	As (ppm)	Sr (ppm)	Y (ppm)	Nb (ppm)	Mo (ppm)	Ag (ppm)	Sn (ppm)	Sb (ppm)	La (ppm)	Ce (ppm)	Pr (ppm)	Nd (ppm)	Sm (ppm)	Eu (ppm)	Gd (ppm)	Tb (ppm)	Dy (ppm)	Ho (ppm)	Er (ppm)	Tm (ppm)	Yb (ppm)	Lu (ppm)	Hf (ppm)	Ta (ppm)	Pb (ppm)	Bi (ppm)	Th (ppm)	U (ppm)	LREE	HREE
DL min		*0.26*	*0.008*	*45.1*	*0.48*	*0.067*	*0.001*	*0.10*	*0.03*	*0.04*	*0.04*	*0.03*	*0.001*	*0.0007*	*0.001*	*0.005*	*0.003*	*0.009*	*0.004*	*0.0009*	*0.001*	*0.0008*	*0.004*	*0.003*	*0.002*	*0.005*	*0.0006*	*0.002*	*0.0006*	*0.002*	*0.0007*	*0.002*	*0.0006*	*0.003*	*0.0005*	*0.002*	*0.001*	*0.001*	*0.001*		
DL max		*0.78*	*0.20*	*175.6*	*2.10*	*0.55*	*0.64*	*0.31*	*0.4*	*0.5*	*0.7*	*0.1*	*0.8*	*0.09*	*0.5*	*0.09*	*1.3*	*0.95*	*3.5*	*0.20*	*0.58*	*0.39*	*0.13*	*0.48*	*0.80*	*0.49*	*0.29*	*0.47*	*0.19*	*0.23*	*0.20*	*0.58*	*0.23*	*0.22*	*0.22*	*0.15*	*0.13*	*0.24*	*0.22*		
Greisen-/greisenized Q vein - related deposits																																									
H.Babákov	Mean	452.0	278.5	67.3	12.2	2.7	0.3	76.3	1.4	1.2	5.9	10.6	269.6	514.5	44.1	10.9	0.05	0.39	0.02	100.93	586.23	99.73	818.59	311.08	18.73	357.43	46.15	346.05	46.92	124.50	11.98	72.74	5.68	0.16	0.84	5.50	0.04	0.11	0.06	2292.73	654.03
n=12	SD	125.2	24.9	41.1	3.1	0.7	0.3	6.7	3.8	3.4	19.2	9.8	25.1	176.2	18.9	1.2	0.11	0.09	0.02	5.11	43.19	9.24	39.77	7.41	1.17	13.18	2.62	40.95	7.11	26.01	2.92	19.34	1.61	0.02	0.29	1.00	0.06	0.21	0.07	87.01	100.13
SCH-37	Max	792.3	318.3	132.1	17.4	4.6	1.3	93.8	13.9	12.5	69.5	43.1	333.3	950.8	73.3	13.2	0.42	0.65	0.06	107.03	642.18	113.29	899.33	324.57	21.60	381.42	52.13	443.41	63.11	182.23	18.26	113.56	9.23	0.20	1.30	7.05	0.21	0.80	0.28	2470.22	881.64
	Min	331.4	243.0	bdl	7.4	1.8	0.1	69.5	0.2	bdl	bdl	6.9	233.4	373.1	23.8	9.2	0.00	0.29	0.01	89.93	517.08	83.96	739.48	299.41	17.38	336.66	42.91	306.50	40.05	100.91	9.20	54.21	4.10	0.13	0.55	4.32	0.01	0.02	0.01	2136.93	558.62
	Median	431.7	285.2	67.4	11.7	2.6	0.1	74.0	0.2		0.1	7.9	264.1	465.0	39.5	10.8	0.02	0.38	0.01	102.44	601.18	102.37	821.49	309.34	18.57	359.59	45.78	335.96	45.34	119.40	11.38	68.18	5.25	0.17	0.64	5.08	0.02	0.04	0.04	2295.92	632.58
	RSD (%)	0.3	0.1	0.6	0.3	0.2	1.2	0.1	2.7	2.8	3.2	0.9	0.1	0.3	0.4	0.1	213.73%	23.69%	91.21%	5.06%	7.37%	9.26%	4.86%	2.38%	6.25%	3.69%	5.68%	11.83%	15.15%	20.89%	24.40%	26.59%	28.40%	10.62%	35.02%	18.24%	129.23%	189.13%	114.61%	3.79%	15.31%
Ovesná Lhota	Mean	140.0	4.6	60.5	10.7	1.5	0.02	38.0	8.2	2.4	9.7	1.0	241.1	531.6	46.2	2.2	0.05	0.41	0.09	79.55	296.43	30.39	146.29	42.79	45.31	54.12	9.90	92.93	15.27	52.03	6.66	54.71	5.68	0.04	2.99	11.53	1.77	0.23	0.09	694.87	237.18
n=9	SD	54.6	0.3	53.4	2.5	0.3	0.04	4.4	14.7	6.5	19.0	0.5	20.5	257.2	28.5	1.4	0.06	0.11	0.20	34.92	96.29	11.46	80.19	30.43	18.43	46.23	8.24	73.48	11.92	34.89	3.38	21.64	2.09	0.04	1.82	1.61	3.88	0.23	0.07	265.26	154.01
SCH-38	Max	237.0	5.3	154.3	15.6	1.9	0.1	46.4	44.5	20.9	57.0	2.0	272.3	1081.4	108.8	6.1	0.19	0.67	0.65	158.46	471.91	55.88	333.18	113.70	90.07	167.50	29.83	268.69	43.98	134.00	14.19	99.52	9.65	0.14	7.14	14.14	12.61	0.61	0.22	1291.77	599.85
	Min	59.8	4.1	bdl	7.8	1.0	0.001	31.5	0.2	bdl	bdl	0.5	209.3	294.7	20.7	1.5	0.01	0.30	0.00	36.75	153.60	18.01	76.73	15.01	24.78	17.49	3.21	32.55	5.43	22.48	3.60	29.16	2.96	0.01	1.31	8.67	0.01	0.03	0.01	368.84	104.85
	Median	125.9	4.5	44.5	10.3	1.5	0.01	37.9	0.3	0.1	0.2	1.0	239.6	357.0	30.1	1.7	0.03	0.38	0.02	74.92	286.62	24.78	97.86	27.08	40.10	31.25	5.42	51.15	8.37	30.29	4.66	50.46	6.30	0.03	1.90	11.63	0.06	0.09	0.07	739.02	143.40
	RSD (%)	39.0	7.6	88.1	23.2	19.6	187.2	11.6	180.0	265.7	195.3	45.8	8.5	48.4	61.7	64.5	124.19	26.00	213.39	43.90	32.49	37.70	54.81	71.11	40.67	85.42	83.26	79.07	78.05	67.06	50.77	39.55	36.83	90.18	61.01	13.97	219.39	98.65	79.90	38.17	64.93
Cetoraz	Mean	153.2	6.3	75.8	10.8	3.9	0.3	279.8	6.8	6.4	0.4	10.0	651.1	301.7	177.1	35.0	1.4	1.4	0.01	117.98	408.06	49.32	256.52	64.66	30.57	57.05	7.04	51.43	7.37	25.63	3.80	37.49	3.88	0.03	2.54	41.74	2.64	1.63	2.15	984.18	136.65
n=11	SD	111.4	4.5	50.7	2.4	4.8	0.6	106.4	13.9	11.1	0.9	8.8	313.9	213.8	126.1	48.0	4.3	1.3	0.01	93.52	347.89	43.65	228.54	56.10	23.40	46.35	5.13	34.14	4.43	13.71	1.76	14.83	1.34	0.02	1.87	28.04	3.31	1.17	3.42	828.07	74.74
SCH-39	Max	304.4	15.3	180.7	15.6	16.7	2.1	481.5	37.5	33.4	2.9	23.1	1494.3	583.8	361.4	153.5	15.0	5.1	0.03	257.29	824.27	105.78	522.64	130.24	65.61	110.92	13.04	91.32	12.70	43.65	6.34	61.44	6.19	0.07	7.37	123.02	12.23	4.82	12.65	1961.85	231.56
	Min	15.7	3.2	bdl	6.7	1.0	0.0	156.4	0.2	bdl	bdl	0.4	296.8	56.3	9.6	0.4	bdl	0.1	0.00	11.63	14.82	1.30	5.25	2.21	7.37	3.38	0.85	10.16	1.98	8.92	1.72	20.02	2.31	bdl	0.50	21.32	0.06	0.40	0.14	45.96	48.29
	Median	189.7	3.7	63.9	10.4	1.3	0.1	283.4	0.2			14.0	567.1	294.8	243.9	5.1		1.4	0.01	163.60	601.87	55.32	271.33	60.74	22.16	57.82	7.13	53.65	7.99	27.66	3.93	38.27	3.83	0.04	2.66	31.00	2.06	1.56	1.09	1326.53	142.47
	RSD (%)	72.7	72.4	66.8	22.0	121.5	189.3	38.0	205.0	174.4	206.9	88.2	48.2	70.9	71.2	137.3	296.0	98.8	84.21	79.26	85.26	88.50	89.09	86.76	76.55	81.24	72.88	66.39	60.16	53.47	46.33	39.57	34.44	62.38	73.87	67.17	125.18	71.78	159.22	84.14	54.69
Krásno-Huber	Mean	7.6	11.8	63.8	11.3	0.8	0.2	3.7	1.6	1.1	5.4	2.4	234.3	0.4	7.9	1.5	0.2	0.2	0.27	0.37	0.43	0.05	0.37	0.11	0.12	0.15	0.02	0.12	0.02	0.05	0.01	0.07	0.01	0.001	0.39	0.20	0.44	0.03	0.11	1.61	0.29
n=8	SD	11.8	3.8	95.1	3.5	0.5	0.3	1.1	4.1	2.3	11.0	6.3	51.8	0.7	1.4	3.1	0.4	0.2	0.39	0.11	0.35	0.05	0.72	0.29	0.12	0.34	0.04	0.26	0.04	0.08	0.01	0.07	0.01	0.002	0.01	0.12	1.06	0.02	0.09	1.81	0.48
SCH-43	Max	37.5	16.7	290.5	18.1	1.3	0.8	6.0	12.5	7.1	33.4	19.2	311.2	2.2	10.1	9.7	1.3	0.6	1.11	0.53	1.25	0.15	2.21	0.88	0.28	1.06	0.12	0.80	0.12	0.27	0.03	0.19	0.02	0.01	0.41	0.36	3.24	0.08	0.33	6.35	1.54
	Min	0.4	8.4	bdl	7.2	bdl	bdl	2.7	bdl	bdl	bdl	bdl	157.8	bdl	6.3	bdl	bdl	0.0	0.00	0.20	0.00	0.00	0.00	0.00	bdl	0.01	bdl	bdl	bdl	bdl	bdl	0.02	bdl	bdl	0.38	0.01	bdl	0.01	0.04	0.52	0.04
	Median	2.1	9.8	10.4	10.4	0.9	0.1	3.5	0.1	0.1			232.4	0.1	7.8	0.4		0.1	0.01	0.35	0.32	0.02	0.05		0.09	0.01		0.01		0.01		0.03	0.01		0.38	0.22	0.01	0.02	0.08	1.03	0.06
	RSD (%)	155.2	31.8	149.1	30.9	63.1	127.5	28.1	252.4	215.2	204.0	263.8	22.1	186.2	17.3	205.9	263.8	127.4	146.34	29.74	81.26	108.00	192.67	257.37	93.80	224.42	222.99	223.92	218.62	169.62	156.13	94.13	101.42	153.30	2.35	61.83	242.98	79.81	80.32	112.71	167.78
Cínovec 1-Voj.jáma 3.p.	Mean	14.6	23.7	46.8	13.8	7.2	5.0	85.3	0.3	14.3	55.8	11485.6	283.4	24.7	35.2	4639.1	9.0	9.5	0.71	0.60	8.76	2.94	17.87	11.45	0.66	8.59	1.83	12.31	1.76	5.77	1.10	11.91	1.66	1.35	3.57	5947.81	3187.69	219.77	2534.25	50.87	36.35
n=9	SD	4.9	5.8	48.8	4.2	3.7	2.5	24.5	0.2	8.7	15.5	1171.3	36.7	34.8	11.4	1035.9	3.7	8.5	0.57	0.73	11.97	3.70	20.82	10.13	0.34	8.31	1.76	13.30	2.18	7.91	1.61	18.33	2.71	1.57	1.95	5101.23	4085.02	114.03	283.89	54.35	47.08
SCH-47	Max	20.3	34.8	141.8	18.8	14.3	10.3	110.5	0.6	30.6	73.9	14442.1	339.4	98.1	53.0	6171.6	15.6	32.8	1.64	2.06	35.72	10.90	68.25	36.82	1.17	29.50	6.28	46.57	7.39	26.01	5.12	54.07	7.34	4.52	7.85	14859.10	11662.10	444.52	2998.23	177.69	152.77
	Min	4.2	13.8	bdl	7.5	3.3	1.2	34.9	0.0	0.0	26.1	10049.7	231.3	2.3	16.0	3405.5	1.1	bdl	0.08	0.06	0.58	0.28	2.17	1.75	0.10	1.33	0.28	1.89	0.26	0.62	0.09	0.71	0.04	0.11	1.18	1220.42	183.48	33.36	2051.64	6.28	4.74
	Median	14.3	23.6	36.1	15.2	5.9	4.7	94.9	0.3	12.5	59.4	11370.2	270.9	5.6	40.5	4119.3	9.3	8.0	0.67	0.28	3.41	1.26	8.41	7.72	0.72	5.19	1.09	6.23	0.70	1.61	0.21	1.56	0.13	0.51	3.02	3704.35	939.64	223.23	2585.40	26.93	11.94
	RSD (%)	33.7	24.7	104.2	30.1	51.5	50.7	28.7	62.5	60.9	27.7	10.2	12.9	140.5	32.5	22.3	40.9	89.7	81.22	121.49	136.67	125.90	116.53	88.42	51.19	96.73	96.37	108.05	123.94	137.05	146.45	153.80	163.47	115.59	54.69	85.77	128.15	51.88	11.20	106.83	129.54
Cínovec 2 - 3.p.	Mean	8.1	5.7	88.2	8.9	2.0	0.3	1.5	0.2	2.6	12.7	4892.5	368.1	6.6	17.6	7175.3	0.1	5.1	0.02	0.21	0.22	0.28	1.80	1.49	0.09	1.84	0.56	6.66	1.53	8.01	2.31	32.79	5.01	0.55	1.67	4.49	89.86	0.65	3678.32	5.92	56.87
n=11	SD	5.5	0.9	86.5	1.7	1.9	0.5	2.3	0.1	3.7	7.9	1682.3	71.0	3.5	11.3	4000.8	0.1	9.5	0.03	0.21	0.30	0.31	1.86	1.45	0.19	1.69	0.52	5.61	1.18	5.82	1.60	21.11	3.04	0.61	0.97	8.07	132.79	1.24	1615.56	5.51	38.73
SCH-48	Max	18.1	8.2	321.1	13.5	7.4	1.5	6.8	0.4	12.5	25.3	6769.3	467.0	14.8	41.8	13886.1	0.4	34.8	0.10	0.79	1.11	1.17	7.20	5.55	0.70	6.49	1.99	21.29	4.48	21.81	5.99	79.51	11.72	1.98	3.74	29.61	358.62	4.50	6908.30	21.46	146.79
	Min	0.1	4.7	bdl	6.8	bdl	bdl	bdl	0.1	0.1	1.9	1481.7	207.8	2.8	2.5	1579.0	0.0	bdl	bdl	bdl	bdl	0.05	0.29	0.22	bdl	0.28	0.08	1.14	0.30	1.71	0.50	8.16	1.31	0.06	0.51	0.26	0.59	0.02	1424.75	1.33	13.20
	Median	6.9	5.6	80.6	8.6	1.9	0.1	0.2	0.2	0.9	14.6	5615.6	360.0	5.4	16.3	7478.2	0.0	2.1	0.01	0.16	0.10	0.15	1.07	1.04	0.02	1.35	0.42	5.28	1.25	6.71	1.95	27.80	4.32	0.25	1.36	1.49	9.76	0.20	2995.45	3.93	49.39
	RSD (%)	67.8	15.3	98.0	19.5	94.6	184.3	158.0	33.4	142.4	62.6	34.4	19.3	53.6	64.4	55.8	165.7	185.4	155.36	100.14	135.75	108.85	103.60	97.63	220.50	91.71	92.29	84.12	77.44	72.66	69.31	64.39	60.79	110.43	58.20	179.69	147.78	191.15	43.92	93.14	68.10
Au-orogenic-related	Mean	70.3	10.4	9.0	16.3	1.1	0.3	3.4	2.6	2.6	0.2	19.8	349.1	404.4	2.6	19.2	0.1		0.09	41.45	184.45	29.42	217.71	97.92	218.15	128.88	18.24	117.29	14.63	30.54	2.71	14.79	1.10	0.07	0.41	9.71	0.09	0.11	0.53	917.98	199.29
Jílové	SD	42.1	12.2	15.8	8.2	1.9	0.4	0.7	5.5	4.6	0.4	17.6	29.8	173.9	1.2	8.9	0.1	0.1	0.16	10.55	59.62	12.76	123.17	65.65	97.98	88.99	12.27	75.14	8.85	16.14	1.15	5.51	0.47	0.03	0.04	2.36	0.14	0.07	0.68	321.33	115.85
n=12	Max	152.9	47.3	51.4	37.5	7.4	1.4	4.6	19.5	12.5	1.5	64.2	392.0	653.3	4.5	31.4	0.2	0.2	0.50	58.24	261.32	44.06	369.74	179.17	450.36	238.94	32.64	203.77	24.74	50.87	4.25	25.16	2.14	0.11	0.50	16.82	0.40	0.23	2.30	1233.35	330.92

SCH-41	Min	18.1	2.7	0.0	8.5	bdl	bdl	2.2	0.2	bdl	bdl	4.0	308.6	100.9	1.3	5.9	0.0	bdl	0.00	27.22	67.00	7.09	34.61	10.95	110.09	13.61	2.07	15.12	2.13	5.87	0.78	6.64	0.60	0.01	0.36	7.46	bdl	0.02	bdl	358.58	33.22
	Median	84.3	5.8	0.0	13.6	0.7	0.1	3.3	0.2	0.1		13.8	345.4	462.2	2.3	22.0	0.0		0.00	39.75	209.26	34.61	234.91	95.98	187.51	125.10	18.14	119.61	15.45	34.54	2.96	15.30	0.98	0.07	0.41	9.12	0.01	0.13	0.19	1079.82	213.21
	RSD (%)	59.8	117.4	174.5	50.5	174.0	146.5	20.7	212.8	181.5	260.8	88.8	8.5	43.0	45.0	46.5	107.1		185.22	25.45	32.32	43.38	56.58	67.04	44.92	69.05	67.27	64.06	60.50	52.87	42.21	37.23	43.09	52.17	9.14	24.28	157.86	60.17	129.34	35.00	58.13
Sobětice	Mean	21.2	4.3	23.6	5.0	1.0	0.1	6.4	2.1	1.7	0.3	1.6	34.6	55.8	2.1	20.0	0.1		3.11	8.66	24.98	3.77	23.59	7.22	7.70	9.37	1.35	11.54	1.92	5.97	0.64	4.55	0.42	0.01	0.34	15.26	0.11	0.04	0.04	85.28	26.39
n=12	SD	20.1	2.3	36.6	4.6	0.2	0.1	0.9	6.1	5.4	0.6	1.9	1.9	21.1	0.4	2.8	0.2	bdl	7.32	2.52	7.92	1.72	14.53	5.45	2.77	7.76	1.05	8.37	1.24	3.02	0.21	0.87	0.06	bdl	0.01	10.28	0.21	0.03	0.05	36.49	14.59
SCH-42	Max	83.4	10.1	116.8	15.3	1.2	0.5	8.6	22.2	19.5	2.4	7.3	39.1	101.3	2.7	26.0	0.5	bdl	25.44	14.32	39.34	7.28	54.49	19.25	11.40	26.45	3.60	28.86	4.56	12.72	1.13	6.57	0.57	0.02	0.35	47.12	0.75	0.10	0.14	163.49	57.23
	Min	3.6	2.6	bdl	bdl	0.7	bdl	5.3	0.2	bdl	bdl	0.3	31.1	27.5	1.5	15.8	bdl	bdl	0.02	5.39	14.04	1.67	8.99	2.28	3.79	2.77	0.43	4.06	0.75	2.83	0.36	3.16	0.34	bdl	0.32	10.08	0.01	0.01	0.01	39.93	11.93
	Median	15.6	3.0		4.7	1.0		6.2	0.2		0.1	0.9	34.7	46.5	2.1	20.8			0.11	8.37	24.81	3.18	17.51	4.39	8.65	5.36	0.82	7.44	1.31	4.46	0.56	4.30	0.40	0.01	0.33	11.21	0.02	0.04	0.02	74.15	19.01
	RSD (%)	94.8	54.0	155.0	92.7	17.0	138.1	13.9	288.6	319.4	249.8	115.0	5.6	37.9	17.8	14.2	163.5		235.52	29.06	31.69	45.63	61.57	75.54	35.95	82.85	78.05	72.50	64.37	50.65	32.97	19.25	15.17		2.49	67.36	195.83	59.95	104.93	42.79	55.28
Kašperské hory-Naděje	Mean	19.8	4.9	45.1	8.9	1.8	0.1	14.7	0.2	1.3	5.7	1.1	83.2	47.9	7.0	110.3		0.1	0.05	12.03	26.38	3.01	13.39	3.11	10.39	3.27	0.51	5.16	1.00	4.64	0.91	11.36	1.44		0.43	7.79	0.05	0.20	0.14	71.58	25.02
n=12	SD	2.1	199.7	268.2	7.6	0.6	0.3	0.8	22.9	2.0	0.5	1.1	3.4	5.9	10.4	39.1		0.1	0.01	0.34	1.27	0.29	3.00	1.41	0.28	2.40	0.25	2.03	0.34	1.02	0.09	0.55	0.05		0.01	0.61	0.05	0.02	0.06	8.34	4.21
SCH-5	Maximum	42.4	20.4	204.3	21.4	7.1	0.7	18.9	0.4	11.1	66.7	1.8	93.0	158.2	12.6	123.4	0.2	0.2	0.21	28.66	57.41	6.09	25.01	5.02	15.55	5.34	1.10	12.94	2.75	14.43	2.88	30.83	3.47	0.01	0.52	12.29	0.22	0.39	0.23	138.35	68.41
	Minimum	10.1	2.7	bdl	bdl	0.8	bdl	9.2	0.2	bdl	bdl	0.3	74.9	19.1	3.1	90.4	bdl	0.0	0.01	4.11	13.84	1.77	6.71	1.28	5.17	1.30	0.20	2.11	0.41	1.87	0.36	4.81	0.64	bdl	0.36	5.57	0.01	0.04	0.07	41.75	10.76
	Median	16.2	3.1	12.5	7.8	1.3		15.2	0.2	0.1		1.1	82.4	33.1	6.5	112.9		0.1	0.02	10.90	24.19	2.71	11.70	2.70	10.61	2.92	0.43	4.20	0.80	3.45	0.61	7.62	1.01		0.43	7.05	0.02	0.19	0.14	66.76	17.16
	RSD (%)	10.9	4103.5	595.3	85.1	30.8	346.9	5.4	10335.2	148.1	8.1	106.9	4.1	12.3	148.1	35.4		71.9	20.44	2.79	4.79	9.80	22.42	45.45	2.67	73.24	48.57	39.25	33.94	21.95	9.85	4.85	3.30		2.03	7.79	98.17	11.07	41.92	11.65	16.83
Kašperské hory-Lohbach	Mean	26.3	24.8	279.2	12.2	0.7	0.2	29.9	7.8	4.4	8.4	2.7	182.6	68.8	8.9	138.1		0.2	0.09	36.48	80.89	8.36	37.71	8.56	17.94	8.28	1.31	11.34	2.04	7.57	1.22	12.01	1.53	0.004	0.54	13.37	0.26	2.14	6.34	198.22	37.01
n=12	SD	20.9	68.8	696.8	5.9	0.6	0.4	21.8	13.3	10.1	19.3	4.6	94.5	70.8	3.7	118.3		0.2	0.06	42.19	87.50	8.53	38.22	8.67	16.73	8.40	1.36	11.88	2.12	7.82	1.25	12.30	1.53	0.01	0.05	10.41	0.16	1.81	6.81	203.38	38.17
SCH-6	Maximum	84.4	253.0	2557.6	29.2	2.2	1.4	67.0	40.3	34.8	69.5	16.9	292.7	191.5	15.6	309.7	bdl	0.7	0.22	137.61	229.35	20.42	100.50	23.88	40.31	22.34	3.60	30.58	5.34	19.75	3.13	30.80	3.78	0.02	0.62	35.00	0.67	4.77	25.30	523.61	95.82
	Minimum	0.1	1.7	bdl	6.1	bdl	bdl	10.2	bdl	bdl	bdl	0.3	59.4	0.8	3.3	15.0	bdl	bdl	0.01	1.89	1.47	0.14	0.42	0.07	0.36	0.07	bdl	0.08	0.01	0.07	0.02	0.15	0.02	bdl	0.49	3.70	0.07	0.07	0.08	4.42	0.35
	Median	20.6	4.1	36.8	11.4	0.8		15.1	0.3	0.1	0.8	0.8	189.6	27.0	8.5	105.8			0.08	12.93	29.36	3.72	18.30	4.28	8.81	3.82	0.51	4.18	0.74	2.79	0.45	4.32	0.61		0.51	7.19	0.22	1.27	6.07	80.82	13.60
	RSD (%)	79.7	277.6	249.6	48.7	85.5	239.1	72.9	171.6	230.5	229.5	171.9	51.7	102.9	41.1	85.6		163.5	66.11	115.65	108.17	101.99	101.35	101.35	93.24	101.39	104.35	104.77	104.16	103.33	102.28	102.44	99.96	128.21	9.34	77.87	62.77	84.27	107.27	102.60	103.15
Orlík u Humpolce	Mean	20.9	4.7	47.1	17.5	1.2	0.1	4.3	3.4	4.5	5.3	6.5	2236.9	36.9	2.7	0.9	0.1	0.1	0.01	5.75	18.35	2.86	18.13	5.82	13.68	7.95	1.19	8.74	1.36	3.54	0.32	1.67	0.16	0.005	0.54	8.68	0.09	0.11	1.88	72.54	16.99
n=12	SD	10.9	6.4	67.5	6.4	1.1	0.1	0.9	6.8	6.5	16.8	1.2	985.3	18.2	0.9	0.5	0.1	0.2	0.03	0.59	2.98	0.67	4.35	1.79	7.41	2.50	0.44	3.53	0.55	1.51	0.15	0.87	0.12	0.004	0.02	7.30	0.19	0.16	3.42	18.78	7.00
SCH-7	Maximum	38.9	25.4	237.7	33.4	4.4	0.3	6.0	25.0	19.5	61.2	8.4	3600.1	72.0	5.6	2.1	0.4	0.6	0.10	6.99	25.77	4.52	27.24	9.92	28.63	13.93	2.15	15.72	2.37	6.44	0.60	3.21	0.50	0.01	0.57	21.41	0.70	0.51	10.29	111.67	30.02
	Minimum	6.9	bdl	bdl	7.8	bdl	bdl	3.4	bdl	bdl	bdl	3.9	843.7	14.7	1.6	0.5	bdl	bdl	bdl	4.95	15.14	2.33	14.08	4.31	4.73	5.57	0.75	4.85	0.75	1.66	0.13	0.61	0.06	0.001	0.51	1.41	bdl	bdl	bdl	54.55	8.87
	Median	18.9	2.5	10.4	16.7	1.1	0.1	4.0	0.2	0.7		6.9	2117.7	35.1	2.5	0.7				5.58	16.87	2.52	16.01	5.18	12.91	7.00	1.06	7.71	1.19	3.38	0.32	1.67	0.15	0.004	0.54	6.08	0.01	0.02	0.01	65.34	15.32
	RSD (%)	52.2	136.6	143.2	36.7	89.4	71.6	19.9	199.3	144.8	317.9	19.0	44.1	49.4	35.2	52.7	139.1	159.5	205.31	10.26	16.26	23.32	24.00	30.79	54.15	31.40	36.87	40.40	40.30	42.71	46.62	51.77	72.80	71.80	3.22	84.09	223.22	140.71	181.77	25.89	41.23
Au-RIRGS-related	Mean	36.7	35.2	137.6	11.7	1.8	0.6	12.1	6.7	8.0	4.4	12.1	29.1	109.4	23.9	3021.4	0.3	0.1	0.46	3.94	14.81	3.06	29.52	12.44	2.79	24.67	2.72	19.75	3.85	10.40	0.84	4.19	0.38	0.01	0.48	1.85	0.05	0.01	0.02	91.21	42.11
Čelina	SD	19.7	50.0	255.3	6.8	1.6	0.3	5.6	14.4	12.2	11.1	4.8	4.8	45.7	14.3	1062.5	0.6	0.3	1.16	1.87	5.95	1.03	9.61	3.37	0.62	7.04	0.79	5.93	1.28	4.05	0.38	2.12	0.18	0.01	0.04	0.52	0.06	0.01	0.02	26.51	14.09
n=13	Max	89.0	168.2	973.0	32.0	6.0	1.2	27.2	51.4	37.5	38.9	19.8	37.4	240.3	66.4	6199.4	2.1	1.0	4.45	7.94	27.69	5.50	53.38	19.68	4.17	37.39	4.34	33.32	7.20	22.42	2.02	10.40	0.79	0.02	0.60	2.53	0.19	0.03	0.05	154.92	80.48
SCH-3	Min	10.3	0.4	bdl	4.6	bdl	0.2	7.9	bdl	bdl	bdl	4.7	19.6	52.8	8.9	2275.4	bdl	bdl	0.00	2.11	7.30	1.66	18.33	8.63	1.89	15.50	1.60	11.33	2.15	6.00	0.50	1.72	0.12	bdl	0.42	0.52	bdl	bdl	bdl	62.75	25.36
	Median	33.4	10.7	29.2	10.3	1.4	0.5	9.6		0.1		11.8	28.0	100.6	20.5	2588.2			0.03	3.00	14.03	2.70	25.97	11.80	2.68	23.32	2.67	20.16	3.86	9.62	0.73	3.38	0.36	0.01	0.48	1.92	0.01	0.01		81.80	40.02
	RSD (%)	53.7	142.1	185.5	58.2	93.0	57.1	46.3	215.8	153.5	250.5	39.8	16.5	41.8	59.7	35.2	231.2	189.1	252.99	47.50	40.14	33.72	32.57	27.13	22.14	28.53	28.89	30.04	33.11	38.93	45.88	50.58	47.96	58.15	8.69	28.30	127.71	67.48	114.20	29.07	33.45
Vacíkov	Mean	33.4	10.7	29.2	10.3	1.4	0.5	9.6		0.1		11.8	28.0	100.6	20.5	2588.2			0.03	3.00	14.03	2.70	25.97	11.80	2.68	23.32	2.67	20.16	3.86	9.62	0.73	3.38	0.36	0.01	0.48	1.92	0.01	0.01		81.80	40.02
n=11	SD	32.0	78.0	149.1	3.5	0.6	0.6	0.9	17.7	13.9	28.1	8.5	14.9	16.1	9.8	535.8	bdl	0.4	0.26	90.25	110.53	8.27	38.62	9.00	0.43	8.93	0.92	5.53	0.82	1.96	0.17	0.91	0.10	0.003	0.20	0.93	0.17	0.15	0.63	247.36	10.37
SCH-1	Maximum	153.2	262.7	542.1	21.7	2.2	2.1	9.9	62.6	45.9	69.5	39.1	180.8	87.8	57.0	2760.5	bdl	1.4	0.97	403.10	622.72	52.26	247.00	50.87	3.11	47.82	4.77	28.26	4.23	10.47	0.97	5.60	0.61	0.01	1.36	8.41	0.61	0.53	2.25	1335.12	54.90
	Minimum	53.7	0.0	bdl	7.9	bdl	bdl	6.4	bdl	bdl	bdl	8.0	133.2	30.9	20.8	1035.6	bdl	bdl	0.02	122.74	275.22	24.88	122.88	19.89	1.76	17.61	1.51	8.58	1.30	3.49	0.37	2.34	0.25	bdl	0.63	5.64	0.01	bdl	0.02	593.43	18.07
	Median	113.4	5.3	253.0	15.0	1.1	1.2	7.7	0.3	15.3	0.2	12.9	155.8	37.8	37.9	1815.3			0.06	225.46	440.49	38.84	173.75	22.66	2.61	19.36	1.83	10.73	1.67	4.46	0.48	2.97	0.34	0.005	0.67	6.69	0.01	0.02	0.10	919.40	22.28
	RSD (%)	96.0	728.8	510.7	34.4	42.6	131.5	9.2		16683.0		71.7	53.4	16.0	48.1	20.7			756.07	3005.81	788.06	306.10	148.75	76.23	15.93	38.31	34.47	27.43	21.30	20.40	23.17	27.00	27.98	40.05	42.60	48.55	1406.64	1336.58		302.41	25.91
Oxidized skarn	Mean	79.6	5.6	115.0	16.6	2.6	0.7	12.7	1.7	2.6	1.3	14.2	42.8	169.7	162.7	9764.2	0.1	0.4	0.09	46.10	168.82	24.03	140.26	38.08	2.88	38.32	5.25	36.57	6.40	19.24	2.34	15.57	1.62	0.02	2.03	11.42	1.58	0.45	0.34	458.48	86.98
Obří důl	SD	66.8	9.0	161.2	13.5	2.1	0.7	11.7	5.6	6.7	2.7	12.7	10.0	246.1	203.7	10247.5	0.4	1.1	0.22	33.20	143.73	19.78	121.96	41.84	2.35	46.65	7.17	51.49	9.07	27.09	3.33	22.89	2.54	0.03	4.51	27.08	6.44	0.92	0.93	375.16	123.08
n=80	Maximum	305.8	73.0	941.0	73.7	18.1	3.3	88.0	36.1	30.6	16.7	69.4	71.2	1476.2	1167.6	53932.0	3.2	7.0	1.70	160.68	686.66	86.18	508.74	226.71	12.47	286.06	44.62	319.70	56.99	167.50	19.86	132.88	14.98	0.16	35.31	236.30	55.60	6.39	7.91	1516.45	756.54
	Minimum	bdl	bdl	bdl	0.7	bdl	bdl	bdl	bdl	bdl	bdl	bdl	22.8	0.1	2.7	515.7	bdl	bdl	bdl	1.83	7.51	1.57	11.12	0.98	bdl	0.73	0.03	0.07	0.01	0.01	bdl	bdl	bdl	bdl	0.51	1.23	bdl	0.01	bdl	33.90	0.12
	Median	59.8	3.2	63.9	13.6	2.1	0.6	10.4	0.2	0.1	0.4	10.7	42.3	92.2	97.7	7214.1		0.1	0.03	34.89	109.95	17.71	101.89	25.88	2.24	26.13	3.03	20.41	3.67	11.06	1.28	7.73	0.70	0.01	0.83	6.02	0.06	0.10	0.07	334.59	48.42
	RSD (%)	84.0	160.5	140.2	81.4	81.9	95.0	91.9	320.7	258.8	217.6	89.6	23.3	145.0	125.2	104.9	373.7	297.0	239.04	72.02	85.14	82.34	86.96	109.89	81.65	121.74	136.67	140.82	141.70	140.80	142.44	146.99	156.91	141.55	221.57	237.01	408.37	206.05	269.73	81.83	141.50
Kovářská	Mean	4.7	11.8	194.6	40.9	1.6	1.6	37.3	0.4	27.8	0.8	0.5	106.9	3.8	1.6	1014.7			0.01	0.29	4.80	0.13	0.75	0.24	0.04	0.51	0.05	0.58	0.13	0.60	0.07	0.58	0.05	0.02	0.39	4.19	0.01	0.28	0.01	6.76	2.07

n=3	SD	4.3	3.9	275.2	6.1	0.3	1.9	49.3	0.2	39.3	0.7	0.1	3.6	0.8	0.1	30.6			0.01	0.35	6.44	0.11	0.45	0.08	0.01	0.32	0.02	0.12	0.04	0.12	0.02	0.10	0.01	0.02	0.03	3.63	0.01	0.32	0.02	7.23	0.40
SCH-16	Maximum	10.8	16.7	583.8	45.9	1.9	4.2	107.0	0.6	83.4	1.7	0.7	111.9	4.5	1.7	1052.2	bdl	bdl	0.02	0.78	13.90	0.28	1.29	0.32	0.05	0.96	0.06	0.67	0.17	0.75	0.09	0.71	0.06	0.05	0.42	9.27	0.03	0.73	0.04	16.93	2.50
	Minimum	1.5	7.2	bdl	32.2	1.1	0.0	2.1	0.2	bdl	bdl	0.3	103.4	2.7	1.5	977.2	bdl	bdl	bdl	0.01	0.10	0.02	0.18	0.13	0.03	0.26	0.03	0.41	0.08	0.44	0.05	0.48	0.04	bdl	0.36	0.97	0.002	0.04	bdl	0.74	1.53
	Median	1.7	11.5		44.5	1.7	0.5	2.8	0.3	0.1	0.8	0.5	105.5	4.2	1.6	1014.7			0.01	0.06	0.40	0.07	0.78	0.28	0.04	0.32	0.06	0.66	0.14	0.61	0.08	0.55	0.05		0.40	2.34	0.01	0.05		2.61	2.17
	RSD (%)	92.5	32.9	141.4	15.0	21.7	118.6	132.1	50.4	141.2	80.1	29.0	3.4	20.6	4.6	3.0			86.02	122.47	134.04	88.75	60.42	33.44	24.15	61.82	32.38	21.14	29.26	20.61	23.31	16.81	19.07	141.42	6.89	86.64	91.42	116.60	141.42	106.99	19.54
Vykmanov	Mean	23.2	75.6	478.0	26.1	2.5	1.2	13.9	0.2	0.2	12.1	0.6	114.8	3.1	1.6	1573.9	1.1	0.3	0.05	0.83	2.02	0.36	2.18	0.73	0.22	0.89	0.09	0.75	0.13	0.35	0.03	0.19	0.02		0.51	8.64	1.19	0.62	0.23	7.23	1.57
n=7	SD	20.4	38.3	383.3	25.3	1.9	2.0	12.9	0.1	0.1	23.6	0.3	25.8	0.3	0.3	483.6	1.4	0.5	0.04	0.66	0.31	0.14	0.82	0.29	0.07	0.22	0.04	0.16	0.02	0.04	0.00	0.07	0.01	0.003	0.02	4.23	1.17	0.50	0.09	1.39	0.24
SCH-44	Maximum	69.5	127.9	875.7	82.0	7.0	6.1	34.6	0.4	0.4	69.5	1.2	159.2	3.6	2.2	2446.4	4.3	1.5	0.11	2.36	2.59	0.65	3.29	1.24	0.36	1.32	0.15	1.01	0.16	0.42	0.04	0.27	0.03	0.01	0.54	17.38	3.48	1.77	0.37	9.81	2.02
	Minimum	5.0	21.4	bdl	bdl	1.0	0.1	4.0	0.1	bdl	bdl	0.0	74.6	2.7	1.4	949.4	0.1	bdl	bdl	0.18	1.64	0.17	1.25	0.38	0.15	0.64	bdl	0.58	0.10	0.29	0.03	0.07	0.02	bdl	0.47	3.28	0.07	0.20	0.09	5.50	1.30
	Median	21.1	92.4	569.9	15.3	1.6	0.3	5.3	0.3	0.2	1.3	0.7	107.3	3.0	1.5	1495.6	0.4	0.1	0.05	0.73	1.88	0.33	1.68	0.57	0.17	0.85	0.09	0.65	0.12	0.35	0.04	0.23	0.02	0.003	0.52	7.92	0.56	0.52	0.27	7.47	1.50
	RSD (%)	88.1	50.7	80.2	97.2	77.5	167.8	93.0	45.5	75.6	194.6	54.1	22.5	8.8	17.8	30.7	131.3	186.5	75.38	78.87	15.14	40.04	37.83	39.79	32.58	24.64	47.01	20.94	18.04	10.50	12.25	33.37	27.23		4.30	48.93	98.00	81.03	39.03	19.18	15.12
Bílé Labe	Mean	230.6	9.7	61.0	12.9	2.4	1.2	88.2	17.0	12.2		5.3	43.5	522.4	141.5	2724.3		0.4	0.07	256.19	564.37	56.55	286.28	72.27	4.84	74.99	11.13	87.83	15.63	52.92	7.45	66.54	8.30	0.04	9.98	25.62	6.55	0.27	0.11	1315.49	249.81
n=10	SD	41.9	6.7	49.6	3.2	3.4	0.9	5.8	37.1	26.7		1.5	2.4	73.3	30.0	908.1		0.2	0.12	80.10	159.12	13.69	59.66	10.48	0.88	10.22	1.83	15.01	2.63	8.70	1.17	10.72	1.51	0.01	2.86	4.14	8.95	0.23	0.10	316.29	39.00
SCH-28	Maximum	271.1	29.2	161.2	17.0	12.5	3.8	98.6	125.1	86.2	0.1	8.4	50.2	633.8	186.5	3391.6	0.2	0.8	0.42	330.40	697.78	67.28	327.21	84.93	7.20	93.27	13.94	111.90	19.84	67.28	9.20	79.65	9.86	0.05	12.41	33.64	24.60	0.76	0.33	1565.79	311.65
	Minimum	118.0	4.6	bdl	8.1	0.8	0.1	77.8	0.1	bdl	bdl	2.7	41.3	409.1	83.4	154.3	bdl	bdl	bdl	42.53	119.82	17.18	112.31	47.54	4.14	62.41	8.42	66.03	11.70	40.45	6.02	44.33	4.50	0.03	2.32	16.00	0.01	0.05	0.00	411.63	198.71
	Median	244.1	8.2	54.2	11.8	1.5	1.0	89.6	0.2	0.1		4.9	42.7	528.9	143.6	2914.8		0.4	0.01	274.59	594.92	59.42	308.86	73.46	4.45	73.25	11.33	89.79	15.81	52.26	7.47	67.35	8.51	0.04	11.00	25.45	0.65	0.18	0.07	1375.82	249.60
	RSD (%)	18.2	68.6	81.3	24.5	139.5	73.4	6.6	218.9	219.0		28.7	5.6	14.0	21.2	33.3		53.4	173.56	31.26	28.19	24.21	20.84	14.50	18.17	13.63	16.48	17.09	16.85	16.44	15.66	16.11	18.18	20.13	28.64	16.17	136.62	83.23	91.90	24.04	15.61
Chedrbí	Mean	6.0	3.7	74.4	10.3	3.9	0.2	2.9	3.6	4.0		0.7	33.7	2.3	19.4	1808.0		0.1	0.01	4.36	7.78	0.90	5.26	1.31	0.15	1.19	0.11	0.70	0.09	0.25	0.02	0.12	0.01	0.001	1.37	2.60	0.02	0.04	0.06	20.94	1.31
n=11	SD	8.2	1.4	89.1	2.3	5.1	0.1	2.2	7.2	7.3	0.1	0.6	7.8	3.5	38.5	564.1		0.1	0.02	9.14	16.16	1.85	10.55	2.46	0.28	1.96	0.16	0.98	0.12	0.29	0.02	0.14	0.01	0.001	2.10	0.74	0.01	0.06	0.08	42.38	1.73
SCH-9	Maximum	29.2	6.6	318.3	14.3	18.1	0.5	7.8	19.5	23.6	0.2	2.1	50.6	10.6	108.3	2233.7	bdl	0.2	0.06	24.99	43.23	4.96	28.63	6.96	0.76	5.53	0.48	2.95	0.37	0.91	0.07	0.44	0.03	0.003	5.87	3.79	0.04	0.19	0.23	115.08	5.26
	Minimum	0.8	2.5	bdl	7.5	1.1	0.0	1.2	0.2	bdl	bdl	0.2	24.2	0.2	1.2	618.6	bdl	bdl	0.00	0.01	0.03	0.01	0.06	0.04	0.01	0.06	0.01	0.08	0.01	0.02	bdl	0.02	0.00	bdl	0.37	1.38	0.01	0.01	bdl	0.24	0.14
	Median	2.9	2.8	58.4	10.6	1.3	0.1	2.1	0.2			0.6	32.2	0.8	1.3	2037.7			0.01	0.04	0.11	0.03	0.32	0.19	0.02	0.33	0.03	0.29	0.04	0.14	0.01	0.06	0.01	0.001	0.38	2.88	0.01	0.01	0.02	1.15	0.58
	RSD (%)	135.7	39.2	119.7	22.5	130.8	90.3	76.7	198.9	181.6		76.8	23.1	151.4	198.8	31.2		83.8	125.42	209.91	207.67	205.73	200.75	187.25	185.89	164.35	148.64	139.96	129.08	119.35	109.53	111.24	77.52	121.86	153.43	28.30	68.88	142.76	132.47	202.38	132.16
Krouna	Mean	13.3	128.9	195.5	12.5	1.5	0.3	5.3	18.2	0.8	0.3	7.6	104.9	48.3	33.1	483.3		0.1	0.02	4.50	18.50	4.05	39.39	15.92	2.21	22.06	2.28	16.06	2.66	7.36	0.62	3.74	0.37	0.01	0.39	8.99	0.06	0.03	0.09	106.62	33.09
n=9	SD	2.1	199.7	268.2	7.6	0.6	0.3	0.8	22.9	2.0	0.5	1.1	3.4	5.9	10.4	39.1		0.1	0.01	0.34	1.27	0.29	3.00	1.41	0.28	2.40	0.25	2.03	0.34	1.02	0.09	0.55	0.05	0.004	0.01	0.61	0.05	0.02	0.06	8.34	4.21
SCH-45	Maximum	18.1	550.4	720.0	30.6	2.8	1.3	6.8	59.8	6.4	1.5	8.9	109.3	59.8	52.5	589.4	bdl	0.2	0.04	5.05	20.63	4.64	45.18	18.61	2.56	25.80	2.72	19.59	3.28	9.40	0.81	4.99	0.48	0.02	0.41	9.94	0.15	0.09	0.21	122.45	41.27
	Minimum	10.7	2.7	bdl	4.2	0.8	0.1	3.9	0.2	bdl	bdl	5.4	98.4	39.3	20.4	446.2	bdl	bdl	0.01	3.79	16.19	3.57	34.04	13.75	1.73	18.65	1.94	13.21	2.16	5.75	0.46	2.82	0.30	0.002	0.38	7.96	0.01	0.01	0.02	92.03	26.65
	Median	12.9	14.6	51.4	9.5	1.4	0.2	5.4	0.3		0.2	8.4	104.7	46.3	30.4	476.8		0.1	0.02	4.59	18.60	4.02	39.48	16.17	2.36	23.24	2.39	16.26	2.64	7.21	0.61	3.77	0.37	0.01	0.39	9.12	0.03	0.02	0.08	105.25	32.73
	RSD (%)	16.2	154.9	137.2	60.8	37.7	107.2	15.0	125.8	265.2	136.9	14.9	3.3	12.2	31.5	8.1		67.7	43.12	7.45	6.84	7.28	7.63	8.87	12.53	10.86	10.97	12.61	12.73	13.85	14.42	14.74	12.76	48.48	2.25	6.74	93.01	76.68	68.00	7.82	12.73
Mutice	Mean	9.7	22.4	109.5	6.1	1.2	0.2	23.1	0.8	5.6	0.9	1.8	65.6	85.4	256.0	290.8		0.2	0.04	33.31	104.64	14.29	93.35	23.57	2.06	25.11	2.71	18.98	3.06	9.71	1.12	8.76	0.86	0.01	0.40	0.69	0.01	0.20	1.13	296.34	45.20
n=12	SD	4.5	28.5	102.9	5.1	0.4	0.3	8.9	1.3	6.6	1.7	0.4	16.6	44.3	139.6	99.5		0.1	0.06	13.88	40.57	4.06	29.86	9.23	0.51	10.60	1.21	8.59	1.39	4.27	0.44	2.62	0.20	0.01	0.12	0.33	0.01	0.12	1.30	94.56	17.78
SCH-10	Maximum	18.6	86.7	287.7	16.7	2.4	1.1	50.0	4.4	18.1	6.3	2.5	90.2	180.7	531.0	419.8	bdl	0.3	0.18	58.10	187.09	20.72	135.80	36.18	2.81	38.36	4.56	33.36	5.53	17.72	1.99	13.58	1.35	0.03	0.77	1.54	0.03	0.44	4.84	460.48	77.71
	Minimum	3.0	2.8	bdl	bdl	0.8	0.0	14.6	0.1	bdl	bdl	1.1	33.4	30.8	85.2	90.6	bdl	0.1	0.01	16.03	60.05	9.10	45.45	8.58	1.28	7.85	0.83	6.06	1.01	3.49	0.48	4.99	0.62	0.003	0.32	0.35	0.01	0.06	0.21	180.89	17.58
	Median	8.5	8.5	125.8	6.5	1.1	0.1	20.5	0.2	2.0	0.4	1.9	70.8	75.1	214.9	311.4		0.1	0.02	30.78	92.78	12.43	90.91	23.42	2.12	25.81	2.76	18.54	2.97	9.86	1.09	7.91	0.85	0.01	0.36	0.63	0.01	0.15	0.63	257.90	47.09
	RSD (%)	45.9	127.7	94.0	84.4	34.4	149.4	38.6	167.4	117.3	191.8	23.2	25.4	51.9	54.5	34.2		36.7	134.21	41.68	38.76	28.39	31.99	39.15	24.84	42.23	44.62	45.27	45.43	43.97	39.27	29.87	22.69	57.05	28.98	47.56	45.52	61.95	114.37	31.91	39.34
Nekvasovy Chlumy	Mean	19.0	3.1	54.1	10.4	4.6	0.5	12.4	5.5	0.8	11.5	4.3	127.7	66.0	77.5	773.4	0.1	0.3	0.15	12.41	44.86	7.99	60.23	17.94	2.59	22.54	2.61	18.10	2.79	7.42	0.63	3.42	0.26	0.01	0.75	3.21	0.02	0.04	0.09	168.56	35.24
n=12	SD	13.7	1.0	71.6	8.6	2.3	0.9	1.8	15.2	2.7	26.7	4.3	59.0	62.8	97.4	789.2	0.2	0.2	0.26	10.06	38.32	6.65	51.03	16.86	1.72	22.63	2.96	18.12	2.69	7.01	0.61	3.87	0.33	0.01	0.71	1.51	0.03	0.04	0.15	135.13	33.67
SCH-29	Maximum	52.3	6.4	258.5	36.1	9.5	3.6	16.0	55.6	9.7	97.3	18.1	319.7	208.5	361.4	3197.0	0.7	0.8	0.97	36.31	116.20	23.63	194.60	62.55	6.95	86.18	11.12	65.33	9.73	23.63	2.29	15.46	1.24	0.02	2.64	6.53	0.13	0.14	0.56	490.67	115.08
	Minimum	3.4	2.7	bdl	bdl	2.5	bdl	9.9	0.1	bdl	bdl	1.8	87.2	22.4	25.3	107.3	bdl	bdl	bdl	1.17	6.98	2.08	25.17	7.83	1.19	8.16	0.81	5.94	0.96	2.63	0.13	0.39	0.02	bdl	0.33	1.65	0.01	0.01	0.01	64.36	12.95
	Median	14.2	2.8	29.2	7.9	3.3	0.2	12.6	0.2		0.1	3.4	115.6	39.9	38.7	558.1		0.1	0.03	8.21	27.26	5.30	37.25	10.12	1.90	12.13	1.31	9.51	1.57	4.58	0.39	2.29	0.14	0.01	0.38	2.63	0.01	0.03	0.04	111.63	20.52
	RSD (%)	72.0	31.3	132.4	82.2	49.8	188.2	14.3	277.2	316.8	232.2	99.2	46.2	95.0	125.7	102.0	293.6	97.1	181.73	81.09	85.42	83.22	84.73	93.99	66.35	100.41	113.15	100.11	96.45	94.43	96.48	112.89	124.15	75.43	95.36	47.12	152.42	86.69	162.60	80.17	95.55
Proseč	Mean	12.9	2.4	34.5	11.4	1.2	0.2	22.8	0.3	4.2	4.8	2.6	64.0	37.3	15.7	556.7	0.1		0.01	2.89	8.58	1.95	17.61	5.69	1.37	8.98	1.06	7.93	1.48	4.26	0.40	2.31	0.24	0.003	0.59	11.10	0.03	0.01	0.05	47.07	17.68
n=12	SD	5.3	1.0	35.0	2.3	0.3	0.1	2.5	0.3	10.5	14.1	0.9	3.6	10.0	8.9	141.6	0.2		0.03	0.61	1.94	0.42	3.61	1.00	0.41	1.75	0.24	2.14	0.45	1.33	0.11	0.79	0.11	0.002	0.09	5.73	0.06	0.01	0.04	9.24	4.66
SCH-46	Maximum	25.7	4.6	100.1	15.8	1.7	0.3	27.0	1.0	37.5	51.4	4.4	70.9	53.8	36.4	761.7	0.5	0.1	0.11	3.67	11.68	2.67	24.09	7.39	1.91	11.25	1.42	11.19	2.12	6.27	0.56	4.13	0.48	0.01	0.76	23.91	0.22	0.02	0.13	62.26	24.53
	Minimum	5.6	bdl	0.0	7.4	0.7	0.1	18.8	bdl	bdl	bdl	1.1	58.8	18.6	3.8	326.1	bdl	bdl	bdl	1.72	5.10	1.20	11.83	4.20	0.29	6.48	0.74	4.81	0.72	1.75	0.14	0.78	0.03	bdl	0.49	5.14	bdl	0.002	bdl	32.28	9.02
	Median	11.9	2.6	23.6	11.4	1.2	0.2	22.7	0.2			2.3	63.0	39.2	14.3	608.1				3.03	8.73	1.89	18.02	5.93	1.40	8.66	1.06	8.08	1.53	4.54	0.42	2.19	0.23	0.003	0.59	10.43	0.01	0.01	0.04	47.01	18.48

	RSD (%)	41.3	42.8	101.4	20.0	22.4	27.8	11.1	103.6	252.6	291.7	35.0	5.6	26.9	57.0	25.4	166.7		238.75	20.99	22.58	21.43	20.49	17.60	30.29	19.50	22.96	26.92	30.06	31.31	28.85	34.21	45.69	75.04	15.12	51.62	204.84	48.69	84.18	19.62	26.34
Reduced skarn	Mean	18.9	1.8	37.9	12.3	1.5	0.1	16.3	0.4	3.7	1.6	1.1	42.9	67.1	10.2	250.4		0.1	0.01	2.06	8.51	2.03	19.62	8.85	3.44	14.53	1.95	14.85	2.68	8.06	0.82	5.28	0.62	0.01	0.54	4.04	0.10	0.02	0.03	59.03	34.25
Budislav	SD	12.4	1.8	31.8	5.2	1.2	0.2	2.2	0.7	7.4	5.0	0.5	15.3	81.5	10.4	85.6		0.0	0.02	1.08	3.45	0.74	7.19	5.20	1.04	9.77	1.72	14.81	2.75	8.82	1.00	7.10	0.80	0.01	0.13	0.82	0.26	0.01	0.05	25.53	36.97
n=12	Maximum	55.6	5.8	82.0	23.6	5.3	0.8	19.5	2.6	20.9	18.1	2.2	68.5	334.6	41.8	348.9	bdl	0.2	0.04	5.31	16.12	3.81	37.25	24.48	5.13	45.59	7.52	63.25	11.68	36.78	4.06	28.30	3.18	0.03	0.95	5.56	0.97	0.04	0.18	132.65	154.77
SCH-13	Minimum	1.0	bdl	bdl	bdl	0.4	bdl	12.9	bdl	0.0	bdl	0.6	28.0	27.8	3.2	106.1	bdl	bdl	0.00	1.23	5.27	1.31	13.11	5.18	1.82	7.99	1.00	6.96	1.23	3.45	0.28	1.40	0.12	bdl	0.47	3.04	0.004	0.003	bdl	38.84	15.04
	Median	16.3	2.5	34.1	12.7	1.1	0.1	17.0	0.2	0.1		0.9	32.5	41.2	6.3	280.5			0.01	1.64	6.99	1.65	17.07	7.03	3.26	11.90	1.44	10.65	1.93	5.53	0.50	2.84	0.37	0.01	0.50	3.79	0.01	0.01	0.01	49.78	23.26
	RSD (%)	65.7	96.5	83.9	42.2	84.5	151.6	13.3	166.3	198.7	302.0	48.3	35.6	121.5	102.2	34.2		67.3	116.65	52.53	40.50	36.56	36.67	58.81	30.31	67.21	88.09	99.75	102.66	109.47	122.25	134.45	130.36	77.86	23.33	20.38	271.81	81.34	183.88	43.25	107.93
Hazlov	Mean	15.9	28.1	109.1	10.6	1.6	0.3	1.5	4.2	4.1	0.2	0.9	1598.8	0.9	24.6	204.5		0.2	0.07	0.37	0.32	0.06	0.34	0.08	0.02	0.11	0.02	0.13	0.03	0.11	0.01	0.11	0.03		0.63	1.83	0.03	0.02	0.22	1.31	0.44
n=11	SD	24.0	68.5	102.5	4.2	0.5	0.5	1.8	10.7	7.7	0.4	0.7	56.0	0.6	9.0	7.9		0.2	0.11	0.35	0.15	0.05	0.32	0.05	0.03	0.08	0.01	0.05	0.01	0.04	0.01	0.05	0.04		0.12	0.08	0.04	0.01	0.52	0.88	0.17
SCH-31	Max	84.8	244.6	244.6	19.5	3.2	1.4	5.1	37.5	26.4	1.0	2.5	1720.8	2.4	47.3	219.6	bdl	0.4	0.33	1.30	0.74	0.18	1.16	0.16	0.10	0.31	0.04	0.22	0.06	0.19	0.03	0.24	0.14	bdl	0.83	1.95	0.14	0.03	1.81	3.42	0.81
	Min	0.8	4.5	bdl	5.1	1.3	0.0	0.3	0.2	0.0	bdl	0.3	1506.8	0.4	11.1	193.2	bdl	bdl	bdl	0.12	0.18	0.02	0.09	0.04	bdl	0.05	0.01	0.07	0.01	0.06	0.01	0.06	0.01	bdl	0.44	1.68	0.01	0.004	bdl	0.51	0.24
	Median	2.6	5.9	141.8	9.6	1.4	0.0	0.5	0.2	0.1		0.7	1594.3	0.7	23.9	204.2		0.1	0.01	0.18	0.27	0.03	0.22	0.06	0.01	0.07	0.02	0.11	0.03	0.10	0.01	0.11	0.01		0.61	1.84	0.01	0.02		0.86	0.41
	RSD (%)	151.4	243.9	94.0	39.4	32.7	161.0	118.2	257.1	189.3	162.1	74.6	3.5	65.6	36.6	3.9		97.6	162.54	95.86	46.75	83.77	92.32	57.84	113.20	69.78	52.89	39.65	46.21	38.59	49.66	45.00	140.52		19.15	4.46	125.26	50.18	240.64	67.44	37.61
Hostákov	Mean	5.6	9.1	19.8	16.3	1.2	0.1	9.0	3.2	4.1	0.2	1.5	41.2	9.2	97.2	1022.0		0.2	0.14	28.34	61.41	8.23	49.77	9.87	1.11	7.28	0.61	3.15	0.40	0.81	0.05	0.31	0.02	0.002	3.25	1.45	0.13	0.24	0.17	166.02	5.34
n=11	SD	6.7	7.2	21.3	10.8	0.8	0.3	1.8	10.3	13.0	0.6	0.4	4.7	1.7	32.0	721.7		0.3	0.34	8.49	16.90	2.13	13.92	3.66	0.47	2.40	0.18	0.81	0.07	0.15	0.02	0.09	0.01	0.002	1.50	0.56	0.21	0.19	0.17	45.48	1.26
SCH-11	Max	19.5	26.4	66.7	41.7	3.1	1.1	11.3	37.5	47.3	2.1	2.4	50.5	12.5	151.4	2468.6	0.1	1.1	1.25	39.34	90.35	12.66	78.95	16.00	1.95	10.40	0.84	4.46	0.54	1.12	0.08	0.56	0.04	0.01	4.96	2.78	0.71	0.73	0.58	249.65	7.62
	Min	bdl	bdl	bdl	5.4	bdl	bdl	6.2	bdl	bdl	bdl	1.1	35.9	6.4	38.9	568.5	bdl	bdl	bdl	13.71	31.83	4.66	29.00	4.07	0.36	3.20	0.32	1.84	0.26	0.59	0.00	0.22	0.01	bdl	0.95	0.82	bdl	0.05	bdl	86.82	3.32
	Median	2.9	7.5	12.5	11.2	1.2		9.5				1.5	40.2	9.2	107.9	598.4		0.2	0.01	30.26	65.12	8.34	48.44	10.74	1.24	7.99	0.66	3.32	0.40	0.81	0.06	0.28	0.02		3.73	1.37	0.04	0.19	0.11	171.19	5.60
	RSD (%)	118.1	79.1	107.6	66.2	65.8	297.1	20.2	321.7	314.4	283.2	24.7	11.4	18.9	32.9	70.6		113.7	250.55	29.95	27.53	25.82	27.97	37.08	41.84	32.94	28.91	25.65	18.90	18.56	49.80	30.06	41.64	91.36	45.99	38.82	153.61	78.41	98.91	27.39	23.61
Kotel	Mean	5.5	5.5	82.4	11.4	2.9	bdl	1.0	0.7	4.1	77.7	2.2	237.2	14.6	1.8	261.2	0.4	0.1	0.49	0.26	1.19	0.29	2.80	1.57	0.38	2.97	0.42	3.63	0.62	1.73	0.14	0.61	0.04	0.003	0.37	16.33	0.03	0.02	0.10	9.47	7.19
n=12	SD	5.0	3.0	65.3	3.2	3.2	0.1	0.4	1.6	8.4	167.0	1.9	80.7	10.1	0.2	92.5	1.1	0.1	0.99	0.17	0.92	0.23	2.58	1.34	0.19	2.37	0.31	2.52	0.43	1.06	0.08	0.38	0.03	0.002	0.01	35.47	0.04	0.01	0.14	7.54	4.53
SCH-17	Max	13.5	11.4	186.3	17.5	12.5	0.3	1.9	6.0	30.6	514.3	7.4	404.5	32.2	2.1	412.8	3.9	0.3	3.34	0.64	3.20	0.81	9.13	4.67	0.73	8.45	1.08	8.88	1.47	3.68	0.26	1.36	0.12	0.01	0.40	127.88	0.17	0.05	0.40	27.14	16.24
	Min	0.4	2.7	bdl	6.3	0.6	bdl	0.4	0.1	bdl	bdl	0.4	108.0	1.2	1.4	72.1	bdl	0.0	0.00	0.01	0.05	0.02	0.27	0.17	0.04	0.38	0.05	0.42	0.07	0.20	0.02	0.10	0.01	bdl	0.35	1.19	0.01	0.01	0.001	0.94	0.92
	Median	2.1	3.9	68.8	11.3	1.6	bdl	1.0	0.2	0.3	0.1	1.5	244.1	11.3	1.8	245.5		0.1	0.02	0.20	0.90	0.20	1.70	1.13	0.43	2.21	0.32	2.86	0.48	1.57	0.13	0.52	0.03		0.37	2.14	0.01	0.02	0.02	6.78	6.35
	RSD (%)	90.1	55.2	79.3	28.3	108.4		38.0	221.3	208.3	214.9	89.1	34.0	69.0	12.1	35.4	273.2	75.9	201.97	66.94	77.52	77.47	91.94	85.49	51.03	79.56	72.96	69.44	69.28	61.49	56.54	62.54	80.82	55.28	3.31	217.15	138.12	52.53	150.65	79.59	62.98
Vrbík	Mean	16.2	8.7	52.0	9.2	1.0	0.1	6.4	7.2	15.8	0.1	1.7	53.9	2.0	39.0	858.3	0.1	0.1	0.10	8.48	10.43	0.84	2.86	0.44	1.33	0.40	0.03	0.23	0.04	0.20	0.04	0.43	0.07	0.001	0.48	4.80	0.11	0.79	0.93	24.78	1.04
n=12	SD	20.3	10.3	58.0	6.2	0.6	0.2	2.2	15.7	23.4	0.3	1.0	11.4	0.9	22.6	165.6	0.1	0.1	0.23	3.93	5.35	0.59	2.97	0.47	1.11	0.31	0.03	0.16	0.03	0.09	0.02	0.23	0.04	0.004	0.03	1.04	0.15	0.79	0.73	12.54	0.48
SCH-40	Max	73.7	36.1	169.6	22.2	2.1	0.8	11.3	54.2	69.5	1.0	3.8	82.7	4.1	79.2	1187.1	0.3	0.3	0.70	16.22	18.88	2.40	11.79	1.90	4.45	1.38	0.12	0.59	0.12	0.37	0.08	0.95	0.15	0.02	0.53	6.99	0.56	2.86	2.63	44.94	2.12
	Min	1.3	bdl	bdl	bdl	bdl	bdl	4.3	0.1	0.0	0.0	0.3	41.6	0.9	7.4	526.8	bdl	bdl	bdl	1.94	2.78	0.30	0.53	0.08	0.47	0.18	bdl	bdl	bdl	0.08	0.02	0.18	0.03	bdl	0.43	3.63	0.00	0.04	0.00	9.13	0.45
	Median	8.8	2.9	25.7	9.5	1.1		5.5	0.3	0.6		1.7	50.0	1.9	31.1	879.9				7.76	9.06	0.65	1.79	0.31	0.89	0.32	0.02	0.21	0.03	0.20	0.03	0.36	0.06		0.48	4.56	0.05	0.64	0.87	21.72	1.05
	RSD (%)	125.1	118.9	111.4	66.8	55.4	211.2	33.6	217.6	148.0	232.3	59.9	21.2	45.0	57.8	19.3	150.7	148.3	225.65	46.30	51.25	70.25	104.04	105.87	83.87	77.79	112.28	67.46	76.29	45.54	57.28	54.33	58.63	280.34	5.63	21.66	142.57	99.28	78.33	50.60	46.36
Other settings	Mean	29.9	101.6	28.6	9.7	1.9	0.1	18.0	5.1	4.2	1.6	0.7	53.2	13.4	1.8	3.1		0.1	0.04	26.67	58.27	6.70	36.44	7.27	8.72	6.88	0.74	5.27	0.80	2.53	0.31	2.85	0.40	0.003	0.33	3.72	0.04	0.13	0.02	150.96	12.91
Erpružice	SD	31.0	20.3	39.4	6.2	1.2	0.1	2.9	10.2	9.6	3.8	0.8	9.9	6.3	1.0	1.2			0.05	19.51	43.49	4.22	20.50	3.90	5.10	3.78	0.42	2.99	0.45	1.39	0.16	1.47	0.21	0.002	0.01	0.98	0.03	0.10	0.02	89.78	6.83
n=12	Maximum	97.3	139.0	115.4	20.9	4.6	0.5	22.9	34.8	30.6	13.9	3.4	71.0	22.6	4.5	5.7	0.1	0.1	0.14	68.11	143.17	15.75	80.76	14.87	20.03	13.47	1.47	10.49	1.59	5.09	0.62	5.67	0.82	0.01	0.35	6.12	0.10	0.39	0.08	327.64	25.75
SCH-14	Minimum	2.9	73.7	bdl	2.6	0.9	bdl	12.7	0.2	bdl	bdl	0.2	39.0	4.0	1.2	1.3	bdl	0.1	0.00	3.70	10.15	1.06	6.24	1.50	1.42	1.77	0.21	1.49	0.21	0.67	0.09	0.81	0.11	bdl	0.32	2.49	0.01	0.04	0.002	26.61	3.66
	Median	13.3	98.3		8.3	1.3	0.1	17.8	0.3		0.1	0.5	52.8	14.6	1.3	2.6		0.1	0.02	23.21	49.90	6.15	31.98	6.55	10.22	5.96	0.64	4.73	0.75	2.54	0.29	2.85	0.42		0.33	3.45	0.03	0.09	0.02	155.76	12.96
	RSD (%)	103.8	20.0	137.9	63.7	60.5	137.2	15.9	199.2	226.4	238.8	114.5	18.6	46.6	55.9	38.2			120.60	73.15	74.64	62.97	56.24	53.59	58.46	54.96	56.48	56.64	56.61	55.09	52.06	51.48	53.18	74.71	2.80	26.38	75.79	80.56	91.61	59.47	52.94
Tehov	Mean	14.1	47.8	43.1	14.4	1.2	0.4	28.0	0.2	0.2	3.7	2.4	127.6	25.2	7.6	44.5	bdl	0.4	0.02	30.38	69.54	8.59	42.23	7.56	6.74	6.45	0.69	4.48	0.74	2.37	0.29	2.43	0.35	0.002	0.49	7.01	0.26	1.13	0.51	171.48	11.36
n=11	SD	14.3	11.7	47.5	2.5	0.4	0.9	7.0	0.1	0.5	8.9	3.5	5.4	5.9	2.1	8.0	0.1	0.1	0.03	15.66	21.05	2.41	14.62	3.02	1.85	2.34	0.25	1.47	0.23	0.64	0.06	0.53	0.08	0.003	0.01	0.37	0.47	1.76	0.84	47.63	3.01
SCH-36	Maximum	42.8	68.7	148.7	19.5	2.2	2.6	42.5	0.3	1.8	30.6	12.9	133.9	34.6	13.0	58.7	0.5	0.6	0.08	61.02	106.89	14.60	81.04	15.33	9.90	12.04	1.25	7.37	1.10	3.21	0.37	3.00	0.45	0.01	0.51	8.02	1.74	5.67	2.61	244.93	16.55
	Minimum	bdl	29.3	bdl	9.3	0.5	bdl	22.9	bdl	bdl	bdl	0.4	118.3	16.4	5.1	34.3	bdl	0.3	bdl	12.09	43.09	5.31	23.12	3.82	4.20	3.35	0.36	2.59	0.44	1.45	0.18	1.33	0.19	bdl	0.48	6.49	0.03	0.02	bdl	98.63	7.03
	Median	7.2	44.6	23.6	14.3	1.1		25.7	0.2			0.9	128.4	26.0	7.1	42.6		0.4	0.01	23.88	66.72	8.26	42.67	7.67	6.35	6.44	0.74	4.64	0.83	2.52	0.30	2.61	0.35		0.49	6.95	0.11	0.26	0.11	161.42	11.65
	RSD (%)	101.4	24.5	110.2	17.5	32.6	208.0	25.0	57.5	241.3	241.3	146.8	4.2	23.4	27.1	18.0		21.7	139.44	51.54	30.27	28.04	34.63	39.99	27.47	36.32	36.76	32.91	30.94	26.83	22.23	21.76	23.54	127.51	2.10	5.33	179.06	156.08	165.09	27.78	26.54

Data for Obří důl, Kovářská and Vykmanov (oxidized skarns) and Kotel, Vrbík, Hazlov and Hostákov (reduced skarns) are from Miranda et al. (2024); bdl – below detection limit

APPENDIX 2

Electron microprobe analyses of scheelite from different localities representing different types of mineralization in the Bohemian Massif

Sample	Point	Locality	Type of mineralization/deposit	Oxide			Weight%				Det.Lim ppm(G)			
				CaO	WO3	Total	Na	Fe	Mo	Sr	Na	Fe	Mo	Sr
SCH1 1	SCH1-1	Vacíkov. Petráčkova hora	RIRGS	19.2	81.2	100.3	0.02	0.00	0.10	0.00	15	35	37	96
SCH1 2	SCH1-2	Vacíkov. Petráčkova hora	RIRGS	19.0	81.4	100.4	0.03	0.00	0.11	0.00	14	35	38	95
SCH1 3	SCH1-3	Vacíkov. Petráčkova hora	RIRGS	19.1	81.0	100.1	0.02	0.00	0.12	0.00	14	35	37	96
SCH1 4	SCH1-4	Vacíkov. Petráčkova hora	RIRGS	19.3	81.8	101.0	0.02	0.00	0.11	0.00	14	35	37	96
SCH1 5	SCH1-5	Vacíkov. Petráčkova hora	RIRGS	19.2	81.5	100.7	0.01	0.01	0.08	0.00	14	35	36	96
SCH1 6	SCH1-6	Vacíkov. Petráčkova hora	RIRGS	19.1	81.9	101.1	0.00	0.00	0.13	0.00	15	35	37	97
SCH1 7	SCH1-7	Vacíkov. Petráčkova hora	RIRGS	19.2	81.7	100.9	0.01	0.00	0.11	0.00	15	35	37	96
SCH3 1	SCH3 1	Čelina. JP-10. 60 m	RIRGS	18.8	79.5	98.4	0.01	0.00	0.15	0.00	14	34	38	95
SCH3 2	SCH3 2	Čelina. JP-10. 60 m	RIRGS	19.3	80.0	99.3	0.01	0.00	0.24	0.00	15	35	40	94
SCH3 3	SCH3 3	Čelina. JP-10. 60 m	RIRGS	19.3	80.1	99.4	0.01	0.00	0.39	0.00	15	34	43	93
SCH3 4	SCH3 4	Čelina. JP-10. 60 m	RIRGS	19.3	80.1	99.4	0.01	0.00	0.19	0.00	14	35	39	94
SCH3 5	SCH3 5	Čelina. JP-10. 60 m	RIRGS	19.1	80.2	99.3	0.01	0.00	0.16	0.00	14	35	38	96
SCH3 6	SCH3 6	Čelina. JP-10. 60 m	RIRGS	19.1	80.2	99.2	0.01	0.00	0.17	0.00	15	35	39	96
SCH3 7	SCH3 7	Čelina. JP-10. 60 m	RIRGS	19.3	80.0	99.3	0.00	0.00	0.18	0.00	15	34	38	95
SCH3 8	SCH3 8	Čelina. JP-10. 60 m	RIRGS	19.2	80.5	99.7	0.00	0.00	0.15	0.00	15	35	38	96
SCH3 9	SCH3 9	Čelina. JP-10. 60 m	RIRGS	19.3	80.7	100.0	0.01	0.01	0.17	0.00	14	34	38	96
SCH3 10	SCH3 10	Čelina. JP-10. 60 m	RIRGS	19.5	79.4	99.0	0.01	0.00	0.36	0.00	14	35	43	96
SCH3 11	SCH3 11	Čelina. JP-10. 60 m	RIRGS	19.2	80.7	99.9	0.00	0.01	0.15	0.00	15	35	38	95
SCH7 1	SCH7 1	Humpolec. Orlík	Orogenic Au	19.2	80.6	99.7	0.01	0.00	0.00	0.15	15	34	35	100
SCH7 2	SCH7 2	Humpolec. Orlík	Orogenic Au	19.0	80.5	99.5	0.00	0.00	0.00	0.15	15	35	35	99
SCH7 3	SCH7 3	Humpolec. Orlík	Orogenic Au	19.0	80.5	99.4	0.02	0.00	0.00	0.19	15	35	35	98
SCH7 4	SCH7 4	Humpolec. Orlík	Orogenic Au	19.0	80.4	99.4	0.01	0.00	0.00	0.17	15	34	35	102
SCH7 5	SCH7 5	Humpolec. Orlík	Orogenic Au	19.1	80.6	99.6	0.02	0.00	0.00	0.20	14	35	36	100
SCH7 6	SCH7 6	Humpolec. Orlík	Orogenic Au	19.0	80.0	99.0	0.04	0.00	0.00	0.16	15	34	35	102
SCH7 7	SCH7 7	Humpolec. Orlík	Orogenic Au	19.0	80.0	99.0	0.01	0.00	0.00	0.17	15	34	36	100
SCH7 7	SCH7 7	Humpolec. Orlík	Orogenic Au	19.0	80.8	99.8	0.01	0.00	0.00	0.15	14	35	35	101
SCH7 8	SCH7 8	Humpolec. Orlík	Orogenic Au	18.8	79.9	98.7	0.00	0.00	0.00	0.16	15	34	35	100
SCH7 9	SCH7 9	Humpolec. Orlík	Orogenic Au	18.9	79.0	97.9	0.01	0.00	0.00	0.17	15	35	35	102
SCH7 10	SCH7 10	Humpolec. Orlík	Orogenic Au	18.9	80.0	98.8	0.01	0.00	0.00	0.16	14	35	36	102
SCH9 1	SCH9 1	Chedrbí u Čáslavi	Oxidized skarn	19.3	79.7	99.0	0.01	0.00	0.10	0.00	14	35	38	97
SCH9 2	SCH9 2	Chedrbí u Čáslavi	Oxidized skarn	19.3	80.3	99.6	0.00	0.00	0.10	0.00	14	34	38	97
SCH9 3	SCH9 3	Chedrbí u Čáslavi	Oxidized skarn	19.5	80.9	100.3	0.00	0.00	0.05	0.00	14	35	36	96
SCH9 4	SCH9 4	Chedrbí u Čáslavi	Oxidized skarn	19.3	80.9	100.2	0.00	0.00	0.04	0.00	15	35	37	94
SCH9 5	SCH9 5	Chedrbí u Čáslavi	Oxidized skarn	19.4	80.7	100.2	0.00	0.00	0.15	0.00	15	35	37	96
SCH9 6	SCH9 6	Chedrbí u Čáslavi	Oxidized skarn	19.3	79.8	99.1	0.00	0.00	0.11	0.00	15	35	38	97
SCH9 7	SCH9 7	Chedrbí u Čáslavi	Oxidized skarn	19.5	80.4	99.8	0.01	0.00	0.13	0.00	14	35	38	96
SCH9 8	SCH9 8	Chedrbí u Čáslavi	Oxidized skarn	19.5	80.6	100.1	0.00	0.00	0.12	0.00	15	34	38	96
SCH39 1	SCH39 1	Cetoraz u Pacova	Greisen Sn-W and related quartz vein	19.4	81.3	100.8	0.01	0.00	0.00	0.01	14	35	35	99
SCH39 2	SCH39 2	Cetoraz u Pacova	Greisen Sn-W and related quartz vein	19.1	79.8	98.9	0.02	0.00	0.01	0.00	14	35	35	98
SCH39 3	SCH39 3	Cetoraz u Pacova	Greisen Sn-W and related quartz vein	19.4	80.8	100.2	0.01	0.00	0.00	0.00	14	35	35	97
SCH39 4	SCH39 4	Cetoraz u Pacova	Greisen Sn-W and related quartz vein	19.3	81.2	100.5	0.01	0.00	0.00	0.00	15	35	36	98
SCH39 5	SCH39 5	Cetoraz u Pacova	Greisen Sn-W and related quartz vein	19.4	80.4	99.8	0.03	0.00	0.00	0.01	15	35	35	97
SCH39 6	SCH39 6	Cetoraz u Pacova	Greisen Sn-W and related quartz vein	19.2	80.6	99.8	0.04	0.00	0.00	0.00	15	35	36	100
SCH43 1	SCH43 1	Krásno - Huber	Greisen Sn-W and related quartz vein	19.5	81.0	100.5	0.00	0.00	0.00	0.00	15	35	36	97
SCH43 2	SCH43 2	Krásno - Huber	Greisen Sn-W and related quartz vein	19.5	81.1	100.7	0.01	0.00	0.00	0.00	14	35	35	96
SCH43 3	SCH43 3	Krásno - Huber	Greisen Sn-W and related quartz vein	19.6	81.4	100.9	0.00	0.00	0.00	0.00	14	35	36	97
SCH43 4	SCH43 4	Krásno - Huber	Greisen Sn-W and related quartz vein	19.6	80.9	100.4	0.00	0.00	0.00	0.00	15	34	35	98
SCH41 1	SCH41 1	Jílové. 3. Pepř. ž. Tobola. 1967	Orogenic Au	19.2	81.2	100.4	0.00	0.00	0.00	0.00	15	35	35	94
SCH41 2	SCH41 2	Jílové. 3. Pepř. ž. Tobola. 1968	Orogenic Au	19.1	81.1	100.2	0.01	0.00	0.00	0.00	15	35	35	96
SCH41 3	SCH41 3	Jílové. 3. Pepř. ž. Tobola. 1969	Orogenic Au	19.2	80.3	99.5	0.02	0.00	0.01	0.00	15	35	35	95
SCH41 4	SCH41 4	Jílové. 3. Pepř. ž. Tobola. 1970	Orogenic Au	19.1	81.0	100.1	0.01	0.00	0.00	0.00	15	35	36	95
SCH41 5	SCH41 5	Jílové. 3. Pepř. ž. Tobola. 1971	Orogenic Au	19.4	80.7	100.1	0.01	0.00	0.00	0.00	15	35	36	94
SCH41 6	SCH41 6	Jílové. 3. Pepř. ž. Tobola. 1972	Orogenic Au	19.1	80.7	99.8	0.01	0.00	0.01	0.00	15	35	35	93
SCH41 7	SCH41 7	Jílové. 3. Pepř. ž. Tobola. 1973	Orogenic Au	19.2	81.3	100.5	0.01	0.00	0.00	0.00	15	35	36	94
SCH41 8	SCH41 8	Jílové. 3. Pepř. ž. Tobola. 1974	Orogenic Au	19.3	80.8	100.0	0.01	0.01	0.00	0.00	15	35	36	95
SCH38 1	SCH38 1	Ovesná Lhota u Světlé nad Sázavou	Greisen Sn-W and related quartz vein	19.0	80.6	99.5	0.03	0.00	0.00	0.00	15	35	35	96
SCH38 2	SCH38 2	Ovesná Lhota u Světlé nad Sázavou	Greisen Sn-W and related quartz vein	19.2	80.7	99.9	0.01	0.00	0.00	0.00	15	35	35	96
SCH38 3	SCH38 3	Ovesná Lhota u Světlé nad Sázavou	Greisen Sn-W and related quartz vein	18.9	78.6	97.5	0.04	0.00	0.00	0.00	15	35	35	93
SCH38 4	SCH38 4	Ovesná Lhota u Světlé nad Sázavou	Greisen Sn-W and related quartz vein	19.1	80.2	99.3	0.03	0.00	0.00	0.00	15	35	36	94
SCH10-1	SCH10-1	Mutice u Mladé Vožice	Oxidized skarn	19.1	80.6	99.8	0.00	0.01	0.02	0.00	15	35	37	91
SCH10-2	SCH10-2	Mutice u Mladé Vožice	Oxidized skarn	19.1	79.5	98.6	0.00	0.00	0.04	0.00	15	35	37	90
SCH10-3	SCH10-3	Mutice u Mladé Vožice	Oxidized skarn	19.2	78.9	98.1	0.00	0.00	0.03	0.00	14	35	37	90
SCH10-4	SCH10-4	Mutice u Mladé Vožice	Oxidized skarn	19.2	79.9	99.2	0.00	0.00	0.04	0.00	15	35	37	93
SCH10-5	SCH10-5	Mutice u Mladé Vožice	Oxidized skarn	19.3	79.6	98.9	0.01	0.00	0.01	0.00	15	35	37	90
SCH10-6	SCH10-6	Mutice u Mladé Vožice	Oxidized skarn	19.2	79.3	98.5	0.00	0.00	0.03	0.00	15	35	37	92
SCH10-7	SCH10-7	Mutice u Mladé Vožice	Oxidized skarn	19.2	79.4	98.7	0.00	0.01	0.04	0.00	15	35	37	91
SCH10-8	SCH10-8	Mutice u Mladé Vožice	Oxidized skarn	19.3	79.5	98.7	0.00	0.00	0.02	0.00	15	35	37	88
SCH10-9	SCH10-9	Mutice u Mladé Vožice	Oxidized skarn	19.2	79.0	98.2	0.00	0.00	0.03	0.00	15	35	36	90
SCH10-10	SCH10-10	Mutice u Mladé Vožice	Oxidized skarn	19.3	80.1	99.3	0.00	0.00	0.02	0.00	15	35	36	90
SCH13-1	SCH13-1	Budislav u Litomyšle	Reduced skarn	19.2	80.0	99.2	0.00	0.00	0.00	0.00	15	35	36	91
SCH13-2	SCH13-2	Budislav u Litomyšle	Reduced skarn	19.2	80.6	99.8	0.00	0.00	0.01	0.00	15	35	36	90
SCH13-3	SCH13-3	Budislav u Litomyšle	Reduced skarn	19.3	79.8	99.0	0.00	0.00	0.01	0.00	15	35	36	89
SCH13-4	SCH13-4	Budislav u Litomyšle	Reduced skarn	19.3	79.8	99.0	0.00	0.00	0.00	0.00	15	35	36	91
SCH13-5	SCH13-5	Budislav u Litomyšle	Reduced skarn	19.2	80.0	99.3	0.01	0.00	0.02	0.00	15	35	36	92
SCH13-6	SCH13-6	Budislav u Litomyšle	Reduced skarn	19.1	80.5	99.6	0.00	0.00	0.00	0.00	15	35	36	90
SCH13-7	SCH13-7	Budislav u Litomyšle	Reduced skarn	19.2	80.4	99.5	0.00	0.00	0.00	0.00	15	35	36	91
SCH29 1	SCH29 1	Nekvasovy-Chlumy	Oxidized skarn	19.3	81.5	100.8	0.01	0.00	0.01	0.00	15	35	36	97
SCH29 2	SCH29 2	Nekvasovy-Chlumy	Oxidized skarn	19.4	81.5	100.8	0.00	0.00	0.03	0.00	15	35	37	97
SCH29 3	SCH29 3	Nekvasovy-Chlumy	Oxidized skarn	19.3	81.5	100.8	0.00	0.00	0.05	0.00	15	35	38	97
SCH29 4	SCH29 4	Nekvasovy-Chlumy	Oxidized skarn	19.3	81.7	101.0	0.01	0.00	0.03	0.00	14	35	36	98
SCH29 5	SCH29 5	Nekvasovy-Chlumy	Oxidized skarn	19.2	80.5	99.7	0.01	0.00	0.03	0.00	15	35	37	97
SCH29 6	SCH29 6	Nekvasovy-Chlumy	Oxidized skarn	19.4	81.1	100.6	0.00	0.01	0.05	0.00	15	35	36	95
SCH29 7	SCH29 7	Nekvasovy-Chlumy	Oxidized skarn	19.3	81.1	100.5	0.00	0.00	0.07	0.00	15	35	38	96
SCH29 8	SCH29 8	Nekvasovy-Chlumy	Oxidized skarn	19.3	80.8	100.2	0.00	0.00	0.04	0.00	14	35	37	97
SCH29 9	SCH29 9	Nekvasovy-Chlumy	Oxidized skarn	19.2	80.9	100.1	0.00	0.00	0.07	0.00	15	35	37	96
SCH29 10	SCH29 10	Nekvasovy-Chlumy	Oxidized skarn	19.2	80.9	100.1	0.01	0.00	0.08	0.00	15	35	37	97
SCH29 11	SCH29 11	Nekvasovy-Chlumy	Oxidized skarn	19.2	81.1	100.4	0.00	0.01	0.08	0.00	15	35	37	96
SCH29 12	SCH29 12	Nekvasovy-Chlumy	Oxidized skarn	19.2	81.2	100.3	0.00	0.00	0.06	0.00	15	35	38	99
SCH28 1	SCH28 1	Bílé Labe	Oxidized skarn	19.1	80.8	100.0	0.03	0.00	0.13	0.00	15	35	38	95
SCH28 2	SCH28 2	Bílé Labe	Oxidized skarn	19.2	80.9	100.2	0.03	0.00	0.17	0.00	15	35	38	92
SCH28 3	SCH28 3	Bílé Labe	Oxidized skarn	19.3	80.2	99.5	0.04	0.00	0.16	0.00	15	35	40	95
SCH28 4	SCH28 4	Bílé Labe	Oxidized skarn	19.1	79.4	98.6	0.04	0.00	0.21	0.00	15	35	40	94
SCH28 5	SCH28 5	Bílé Labe	Oxidized skarn	19.1	80.1	99.2	0.03	0.00	0.17	0.00	15	35	40	93
SCH6 1	SCH6 1	Kašperské Hory. Lohbach	Orogenic Au	19.2	80.5	99.7	0.01	0.00	0.00	0.00	15	35	36	92
SCH6 2	SCH6 2	Kašperské Hory. Lohbach	Orogenic Au	18.2	79.2	97.4	0.01	0.00	0.01	0.00	15	35	36	95
SCH6 3	SCH6 3	Kašperské Hory. Lohbach	Orogenic Au	19.3	81.7	101.0	0.01	0.00	0.00	0.00	15	35	36	95
SCH6 4	SCH6 4	Kašperské Hory. Lohbach	Orogenic Au	19.2	79.9	99.2	0.01	0.00	0.01	0.00	15	35	36	93
SCH6 5	SCH6 5	Kašperské Hory. Lohbach	Orogenic Au	19.0	78.2	97.3	0.01	0.00	0.00	0.00	15	35	37	93
SCH6 6	SCH6 6	Kašperské Hory. Lohbach	Orogenic Au	19.4	80.5	100.0	0.01	0.00	0.02	0.00	15	35	37	94
SCH6 7	SCH6 7	Kašperské Hory. Lohbach	Orogenic Au	19.4	80.8	100.2	0.00	0.01	0.02	0.00	15	35	37	93
SCH5 1	SCH5 1	Kašperské Hory. št. Naděje	Orogenic Au	19.3	79.6	99.0	0.01	0.00	0.00	0.00	15	35	36	97
SCH5 2	SCH5 2	Kašperské Hory. št. Naděje	Orogenic Au	19.3	78.8	98.1	0.00	0.00	0.00	0.00	15	35	36	98
SCH5 3	SCH5 3	Kašperské Hory. št. Naděje	Orogenic Au	19.5	79.7	99.2	0.00	0.00	0.00	0.00	15	35	36	98
SCH5 4	SCH5 4	Kašperské Hory. št. Naděje	Orogenic Au	19.3	78.4	97.7	0.01	0.00	0.00	0.00	14	35	35	97
SCH5 5	SCH5 5	Kašperské Hory. št. Naděje	Orogenic Au	19.3	78.7	98.1	0.01	0.00	0.00	0.00	15	35	35	97
SCH5 6	SCH5 6	Kašperské Hory. št. Naděje	Orogenic Au	19.2	79.2	98.4	0.02	0.00	0.01	0.00	15	35	35	96
SCH5 7	SCH5 7	Kašperské Hory. št. Naděje	Orogenic Au	19.2	78.9	98.1	0.00	0.00	0.01	0.00	15	34	35	95
SCH5 8	SCH5 8	Kašperské Hory. št. Naděje	Orogenic Au	19.4	79.1	98.5	0.00	0.00	0.01	0.00	15	35	35	98
SCH5 9	SCH5 9	Kašperské Hory. št. Naděje	Orogenic Au	19.4	79.1	98.5	0.01	0.00	0.00	0.00	15	35	35	97
SCH5 10	SCH5 10	Kašperské Hory. št. Naděje	Orogenic Au	19.3	79.4	98.8	0.00	0.00	0.00	0.00	15	35	35	97
SCH5 11	SCH5 11	Kašperské Hory. št. Naděje	Orogenic Au	19.4	78.9	98.3	0.01	0.00	0.01	0.00	14	35	35	97
SCH14 1	SCH14 1	Erpužice u Stříbra	Quartz vein	19.4	79.2	98.6	0.00	0.01	0.00	0.00	15	34	35	96
SCH14 2	SCH14 2	Erpužice u Stříbra	Quartz vein	19.2	78.8	98.0	0.00	0.00	0.00	0.00	15	35	36	97
SCH14 3	SCH14 3	Erpužice u Stříbra	Quartz vein	19.2	78.6	97.8	0.00	0.00	0.00	0.00	14	35	35	98
SCH14 4	SCH14 4	Erpužice u Stříbra	Quartz vein	19.3	79.3	98.7	0.00	0.01	0.00	0.00	15	35	36	97
SCH14 5	SCH14 5	Erpužice u Stříbra	Quartz vein	19.5	79.6	99.1	0.00	0.00	0.00	0.00	14	35	36	97
SCH37 1	SCH37 1	Horní Babákov u Hlinska	Greisen Sn-W and related quartz vein	19.0	79.1	98.1	0.05	0.00	0.00	0.00	15	35	35	99
SCH37 2	SCH37 2	Horní Babákov u Hlinska	Greisen Sn-W and related quartz vein	18.9	79.0	98.0	0.05	0.00	0.00	0.00	15	35	36	95
SCH37 3	SCH37 3	Horní Babákov u Hlinska	Greisen Sn-W and related quartz vein	19.1	80.0	99.1	0.04	0.00	0.00	0.00	15	35	36	93
SCH37 4	SCH37 4	Horní Babákov u Hlinska	Greisen Sn-W and related quartz vein	19.1	80.1	99.2	0.05	0.00	0.00	0.00	15	35	36	94
SCH37 5	SCH37 5	Horní Babákov u Hlinska	Greisen Sn-W and related quartz vein	19.1	79.4	98.5	0.05	0.00	0.00	0.00	15	35	36	96
SCH37 6	SCH37 6	Horní Babákov u Hlinska	Greisen Sn-W and related quartz vein	19.0	79.6	98.6	0.06	0.00	0.00	0.00	15	35	36	96
SCH37 7	SCH37 7	Horní Babákov u Hlinska	Greisen Sn-W and related quartz vein	19.0	79.6	98.6	0.07	0.00	0.00	0.01	15	35	36	94
SCH37 8	SCH37 8	Horní Babákov u Hlinska	Greisen Sn-W and related quartz vein	19.1	80.0	99.1	0.06	0.00	0.00	0.00	15	35	36	95
SCH37 9	SCH37 9	Horní Babákov u Hlinska	Greisen Sn-W and related quartz vein	19.1	79.1	98.2	0.05	0.00	0.00	0.00	15	35	36	96
SCH37 12	SCH37 12	Horní Babákov u Hlinska	Greisen Sn-W and related quartz vein	18.9	78.3	97.2	0.04	0.00	0.01	0.00	15	33	35	92
SCH46 1	SCH46 1	Proseč u Litomyšle	Oxidized skarn	19.5	81.7	101.2	0.01	0.01	0.05	0.00	15	35	37	95
SCH46 2	SCH46 2	Proseč u Litomyšle	Oxidized skarn	19.3	81.0	100.3	0.00	0.01	0.06	0.00	15	35	36	95
SCH46 3	SCH46 3	Proseč u Litomyšle	Oxidized skarn	19.4	81.2	100.5	0.00	0.00	0.04	0.00	15	35	37	97
SCH46 4	SCH46 4	Proseč u Litomyšle	Oxidized skarn	19.3	81.5	100.9	0.00	0.00	0.04	0.00	15	35	37	97
SCH46 5	SCH46 5	Proseč u Litomyšle	Oxidized skarn	19.5	81.3	100.8	0.00	0.00	0.03	0.00	15	35	37	97
SCH46 6	SCH46 6	Proseč u Litomyšle	Oxidized skarn	19.5	81.5	101.1	0.00	0.00	0.04	0.00	15	35	37	97

SCH46 7	SCH46 7	Proseč u Litomyšle	Oxidized skarn	19.6	81.7	101.2	0.01	0.00	0.02	0.00	14	35	36	95
SCH46 8	SCH46 8	Proseč u Litomyšle	Oxidized skarn	19.6	81.3	100.9	0.01	0.00	0.02	0.00	15	35	36	96
SCH45 1	SCH45 1	Krouna u Poličky	Oxidized skarn	19.4	80.7	100.1	0.00	0.00	0.04	0.00	15	35	36	95
SCH45 2	SCH45 2	Krouna u Poličky	Oxidized skarn	19.4	80.2	99.6	0.03	0.00	0.03	0.00	14	35	37	97
SCH45 3	SCH45 3	Krouna u Poličky	Oxidized skarn	19.3	80.0	99.3	0.02	0.00	0.05	0.00	15	35	36	95
SCH45 4	SCH45 4	Krouna u Poličky	Oxidized skarn	19.3	80.5	99.8	0.00	0.00	0.03	0.00	15	35	37	98
SCH45 5	SCH45 5	Krouna u Poličky	Oxidized skarn	19.3	80.6	99.9	0.00	0.00	0.03	0.00	15	35	37	97
SCH45 6	SCH45 6	Krouna u Poličky	Oxidized skarn	19.3	79.7	99.1	0.00	0.00	0.06	0.00	15	35	36	97
SCH36 1	SCH36 1	Tehov u Říčan	Quartz vein	19.3	79.4	98.6	0.01	0.00	0.00	0.00	15	35	36	95
SCH36 2	SCH36 2	Tehov u Říčan	Quartz vein	19.2	79.4	98.7	0.01	0.01	0.00	0.00	14	34	35	95
SCH36 3	SCH36 3	Tehov u Říčan	Quartz vein	19.3	79.7	98.9	0.00	0.00	0.00	0.00	15	35	36	96
SCH36 4	SCH36 4	Tehov u Říčan	Quartz vein	19.2	79.1	98.3	0.01	0.00	0.00	0.00	14	35	36	97
SCH36 5	SCH36 5	Tehov u Říčan	Quartz vein	18.6	74.5	93.0	0.01	0.00	0.00	0.00	14	34	36	94
SCH36 6	SCH36 6	Tehov u Říčan	Quartz vein	19.3	79.2	98.5	0.00	0.00	0.01	0.00	15	35	35	97
SCH36 7	SCH36 7	Tehov u Říčan	Quartz vein	19.1	78.9	98.0	0.00	0.00	0.00	0.00	15	35	36	95
SCH36 8	SCH36 8	Tehov u Říčan	Quartz vein	19.1	78.9	98.0	0.01	0.00	0.00	0.00	14	35	36	96
SCH48 1	SCH48 1	Cínovec 2	Greisen Sn-W and related quartz vein	19.6	75.7	95.4	0.00	0.00	0.52	0.00	15	34	45	94
SCH48 3	SCH48 3	Cínovec 2	Greisen Sn-W and related quartz vein	19.8	75.5	95.3	0.00	0.01	0.52	0.00	14	34	45	95
SCH48 4	SCH48 4	Cínovec 2	Greisen Sn-W and related quartz vein	19.4	77.2	96.7	0.00	0.00	0.14	0.00	14	34	38	96
SCH48 5	SCH48 5	Cínovec 2	Greisen Sn-W and related quartz vein	17.7	76.4	94.1	0.01	0.02	0.12	0.00	14	35	39	94
SCH48 6	SCH48 6	Cínovec 2	Greisen Sn-W and related quartz vein	19.6	75.9	95.5	0.00	0.00	0.54	0.00	14	34	45	94
SCH48 7	SCH48 7	Cínovec 2	Greisen Sn-W and related quartz vein	20.2	76.7	96.9	0.00	0.00	0.09	0.00	14	35	38	93
SCH47 2	SCH47 2	Cínovec 1	Greisen Sn-W and related quartz vein	18.5	74.9	93.3	0.02	0.03	0.25	0.00	14	34	41	93
SCH47 3	SCH47 3	Cínovec 1	Greisen Sn-W and related quartz vein	18.6	74.1	92.7	0.00	0.02	0.41	0.00	14	34	42	91
SCH42 1	SCH42 1	Sobětice u Klatov	Orogenic Au	19.0	79.3	98.3	0.01	0.01	0.00	0.00	15	35	35	94
SCH42 2	SCH42 2	Sobětice u Klatov	Orogenic Au	19.2	80.2	99.4	0.01	0.00	0.00	0.00	14	35	35	98
SCH42 3	SCH42 3	Sobětice u Klatov	Orogenic Au	19.1	80.0	99.1	0.01	0.00	0.00	0.00	14	35	36	97
SCH42 4	SCH42 4	Sobětice u Klatov	Orogenic Au	19.2	80.0	99.2	0.02	0.00	0.00	0.00	15	35	36	97
SCH42 5	SCH42 5	Sobětice u Klatov	Orogenic Au	19.4	79.8	99.2	0.00	0.00	0.00	0.00	15	35	36	96
SCH33 1	SCH33 1	Supíkovice u Jeseníku	Orogenic Au	19.3	80.0	99.3	0.00	0.00	0.03	0.00	14	35	36	94
SCH33 2	SCH33 2	Supíkovice u Jeseníku	Orogenic Au	19.2	80.5	99.7	0.00	0.00	0.02	0.00	14	35	36	96
SCH33 3	SCH33 3	Supíkovice u Jeseníku	Orogenic Au	19.2	78.6	97.7	0.00	0.00	0.03	0.00	14	35	36	96
SCH33 4	SCH33 4	Supíkovice u Jeseníku	Orogenic Au	19.4	79.9	99.3	0.00	0.00	0.02	0.00	14	35	36	95
SCH33 5	SCH33 5	Supíkovice u Jeseníku	Orogenic Au	19.2	80.5	99.6	0.00	0.00	0.03	0.00	14	35	36	95

Data for Obří důl, Kovářská and Vykmanov (oxidized skarns) and Kotel, Vrbík, Hazlov and Hostákov (reduced skarns) are from Miranda et al. (2024)

APPENDIX 3

Detailed laser setting specifications

Laser make, model and type	Resolution M-50 Excimer
Laser wavelength	193 nm
Laser pulse duration	5 ns
Laser energy density	3 J cm-2
Laser repetition rate	15 Hz
Laser spot diameter	33 to 55 µm spot
Ablation cell	S-155 (Laurin Technic)
He carrier gas flow	350 ml/min
N2 additional gas	2 ml/min
Gas blank acquisition time	30 s
ICP-MS model and type	7900 Agilent quadrupole
Ar plasma gas flow	14 L/min
Ar auxiliary gas flow	0.0 L/min
Ar makeup gas flow	0.0 L/min
Injector	3.0 mm i.d., quartz
Torch depth/z-position	0.4 mm
RF power	1550 W
Cone	Ni-Pt
m/z monitores (amu)	11, 23, 24, 39, 44, 49, 51, 55, 57, 59, 61, 63, 66, 75, 85, 88, 89, 93, 95, 107, 118, 137, 139, 140, 141, 146, 147, 153, 157, 159, 163, 165, 166, 169, 172, 175, 181, 182, 183, 208, 209, 232, 238.
Dwell time (ti)	5.00 ms
Quad. settling time (τ)	1.90 ms
Total sweep time (Tn)	400 ms

APPENDIX 4

Reference materials

Element	Li7	B11	Na23	Mg24	Si29	K39	Ti49	V51	Cr53	Mn55	Co59	Ni60	Cu63	Zn66	As75	Sr88	Y89	Nb93	Mo95	Ag107
GSD-1 g Working value	43	50	26708.5	21709	248656.8	25300	7431.7	44	42	220	40	58	42	54	27	69.4	42	42	39	23
Stdev	6	20	1483.8	241.2	3739.2	300	359.6	2	3	20	2	4	2	2	8	0.7	2	3	3	3
Average GSD-1 g	48.7	71	27949	22485	274633	26780	7123	43	41.9	228	38.3	55.9	41.8	55.8	37	69	39	37	39	22.1
Stdev (n = 25)	2.1	6	1120	2254	5900	887	104	1	1.9	11	1.0	1.9	1.2	2.5	3	5	3	3	3	0.8
RSD* (%)	4%	9%	4%	10%	2%	3%	1%	3%	5%	5%	3%	3%	3%	4%	9%	8%	8%	9%	8%	4%
GSE-1 g Working value	430	330	28934	21106	250994	21800	450	440	400	590	380	440	380	460	260	447	410	420	390	200
Stdev	60	120	1484	181	7011	200	42	20	80	20	20	30	40	10	90	5	30	40	30	20
Average GSE-1g	467.7	416	29774	21296	270300	23984	416	422	384.3	642	387.3	434.2	396.2	487.6	340	443	398	384	393	197.6
Stdev (n = 25)	12.3	16	1060	1684	6133	993	8	10	8.3	16	8.5	11.0	10.1	9.2	41	19	11	11	15	6.2
RSD (%)	3%	4%	4%	8%	2%	4%	2%	2%	2%	2%	2%	3%	3%	2%	12%	4%	3%	3%	4%	3%
Gprobe6-A Working value	6	n.d	15506	51318	224259	1577	7012	238	300.2	1255	46.9	145.7	89.5	70.8	n.d	166.6	19.33	4.16	n.d	n.d
Stdev	1.39	n.d	1335	6935	9418	166	1319	27.1	21.5	93	3.51	18.9	20.31	16.6	n.d	26.1	1.78	0.41	n.d	n.d
Average Gprobe6-A	6.1		16431	53166	256466.7	1815	6436	255	330.6	1324	52.9	168.8	97.7	96.4		163	17	3		0.6
Stdev (n = 25)	1.6		1175	5970	5800.0	221	55	5	7.9	43	1.5	5.3	3.3	3.4		12	2	0.3		0.1
RSD (%)	26%		7%	11%	2%	12%	1%	2%	2%	3%	3%	3%	3%	3%		7%	9%	8%		12%
NIST-612 Working value	42	35	103858	77	n.d	66.3	44	39	35	38	35.5	38.8	37.7	38	37	78.4	38	40	38	22
Stdev	6	6	n.d	60	n.d	0.8	10	8	3.3	2	1.2	0.2	0.9	8	14	0.2	4	6	4	0.3
Average NIST-612	43.4	41	101657	62		68	39.8	37.6	35.7	40.4	33.9	37.5	35.7	34.9	32.7	75.0	35.5	32.7	37.1	19.7
Stdev (n = 25)	2.0	8	1471	2		8	1.3	1.0	1.8	2.2	1.0	1.5	1.2	1.8	1.2	6.3	3.3	3.1	2.8	0.7
RSD (%)	5%	19%	1%	4%		12%	3%	3%	5%	5%	3%	4%	3%	5%	4%	8%	9%	10%	8%	3%

Element	Sn118	Ba137	La139	Ce140	Pr141	Nd146	Sm147	Eu153	Gd157	Tb159	Dy163	Ho165	Er166	Tm169	Yb172	Lu175	Ta181	Pb208	Bi209	Th232	U238
GSD-1 g Working value	29	67	39.1	41.4	45	44.7	47.8	41	50.7	47	51.2	49	40.1	49	50.9	51.5	40	50	35	41	41
Stdev	6	1	0.4	0.4	1	0.5	0.5	2	0.5	2	0.5	2	0.4	2	0.5	0.5	4	2	4	2	2
Average GSD-1 g	33.0	68	39	39	41	44	47	40	48	45	50	47	37	45	50	48	39	49	31	39	40
Stdev (n = 25)	1.1	3	4	4	4	1	1	3	1	4	1	4	1	4	1	4	3	3	3	5	4
RSD* (%)	3%	4%	9%	10%	10%	2%	2%	7%	2%	9%	2%	9%	3%	9%	2%	8%	9%	7%	10%	13%	9%
GSE-1 g Working value	280	427	392	414	460	453	488	410	514	480	524	501	595	500	520	518	390	378	320	380	420
Stdev	50	5	4	4	10	5	5	20	6	20	6	8	6	20	5	6	40	12	30	20	30
Average GSE-1g	331.6	423	405	411	450	452	491	413	511	501	521	515	571	504	521	526	425	384	316	378	419
Stdev (n = 25)	9.7	12	9	9	12	14	13	14	15	15	15	14	21	14	16	16	14	17	16	11	13
RSD (%)	3%	3%	2%	2%	3%	3%	3%	3%	3%	3%	3%	3%	4%	3%	3%	3%	3%	4%	5%	3%	3%
Gprobe6-A Working value	1.33	173	5.2	12	1.69	8.4	2.36	0.98	2.87	0.51	3.3	0.72	2.1	0.31	2.06	0.32	0.28	3.28	n.d.	0.33	0.29
Stdev	0.71	25.62	0.56	0.7	0.12	0.98	0.31	0.13	0.46	0.06	0.46	0.09	0.34	0.05	0.33	0.04	0.03	0.78	n.d.	0.04	0.06
Average Gprobe6-A	1.3	167	5	10.9	1.50	8.08	2.29	0.99	2.94	0.48	3.18	0.67	1.94	0.27	2.00	0.29	0.23	3.72		0.31	0.31
Stdev (n = 25)	0.2	3	0.5	1	0.15	0.38	0.11	0.11	0.13	0.05	0.11	0.08	0.09	0.03	0.08	0.03	0.04	0.28		0.07	0.04
RSD (%)	14%	2%	10%	10%	10%	5%	5%	11%	4%	10%	4%	12%	5%	12%	4%	10%	18%	8%		22%	13%
NIST-612 Working value	38	39.7	35.8	38.7	37.2	35.9	38.1	35	36.7	36	36	38	38	38	39.2	36.9	40	38.57	30	37.79	37.38
Stdev	4	0.8	0.8	0.8	1.8	0.8	0.8	2	0.8	6	0.8	2	1.8	2	0.8	0.8	4	0.2	12	0.08	0.08
Average NIST-612	34.9	38.2	34.9	35.2	33.7	35.9	38.1	35.2	38.4	35.2	35.5	35.4	35.6	33.3	38.7	33.9	34.9	37.1	29.7	35.1	34.5
Stdev (n = 25)	1.8	1.1	3.7	3.8	3.8	0.8	0.9	2.7	0.8	3.7	0.8	3.7	1.8	3.6	0.8	3.4	3.9	1.9	3.1	3.5	3.5
RSD (%)	5%	3%	11%	11%	11%	2%	2%	8%	2%	10%	2%	10%	5%	11%	2%	10%	11%	5%	10%	10%	10%

* – relative standard deviation